

THE EFFECT OF CAVITATION ON PARTICULATE
CONTAMINATION GENERATION

By

ROBERT ELWIN BOSE

Bachelor of Science
Oklahoma State University
Stillwater, Oklahoma
1960

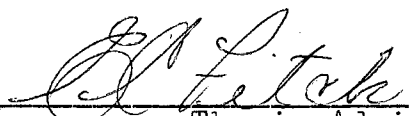
Master of Science
Oklahoma State University
Stillwater, Oklahoma
1962

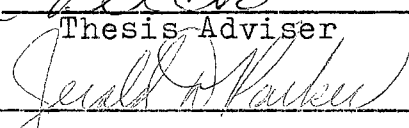
Submitted to the Faculty of the
Graduate College of the
Oklahoma State University
in partial fulfillment of
the requirements for
the Degree of
DOCTOR OF PHILOSOPHY
July, 1966

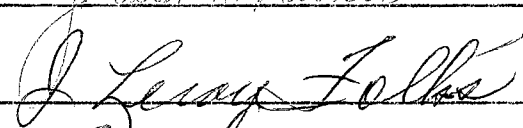
JAN 26 1967

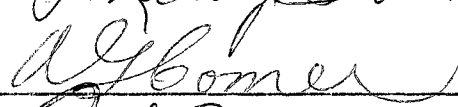
THE EFFECT OF CAVITATION ON PARTICULATE
CONTAMINATION GENERATION

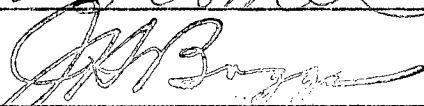
Thesis Approved:



Thesis Adviser








Dean of the Graduate College

626992

ACKNOWLEDGMENT

The writer wishes to acknowledge the Mechanical Engineering School of Oklahoma State University for financial aid in the form of a Graduate Assistantship and the rank of Instructor on the staff.

The following companies are to be extended an expression of thanks for their assistance: Cessna Industrial Hydraulics Division and the Aluminum Company of America for supplying test materials; and the Research Division of Allis-Chalmers for the use of their test apparatus.

The writer would like to thank the members of his advisory committee, Dr. E. C. Fitch, Dr. J. D. Parker, Professor A. G. Comer, and Dr. J. L. Folks, for their assistance and counseling throughout this study. Special acknowledgment is to be given to the writer's major adviser and graduate committee chairman, Dr. E. C. Fitch, for his assistance and guidance throughout the writer's graduate program.

An expression of gratitude and friendship is extended to the writer's fellow graduate students who have added a bit of humor and enjoyment during the author's graduate study.

The writer is especially grateful to Mrs. Vi Snider

and Mrs. Susan Magee for their invaluable assistance in the evaluation of test results. The Mechanical Engineering Laboratory technicians are to be acknowledged for their help in supplying and maintaining special test equipment.

Thanks is also extended to Miss Velda Davis for her careful typing and preparation of the manuscript.

The writer would like to give special recognition and thanks to his father, Edward, for his judgment, encouragement and financial aid throughout his education.

Acknowledgment is also given to my wife, Roberta, for the typing of the first draft and the reading of the manuscript.

TABLE OF CONTENTS

Chapter	Page
I. INTRODUCTION	1
II. LITERATURE SURVEY	5
Introduction	5
Material Failure Theories	6
Experimental Evaluation of Materials	11
Vibratory Type Apparatus	13
Flowing System Apparatus	16
Rotating Disk Apparatus	19
Experimental Correlation of Material Properties	21
Cavitation Intensity	24
III. EXPERIMENTAL APPARATUS AND TEST PROCEDURES	26
Introduction	26
Test Specimens	27
Test Procedure	33
Analysis of Fluid Samples	36
IV. EXPERIMENTAL RESULTS AND CONTAMINATION DATA CORRELATIONS	38
Introduction	38
Largest Particle Size Generated	39
Particle Size Distribution	51
Effect of Fluid Viscosity on Particulate Contamination Generation	69
V. APPLICATIONS OF EMPIRICAL RELATIONSHIPS	72
VI. SUMMARY AND CONCLUSIONS	77
Summary	77
Largest Particle Size Generated	77
Volume of Material Lost	79
Particle Size Distributions	80

Chapter	Page
VI. (Continued)	
Conclusions	81
Recommendations for Future Study	83
SELECTED BIBLIOGRAPHY	85
APPENDIX A - Cleaning and Packaging of Sample Containers Testing Procedure Using Packaged Sample Containers Evaluation of Particle Size Distribution	88
APPENDIX B - Cumulative Weight Loss Curves for Cavitated Specimens	95
APPENDIX C - Photographs of Generated Particulate . .	102

LIST OF TABLES

Table	Page
I. Index of Resistance to Cavitation	
Damage (23)	18
II. Mechanical Properties of Test	
Materials	32

LIST OF FIGURES

Figure	Page
2-1. Deformation Due to Shock Wave as a Result of Cavitation Bubble Collapse (20). .	10
2-2. Deformation Due to Liquid Jet as a Result of Nonsymmetrical Cavitation Bubble Collapse	12
2-3. Magnetostriction Apparatus	14
2-4. Four Zones of Cavitation Damage Rate (21) . .	15
2-5. Rate of Weight Loss Versus Amplitude of Vibration for Various Materials in the Steady State Zone (21)	17
2-6. Rotating Disk Apparatus (24)	20
2-7. Correlation Between Strain Energy and Reciprocal of Rate of Volume Loss (20) . . .	23
3-1. Sketch of Sampling Equipment	28
3-2. Photograph of Experimental Apparatus	29
3-3. Photograph of Environmental Cabinet and Sample Container	30
3-4. Schematic Representation of Calibration Equipment	34
4-1. Rate of Weight Loss and Largest Particle Size Generated for 1100-H18 Aluminum	41
4-2. Rate of Weight Loss and Largest Particle Size Generated for Copper	42
4-3. Rate of Weight Loss and Largest Particle Size Generated for 2024-T351 Aluminum . . .	43
4-4. Rate of Weight Loss and Largest Particle Size Generated for Brass (Free Cutting) . .	44

Figure	Page
4-5. Rate of Weight Loss and Largest Particle Size Generated for Monel	45
4-6. Rate of Weight Loss and Largest Particle Size Generated for 304 Stainless Steel . . .	46
4-7. Correlation Between Largest Particle Size Generated and Strain Energy at Steady State Conditions	48
4-8. Correlation Between Largest Particle Size Generated and Brinell Hardness Number at Steady State Conditions	49
4-9. Correlation Between Volume Loss and Strain Energy at Steady State Conditions	52
4-10. Cumulative Particle Size Distribution Curve for 1100-H18 Aluminum	54
4-11. Cumulative Particle Size Distribution Curve for Copper	55
4-12. Cumulative Particle Size Distribution Curve for 2024-T351 Aluminum	56
4-13. Cumulative Particle Size Distribution Curve for Brass (Free Cutting)	57
4-14. Cumulative Particle Size Distribution Curve for Monel	58
4-15. Cumulative Particle Size Distribution Curve for 304 Stainless Steel	59
4-16. Cumulative Particle Size Distribution Curve of Aircraft Field Data	60
4-17. Correlation Between Particle Cutoff Size and Brinell Hardness Number	61
4-18. Cumulative Particle Size Distribution Curves for all Materials Tested	63
4-19. Correlation Between Slope of the Cumulative Particle Size Distribution Curves and Strain Energy	64
4-20. Sketch Showing the Determination of μ_S for $N(\mu)$ Equal to 7,000	66

Figure	Page
4-21. Correlation Between μ_s and Strain Energy for $N(\mu)$ Equal to 7,000	67
5-1. Estimation of $N(\mu)$ Using Empirical Relationships	75
B-1. Cumulative Weight Loss Curve for 1100-H18 Aluminum	96
B-2. Cumulative Weight Loss Curve for Copper	97
B-3. Cumulative Weight Loss Curve for 2024-T351 Aluminum	98
B-4. Cumulative Weight Loss Curve for Brass (Free Cutting)	99
B-5. Cumulative Weight Loss Curve for Monel	100
B-6. Cumulative Weight Loss Curve for 304 Stainless Steel	101
C-1. Photographs of Generated 1100-H18 Aluminum Particulate at Steady State Conditions	104
C-2. Photograph of Generated Brass Particulate at Steady State Conditions	105
C-3. Photograph of Generated Monel Particulate at Steady State Conditions	105
C-4. Photograph of Generated Copper Particulate at Steady State Conditions	106
C-5. Photograph of Generated 2024-T351 Aluminum Particulate After Initial Five Minute Exposure to Cavitation	106

LIST OF SYMBOLS

BHN	. . Brinell hardness number
cms	. . centimeters
cps	. . cycles per second
D	. . diameter of ball
d	. . diameter of impression
e_f	. . ultimate elongation, per cent
ETP	. . electrolytic tough pitch
gms	. . grams
I	. . Intensity of Cavitation Damage
i	. . average depth of erosion
MDP	. . mean depth of penetration
M_d	. . slope of particle distribution curves
min.	. . minutes
MM ³	. . cubic millimeters
$N(\mu)$. . particle size distribution
$N_1(\mu)$. . particle size distribution of sample 1
$N_2(\mu)$. . particle size distribution of sample 2
P	. . applied load
PSI	. . pounds per square inch
S_e	. . strain energy
t	. . time
U_b	. . approximate strain energy for a brittle material

U_d	. . approximate strain energy for a ductile material
V_L	. . volume loss
σ_o	. . yield strength
σ_u	. . ultimate tensile strength
μ_{CS}	. . particle cutoff size
μ_{LS}	. . largest particle size generated
μ_S	. . particle size at which all materials generate equal numbers of particles
π	. . constant
%	. . per cent

CHAPTER I

INTRODUCTION

The analysis of hydraulic systems with respect to contamination has received considerable attention by design engineers the past ten years. Because of higher pressure component environments and correspondingly narrow clearance spaces and micronic size orifices, these engineers can no longer ignore the effect of contaminant upon the system design characteristics. Examples of increasing clearance spaces so that a component can tolerate its contaminant environment are common everyday occurrences. Engineers in the past have been able to "fix" the system by specifying a better filter and reducing the cause of contaminant build-up. A lower economical filtration limit has been reached and designers are realizing that components now must be designed to operate in or tolerate a certain level of contamination. This level is now commonly referred to as the contaminant tolerance level and may be defined as the contaminant particle size distribution of the fluid such that all components of the system will function properly during its specified operation for an acceptable time interval. It is the assignment of a

quantitative contaminant tolerance level to a system that presents an almost insurmountable task.

Contamination in a system can be classified into two distinct categories: (1) that which may be removed economically by a network of filtration and proper maintenance and (2) that which cannot be removed economically and is referred to as background contaminant. The regulation of the background contaminant normally presents the problems to the design engineer. There are two solutions for eliminating the background contamination, and they are (1) redesign of the contaminant sensitive components and (2) change of the oil in the system. To enable the engineer to predict the contaminant background build-up, contaminant generation mechanisms must be identified and their rates of contribution known. From these known rates of generation, the design engineer then can determine those mechanisms of contaminant generation which can be tolerated and those which must be minimized or eliminated. One such major mechanism of contaminant generation is cavitation.

Cavitation is the formation of partial vacuums or bubbles in a liquid caused by a change in environmental conditions. Cavitation in a system or component may be expected when portions of the fluid are subjected to pressures near the vapor pressure of the particular fluid. It is characterized by the development of minute bubbles which

grow in size, due to the low pressure, from undissolved vapor or gas nuclei in the liquid. In a flowing system, the bubbles are swept downstream and collapse in regions of higher pressure. If the point of collapse of the bubble is near the boundary of the component, structural damage to the component may occur if the shock due to the collapsing of the cavitation bubbles is of sufficient magnitude. Since cavitation often appears downstream from the filtering system, it becomes important to determine the size distribution introduced into the fluid such that the design engineer can initiate corrective measures if necessary. If the sizes of the distribution generated are tolerable in a system, then additional filtration because of the cavitation is not required. However, if the generated particles are of sufficient size and concentration, they may cause failure of the system. An example indicating the importance of knowing the particulate sizes generated as a result of cavitation is in the missile field. A typical missile fluid system, whose lifetime may be in the order of several minutes, is constructed using sophisticated fluid components that require very clean fluid conditions. If the components of the system are not limited by cavitation conditions, then smaller components of lighter weight (such as a pump) could be used to handle larger flow rates and operate in a cavitating environment as long as the particle sizes generated are below the

contaminant tolerance level of the fluid system. Therefore, in specific instances it may be feasible to operate at cavitation conditions providing that the foreign material introduced to the fluid will not be detrimental to the function of the system.

The optimum location, type, and size of filtration components can be designed into a system if the design engineer has an insight into the mechanisms of contamination generation, the contribution of these mechanisms, and the effect of the contamination upon the system.

It is the purpose of this study to determine the parameters which provide the information necessary to predict the particulate contaminant generated in a system as a result of cavitation.

CHAPTER II

LITERATURE SURVEY

Introduction

Since the beginning of the twentieth century when cavitation was first studied extensively, the principal concern of the many investigators has been to (1) identify the mechanism by which the damage occurs, (2) determine the material or material properties which can best resist this damage, and (3) formulate mathematical models and theories of the cavitation bubble growth and collapse and the subsequent material response to this collapsing action.

In the earlier investigations, the difficulty of determining the cause of the material damage was due to the fact that the cavitation occurred at a low rate or intensity in a relatively high corrosive environment. The tests were conducted in sea water on ship propellers over a period of years. Other mechanisms of material removal are initiated as a result of cavitation damage of a material's surface. One such mechanism is erosion which is accelerated by the roughened surface resulting from cavitation damage. Methods of classifying materials or their properties as to their cavitation damage resistance have

been somewhat limited until recently by the inability to identify an acceptable correlation parameter for the broad range and various types of materials that are available to present day designers. Many theoretical expressions have been derived to predict the energy released by the collapse of the many bubbles during the cavitation action. Hydrodynamic and liquid environmental effects have been explored in connection with these expressions to give a broader insight into the growth and collapse of the bubbles. Various experimental devices have been used in order to simulate or model the bubbles during their life cycle of the cavitation action that is encountered in the various field installations.

A review of the literature has revealed little information concerning the size and distribution of the particles generated as a result of cavitation damage. A selected number of theories on the failure of the materials are available and will be presented along with a discussion of the apparatus used in the tests, the various means of measurement, and the analyses of cavitation damage.

Material Failure Theories

A large number of theories on material failure due to cavitation are given in the literature. Theories based on mechanical, chemical, electrochemical, thermo-mechanical, etc., have been theorized and supported in some instances

by experimental data. A majority of the investigators accept the mechanical action theory as the primary cause of cavitation damage to structural members of components in fluid systems. Bubbles due to cavitation release large amounts of kinetic energy during collapse which is converted into a shock wave or liquid jet producing a blow to the metal surface such as a hammering effect. If the blows are of sufficient magnitude, failure of the metal occurs and small particles of the material are removed from the surface.

Parsons and Cook (1)¹ were perhaps the first investigators to attribute the mechanical action as the primary basis for cavitation damage and placed secondary importance upon the other damage contributors (such as mechanical-chemical theories, etc.). Foettinger (2) strengthened this mechanical action theory by producing damage pits, similar to those found on centrifugal pumps and water turbine impeller vanes, in neutral glass. He reasoned that if chemical or electrolytic action was active, then the materials should also be damaged where cavitation was not present.

From the microscopic examination of the surface of materials subjected to cavitation, Boetcher (3), using a flowing system, suggested that the damage was "either a

¹The numbers in parentheses refer to references in the Selected Bibliography.

hammering or the removal of tiny pieces at a time, rather than an erosive action." He proposed that the destruction of the material was caused by either compressive action or cavitation fatigue. The compressive action theory was based upon the fact that if the material was stressed higher than the compressive yield point, then deformation of the material would occur. If this mechanism were repeated by additional blows, either the material would fail and break or strain hardening would occur and prevent further deformation. The second mechanism of damage, cavitation fatigue, assumed "an entirely different aspect" (3). Although the material was stressed below the compressive yield point, damage could occur by the mechanism of fatigue. Boetcher (3) also suggest a progressive type of material damage as a result of the cavitation damage. In this theory, the initial pits, as a result of the removal of small pieces of the material, act as points of stress concentration and result in "a sidewise spreading of the destruction as well as a deepening of the pits."

Poulter (4) proposed that during the repeated stressing of the material, liquid penetrates into small openings of the material and upon the subsequent release of the pressure on the surface, "the cohesive forces of the glass or quartz are not great enough to retain the liquid under the compressed condition." By covering a portion of the test specimen with an oil film, Poulter (4) presented

experimental evidence that the oil film area was undamaged and that the exposed area exhibited a pitted surface.

Wheeler (5) proposed an ejection mechanism whereby particles are exploded from the material due to an accumulation of energy below the surface as a result of the cavitation action upon the surface of the material. An upward extrusion of metal as a result of the hammering action of the cavitation is another mechanism suggested by Wheeler (5). This extrusion of the material is known as "piling up" and forms a raised rim about a crater or pit which is removed by subsequent blows of the cavitation action.

Thiruvengadam (6) with the aid of microscopic examinations of damaged material surfaces concluded:

This [experimental observation] proves beyond doubt that the loss of material is due to the "chipping off" process produced by the repeated overlapping indentations of the shock waves.

Figure 2-1 gives a definition sketch for the shock wave and deformation resulting in a raised coronet or the "piling up" of the material (5).

Plesset and Ellis (7) and Plesset and Devine (8) have shown, by means of X-ray and electrolytic polishing techniques, the depth of this plastic deformation for various materials that have been subjected to cavitation intensities for various intervals of time. Kornfeld and Suvorov (9) attributed the cavitation destructive action to unstable bubbles which upon collapse result in a liquid jet of water impinging upon the material surface (see Figure

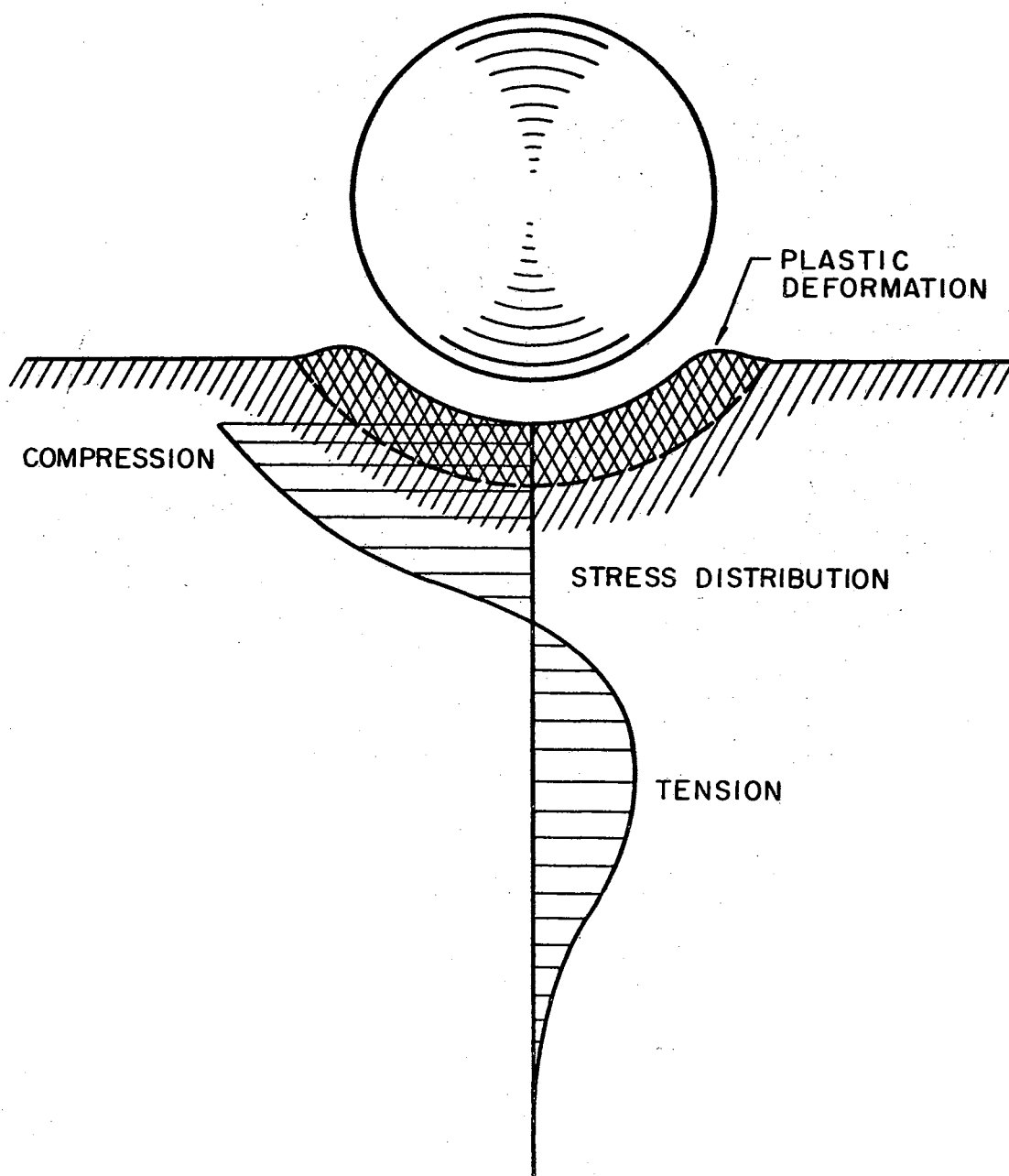


Figure 2-1. Deformation Due to Shock Wave as a Result of Cavitation Bubble Collapse (20)

2-2). Because of the nonsymmetrical location of the crater's raised rim as a result of unsymmetrical bubble collapse, Robinson (10) also supported the "fluid jet damage hypothesis, as opposed to the shock wave impingement hypothesis." Naude and Ellis (11) calculated that pressures of the order to 10^5 to 10^6 PSI were produced upon the boundary of the material as a result of the impingement of this fluid jet.

Hammitt (12) suggests that the sizes of material lost from heavily overlapped damaged surfaces may be at least of the same magnitude as the pits observed in the earlier part of the test. Nowotny (13) is perhaps the only investigator who has reported data concerning the size of particles broken from the material surface as the result of cavitation damage. He (13) found that particles smaller than the grain size appeared in the test liquid and that for a crystal with a grain size of 10^{-3} cms, particles as small as 10^{-4} to 10^{-5} cms were produced.

Experimental Evaluation of Materials

The three most common types of experimental apparatus used to classify materials as to their cavitation damage resistance are the (a) vibratory or magnetostriction device, (b) flow devices such as the venturi section, and (c) the rotating disk. The various types of devices used and their inherent different characteristics have

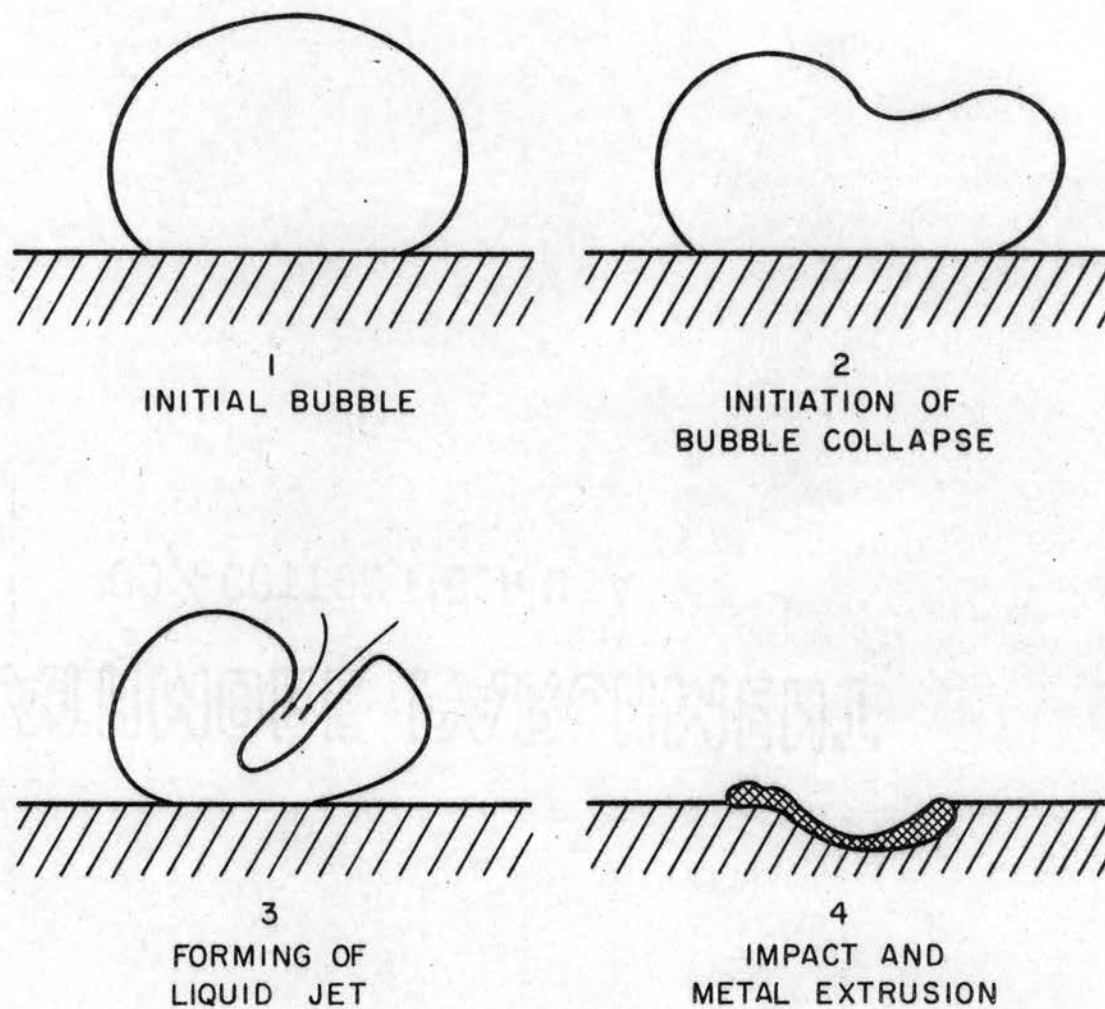


Figure 2-2. Deformation Due to Liquid Jet as a Result of Nonsymmetrical Cavitation Bubble Collapse

prevented the establishment of a standardized test procedure. An attempt was made to standardize a vibratory type test in a report given by Robinson, Holmes, and Leith (14). However, the question still remains as to the length of time the materials are to be subjected to cavitation damage for comparative evaluation. This is a necessary requirement since the damage intensity (energy absorbed by the material/time) is not equal for the various types of experimental apparatus.

Vibratory Type Apparatus

The length of exposure time in many experimental tests using the vibratory type machine (see Figure 2-3) is from a few minutes to four or five hours with measurements of weight loss being taken at various time intervals (7, 14, 15, 16, 17, 18, 19, 20). It has been shown by Thiruvengadam (21) that the rate of weight loss (weight per minute) exhibits four distinct zones of damage for certain types of materials. The four zones of damage, shown in Figure 2-4, are the incubation zone, accumulation zone, attenuation zone, and the steady state zone. The incubation zone is defined as that interval of the rate of weight loss curve where the weight of material loss is not measurable. During the incubation period, soft materials such as lead and pure aluminum are damaged considerably (deep indentations or pits) but do not lose appreciable

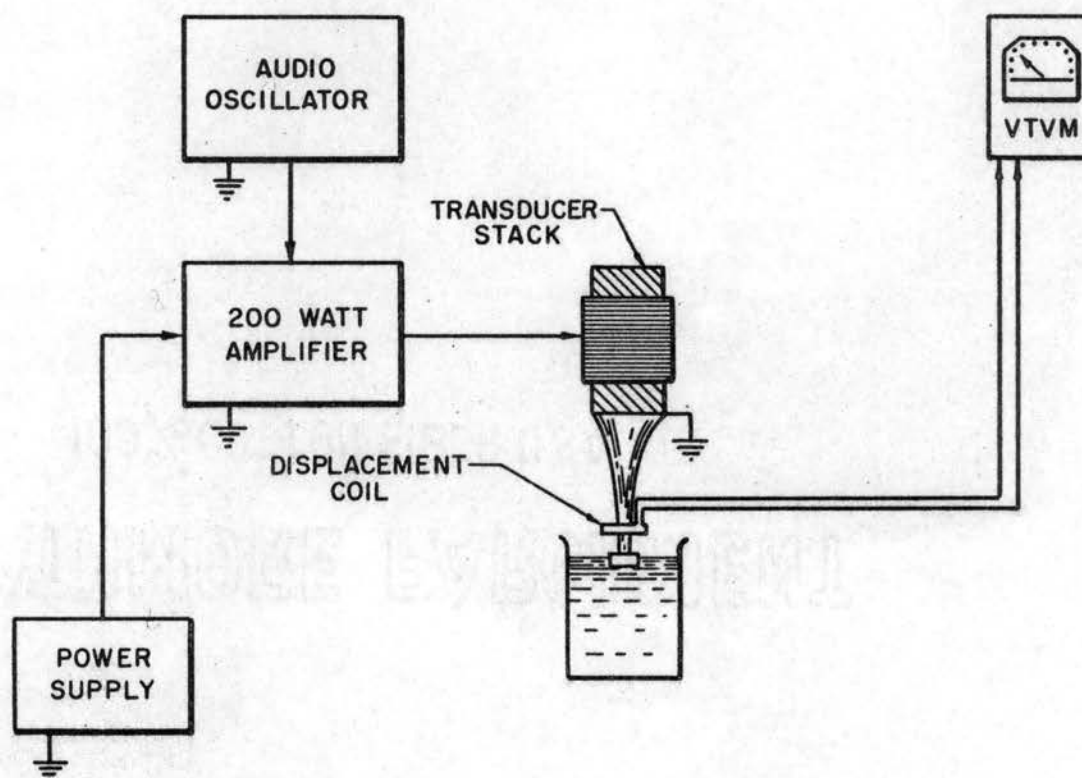


Figure 2-3. Magnetostriction Apparatus

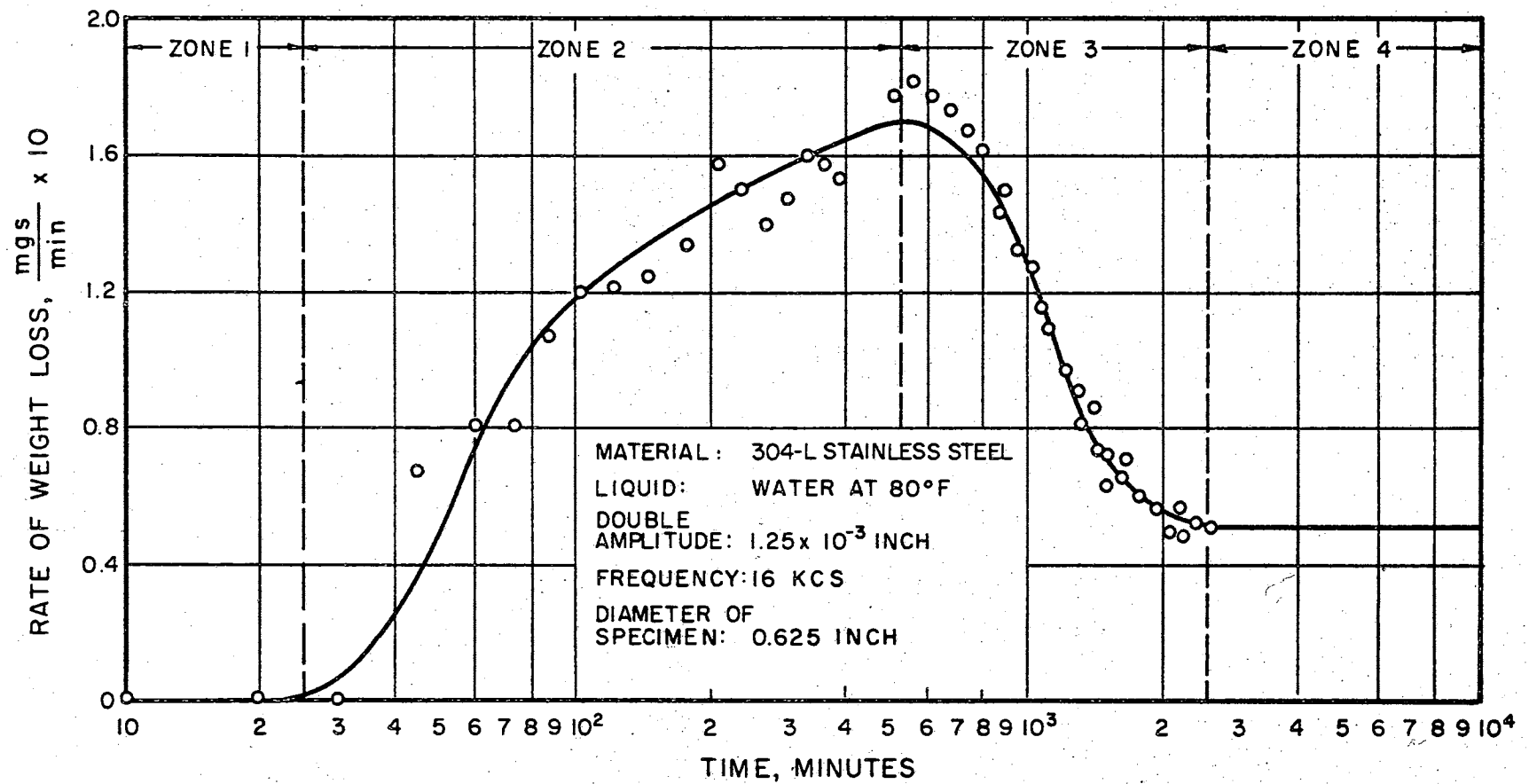


Figure 2-4. Four Zones of Cavitation Damage Rate (21)

weight. Materials such as some cast irons lose weight immediately and exhibit a very short or no incubation interval. Materials such as stainless steel may have an incubation zone in the order of 25 minutes before any weight loss is detected (21).

The second zone or interval of cavitation damage is the accumulation period during which the rate of weight loss increases with time (shown on Figure 2-4 as a positive slope). The third zone is characterized by a negative slope and is referred to as the attenuation zone. The steady state zone (zone four) is the point at which the rate of weight loss remains constant and is the zone suggested by Thiruvengadam and Preiser (21) at which material should be compared as to their cavitation damage resistance. Figure 2-5 is a plot of the rate of weight loss for various materials in the steady state zone (21).

Flowing System Apparatus

Possibly the best reason for using the flowing system as a secondary means for classification of a material's cavitation damage resistance has been the length of time necessary to complete a test. Mousson (22), using a double weir arrangement, lists 266 material specimen tests in which each specimen was subjected to 16 hours of cavitation action, which is about eight times that used for the magnetostriction device. An "Index of Resistance to

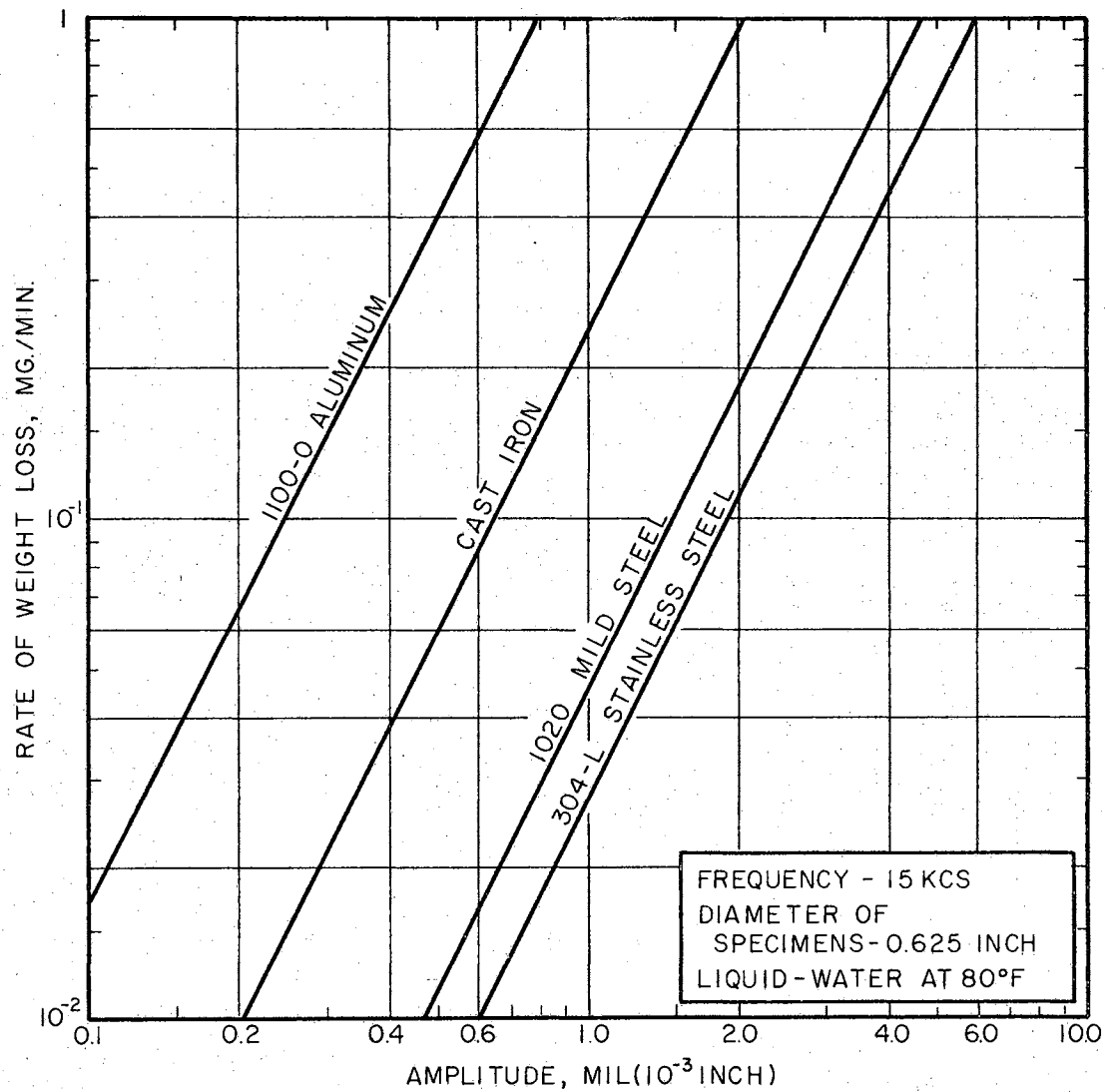


Figure 2-5. Rate of Weight Loss Versus Amplitude of Vibration for Various Materials in the Steady State Zone (21)

Cavitation Damage" has been given by Stiles (23) who concluded that "No known materials are available which will withstand the severe cavitation conditions often encountered today." Stiles classified the materials as to their cavitation resistance using a "globe-style body" with plugs made of various materials with a pressure drop across the valve of 2,000 PSI. The types of materials commonly used in hydraulic valves and the flow conditions under which they would normally be subjected were the conditions under which he conducted his tests. The time necessary for equal damage of each material was determined and the following index (Table I) was constructed by arbitrarily assigning type 316 stainless steel a value of unity.

TABLE I
INDEX OF RESISTANCE TO CAVITATION DAMAGE (23)

Material	Hours Tested	Index
No. 6 Stellite over Type 316 SS	120	>20*
Stainless Steel -- 17-4 PH	12	> 2*
Hardened to 45 RC		1.33
SS Type 316 Electrolyzed	8	
Stainless Steel -- Type 316	6	1.00
Cast Iron -- A126 Class C	4.5	0.75
Chrome Moly Steel -- C5	4.0	0.67
Nodular Iron -- A395	2.5	0.42
Carbon Steel -- WCB	2.25	0.38
Carbon Steel -- AISI C1213	1.0	0.17
Brass -- ASTM B16	0.5	0.08
Aluminum -- 1100-F	(2 min.)	0.006
*Indicates that the damage was less than that of Type 316 SS when the test was discontinued.		

Other classifications of a material's resistance to cavitation damage are given which have been derived using the vibratory test device and, in general, agree with the above classification (15, 18). Hammitt (12), using a flowing system, observed that cavitation damage was "in the form of irregularly shaped pits which do not change with additional exposure to the cavitating field within the limited durations utilized." He suggested a "correlating model in terms of the cavitation bubble density and energy and specimen material strength." Robinson (10), using mercury and water in separate tests, reported the damage data of the materials as a "Mean Depth of Penetration, (MDP)." The values of MDP were obtained by dividing the weight loss by the total exposed area and density of the specimens. He also presented data for the materials in terms of the depth to diameter ratio, which was obtained by the use of profile traces of the cavitated surface.

Rotating Disk Apparatus

The rotating disk device shown in Figure 2-6 used for determining the resistance of materials to cavitation damage utilizes a circular disk with holes drilled at various radii. When the disk is rotated in the fluid, cavities (envelope of bubbles) are produced because of the discontinuity produced by the holes in the disk. Material

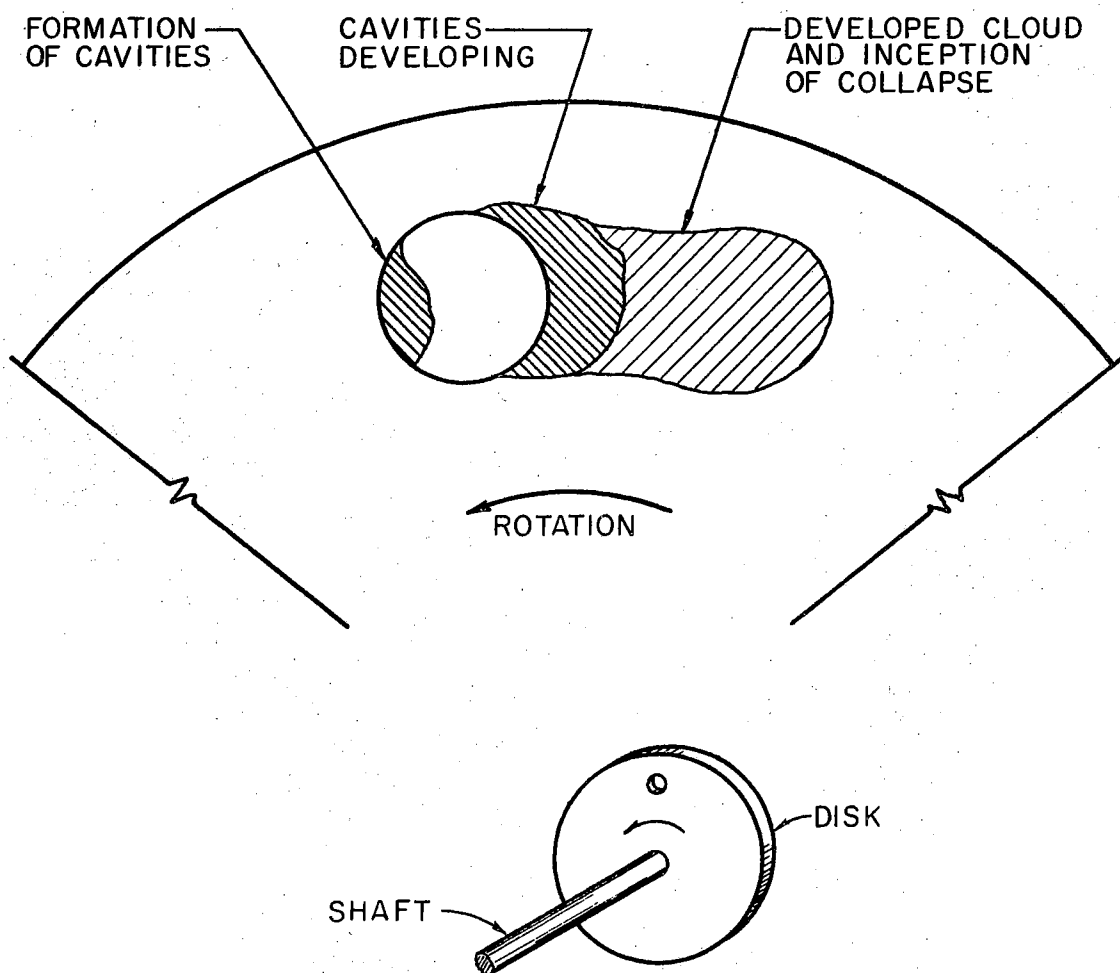


Figure 2-6. Rotating Disk Apparatus (24)

specimens which are to be classified as to their cavitation damage resistance are placed downstream from the holes where the cavities collapse. Lichtman, et al., (24) and Thiruvengadam (6) have used this type of device to classify materials in addition to the magnetostriction device and in some specific instances have shown comparable erosion ratings (volume of eroded material) between the rotating disk and magnetostriction devices (24).

Experimental Correlation of Material Properties

The difficulty experienced by the many investigators in determining correlation parameters for a material's resistance to cavitation damage can obviously be attributed to the following factors: (a) the differences in the atomic coordination of the various materials, (b) differences in fluid environmental effects, (c) differences in various testing techniques, etc. In an effort to identify the mechanical or material property which can best be used to judge a material's response to cavitation attack, materials have been chosen from a specific class (such as ductile or brittle classes of materials) since there was no apparent correlation outside of a specific class. From the data collected by the earlier investigators various correlations were attempted between the damage of the material and its material properties, a parameter of the

fluid or a parameter of the test device. However, it was only recently that a relationship was discovered between cavitation damage and a large range of material properties (25).

Rao and Thiruvengadam (25), using a two-dimensional open circuit tunnel, investigated five specimens of commercially pure aluminum (99%) with different mechanical properties. They showed that the average depth of erosion was inversely proportional to the Brinell hardness number, fatigue strength, and ultimate tensile stress which are proportional to one another. They also found that the weight loss (ounces/hour) was inversely proportional to the compressive stress for brittle materials such as concrete, brick, and stone. Thiruvengadam (26) further experimented with copper, brass, mild steel, stainless steel and aluminum and found a "good correlation" between the intensity of cavitation and the strain energy of the material. The strain energy was taken as the area under the stress-strain curve in a tensile test. Figure 2-7 gives the correlation between the strain energy and the reciprocal of the rate of volume loss for several materials (20).

Robinson (10), using a flowing system, found that either the elastic modulus or acoustic impedance correlated well with the mean depth of penetration of the specimens for a set of materials used with water as the test media. He found that when he used mercury in the flowing

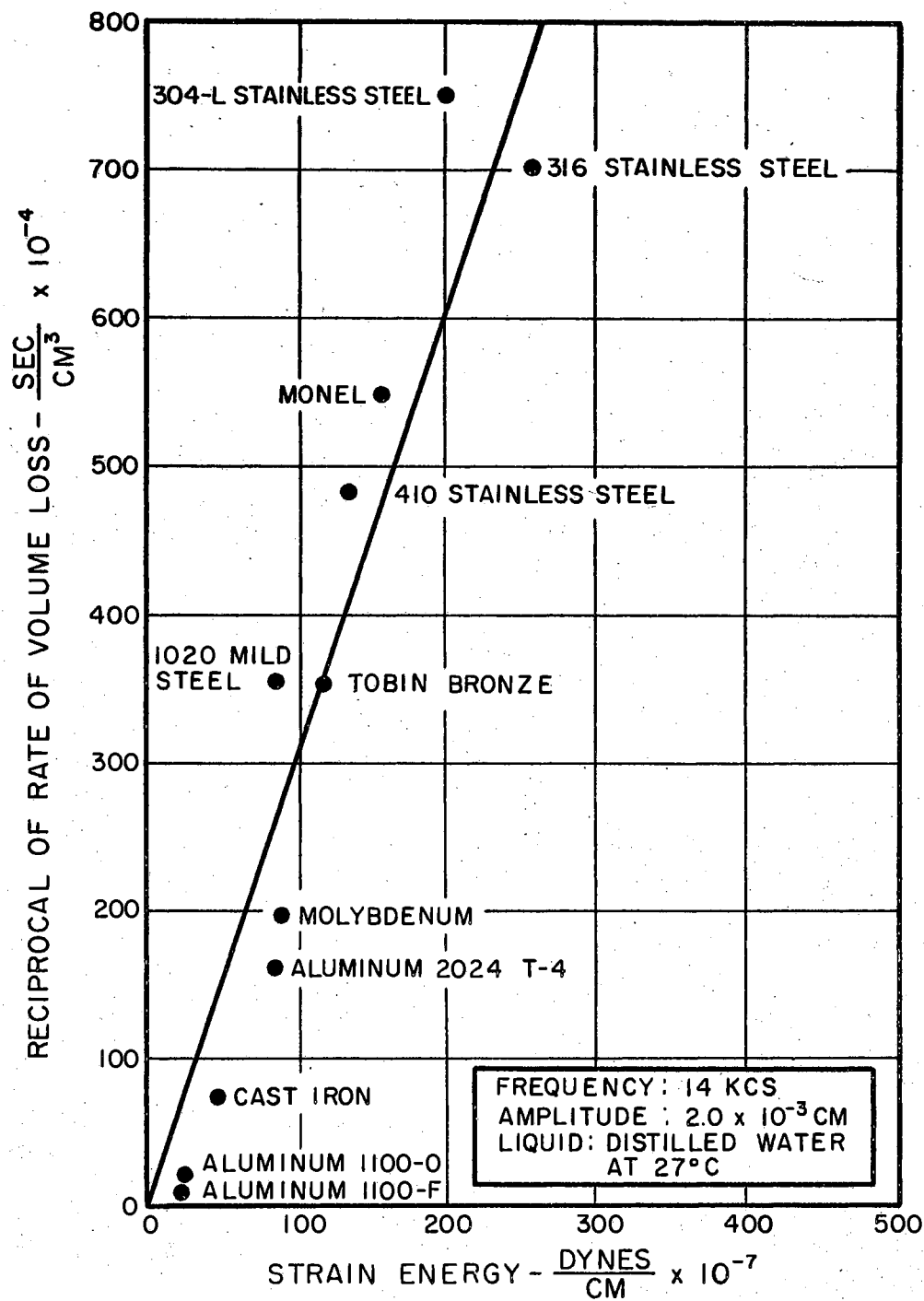


Figure 2-7. Correlation Between Strain Energy and Reciprocal of Rate of Volume Loss (20)

system "it was not possible to correlate the observed damage with any single mechanical property." However, there was a "fairly good correlation" in terms of a function of tensile strength and true breaking stress in the mercury tests. In general, data taken from several investigations show that as the hardness of a specific group of materials increases, the resistance to cavitation damage increases (indicated by a decrease of weight loss for a constant time interval) (18, 22). This relationship is not necessarily true when applied to a large group of different materials. Eisenberg (27) gives in his report a detailed section on the correlation of material properties and susceptibility to cavitation damage.

Cavitation Intensity

Many measurements have been taken from various materials such as weight loss, volume loss, rate of weight or volume loss, and the number of pits per unit area in an attempt to define a "cavitation intensity." The most common method of classifying materials as to their resistance to cavitation damage has been the amount of weight loss in a specific time interval (15, 18, 22, 24). Various devices such as the flowing system and magnetostriction apparatus have been used to classify materials, and in some specific cases the intensity (weight loss/time) of the different devices has been comparable. Knapp (28), by

determining the number of pits per second per square inch, found that the intensity (rate of pitting) increased with an increase of the flow velocity. Thiruvengadam (19) defines an "Intensity of Cavitation Damage" I as

$$I = \frac{iS_e}{t} \quad [2-1]$$

where

i = Average depth of erosion

S_e = Strain energy

t = Time

and is a measure of "the power absorbed per unit eroded area." He (29) compared the intensities of various devices and found that the most intense device was the rotating disk used by Rasmussen (30) and that the least intense was a flow device used by Hammitt (12). The ASME Standard Magnetostriction Device was found to have an intensity of one watt/meter² which is about 30,000 times as intense as Hammitt's (12) flow device and one-fourth as intense as Rasmussen's (30) rotating disk. Intensities of cavitation damage are reported as high as 3,000 watts/meter² for a stainless steel needle valve that failed in 10 minutes of operation (29).

CHAPTER III

EXPERIMENTAL APPARATUS AND TEST PROCEDURES

Introduction

Experimental apparatus used in the determination of contaminant generation mechanisms should satisfy the following general requirements:

- (a) Other mechanisms of contaminant generation such as erosion, abrasion, etc., must be minimized, and
- (b) Environmental and background contaminant should be minimized by using a small fluid testing loop in a relatively clean atmosphere.

An ASME Standard Magnetostriction Apparatus* was used in the test program and is described in detail by Robinson, Holmes, and Leith (14). The vibratory type of cavitation testing machine was chosen for the study for the following reasons:

- (a) Contaminant generation due to cavitation is

*This equipment was made available by the Allis-Chalmers Research Division, Milwaukee, Wisconsin.

- the only mechanism of particulate generation,
- (b) All contaminant generated can be collected in the sample containers (see Figure 3-1),
 - (c) The amount of fluid required for each test is small, thus enabling sub-micronic filtered fluid to be used as the test medium, and
 - (d) The machine produces an accelerated test.

The test apparatus shown in Figures 3-2 and 3-3 consists of a driving oscillator, a field coil which surrounds the driven nickel tube and a "dust free" environmental cabinet. A brass bushing silver-soldered to the nickel tube is used to fasten the individual material test specimens to the oscillating tube (see Figure 3-1). An alternating magnetic field drives the nickel tube in forced vibration at a selected frequency and amplitude. Two cooling loops were necessary, one to keep the testing fluid at 80 ± 5 degrees Fahrenheit and the other to keep the temperature-sensitive nickel tube cool. The "dust free" cabinet not only minimized the environmental contaminant, but served to reduce the noise level, which is an annoying characteristic of this type of testing machine.

Test Specimens

Materials were selected for the tests whose range of properties would include those normally used in hydraulic component design. The materials tested were ductile

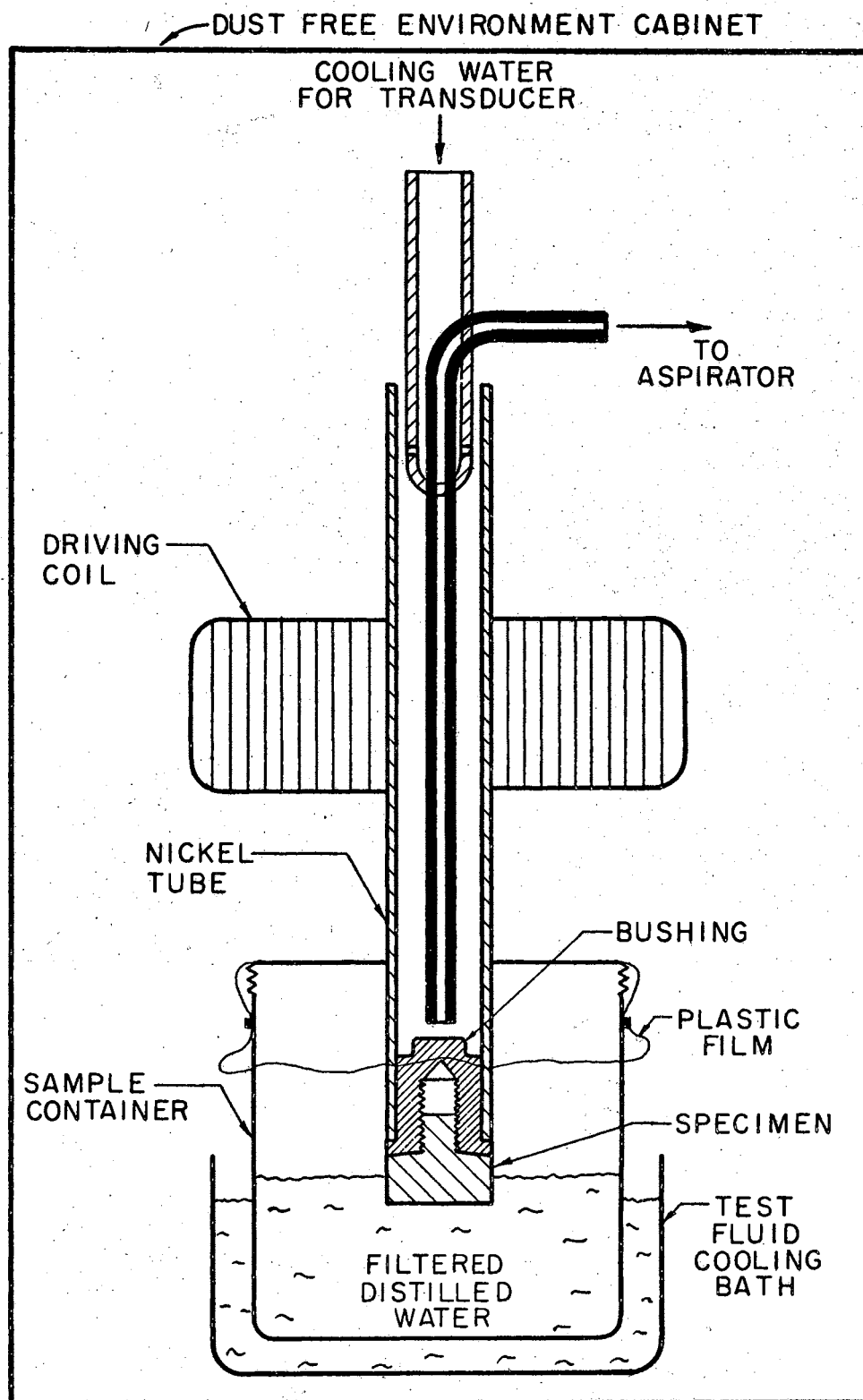


Figure 3-1. Sketch of Sampling Equipment

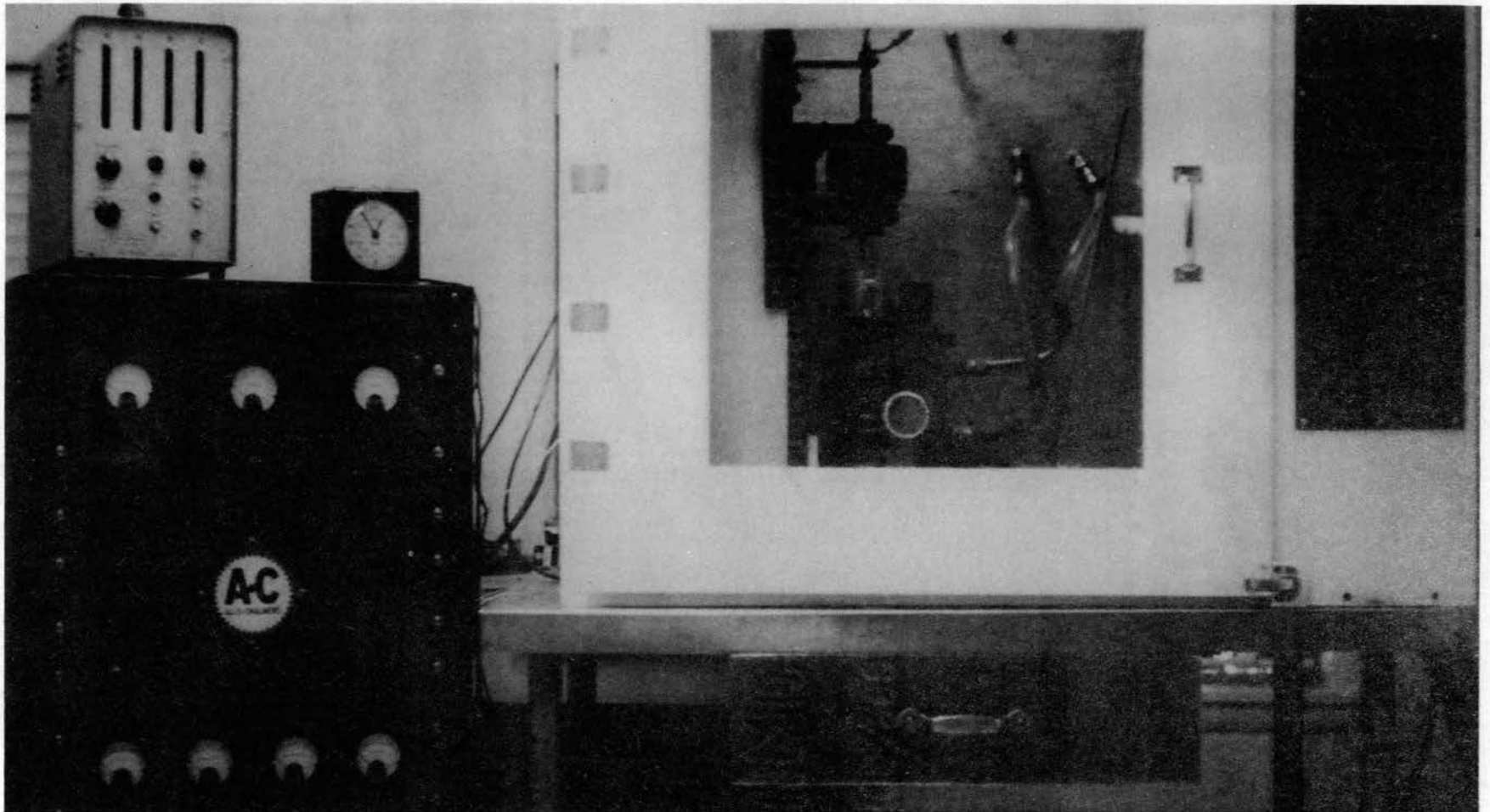


Figure 3-2. Photograph of Experimental Apparatus

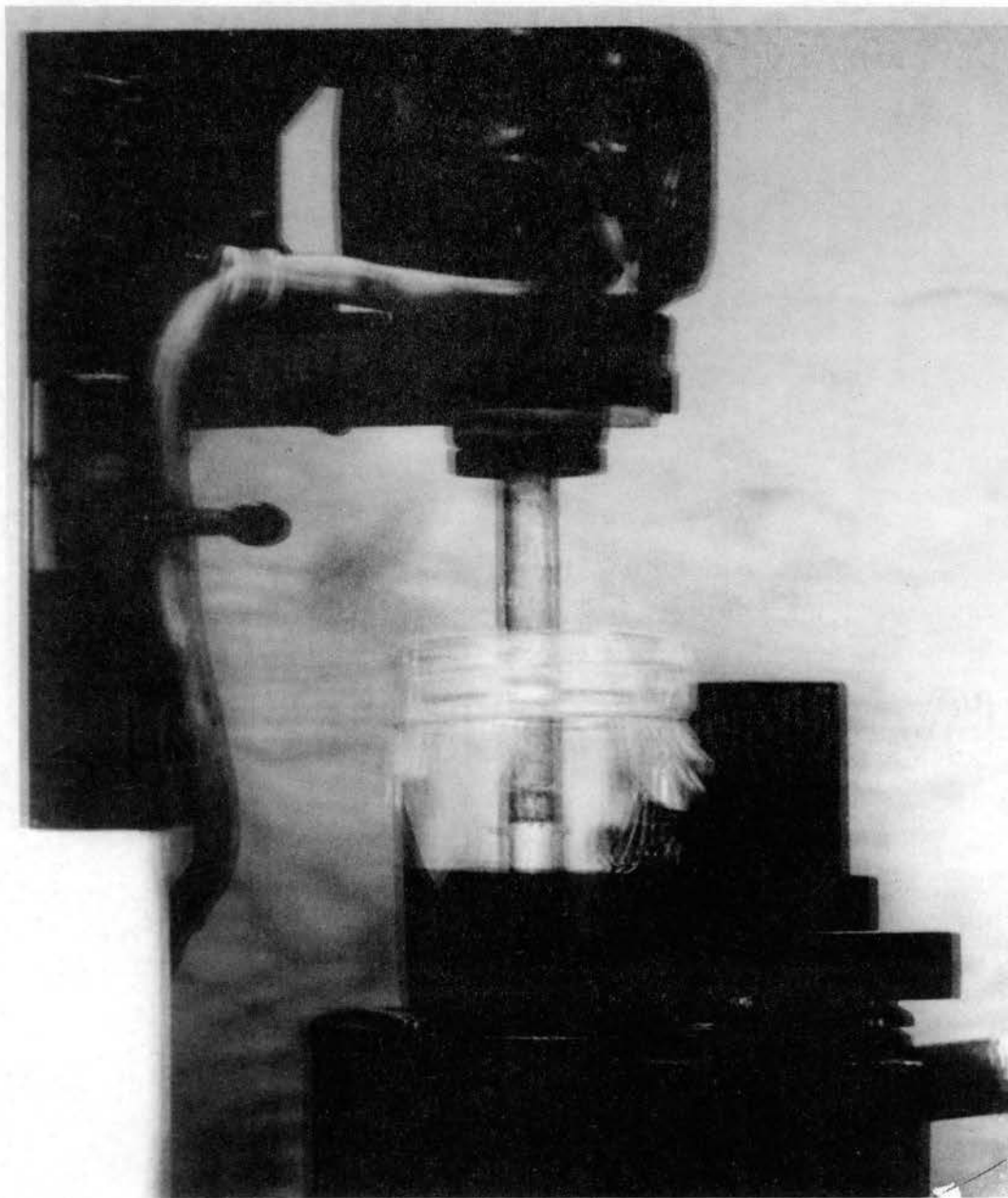


Figure 3-3. Photograph of Environmental
Cabinet and Sample
Container

rather than brittle since they are more commonly used in applications where cavitation damage may occur. The materials used were:

- (a) 1100-H18 aluminum, strain hardened commercially pure aluminum,
- (b) Free cutting Brass, 61.50% copper, 35.25% zinc and 3.25% lead,
- (c) 2024-T351 aluminum, solution heat treated and then cold worked,
- (d) Monel, 67% nickel, 30% copper plus small amounts of iron, manganese, silicon, carbon and sulphur,
- (e) 304 Stainless Steel, chromium-nickel austenitic steel, and
- (f) Electrolytic Tough Pitch Copper (99.9+% copper).

Table II is a list of the mechanical properties of these materials, which were used in correlating the various generated contaminant data with the material properties. The Brinell hardness numbers were determined using the Brinell hardness machine located in the Metals Technology Laboratory of the Technical Institute at Oklahoma State University. The values for the ultimate elongation, ultimate tensile strength and yield strength were taken from tables provided from the metal supplier. An approximate value for these properties was determined by an

TABLE II
MECHANICAL PROPERTIES OF TEST MATERIALS

Material	Approximated Strain Energy PSI	Hardness BHN	Yield Strength PSI	Ultimate Tensile Strength PSI	Ultimate Elongation %	Density gms/cm ³
1100-H18 Aluminum	3,450	44	22,000	24,000	15	2.70
Copper E.T.P.	6,375	83	40,000	45,000	15	8.90
Brass (Free Cutting)	9,000	140	42,000	58,000	18	8.41
2024-T351 Aluminum	13,250	137	56,000	70,000	21	2.70
Monel	16,850	217	98,000	112,000	16	8.84
304 Stainless Steel	32,000	212	71,000	117,000	34	7.98

interpolation based on the Brinell hardness numbers of the materials. The strain energy (area under the stress-strain curve to rupture) for the ductile materials was approximated by the following relationship (31)

$$U_d \approx (\sigma_u + \sigma_o)e_f/2 \quad [3-1]$$

where

U_d = Approximate strain energy, PSI

σ_u = Ultimate tensile strength, PSI

σ_o = Yield strength, PSI

e_f = Ultimate elongation, %.

For brittle materials ($e_f < 5\%$) the stress-strain curve can be assumed to be a parabola and the area under the curve can be approximated by

$$U_b \approx \frac{2}{3} \sigma_u e_f. \quad [3-2]$$

Test Procedure

The material specimens tested were machined from five-eighths inch diameter bar stock with the surface of the specimen polished using triple-zero emery paper. The tests were performed at a frequency of $6,500 \pm 50$ cps and a measured displacement of $0.0034 \pm .0005$ inches (peak-to-peak). The displacement was measured (see Figure 3-4) by placing a Strobotac light source behind a stud on the specimen such that the light shined across the stud of the test specimen. A filar microscope was focused on the

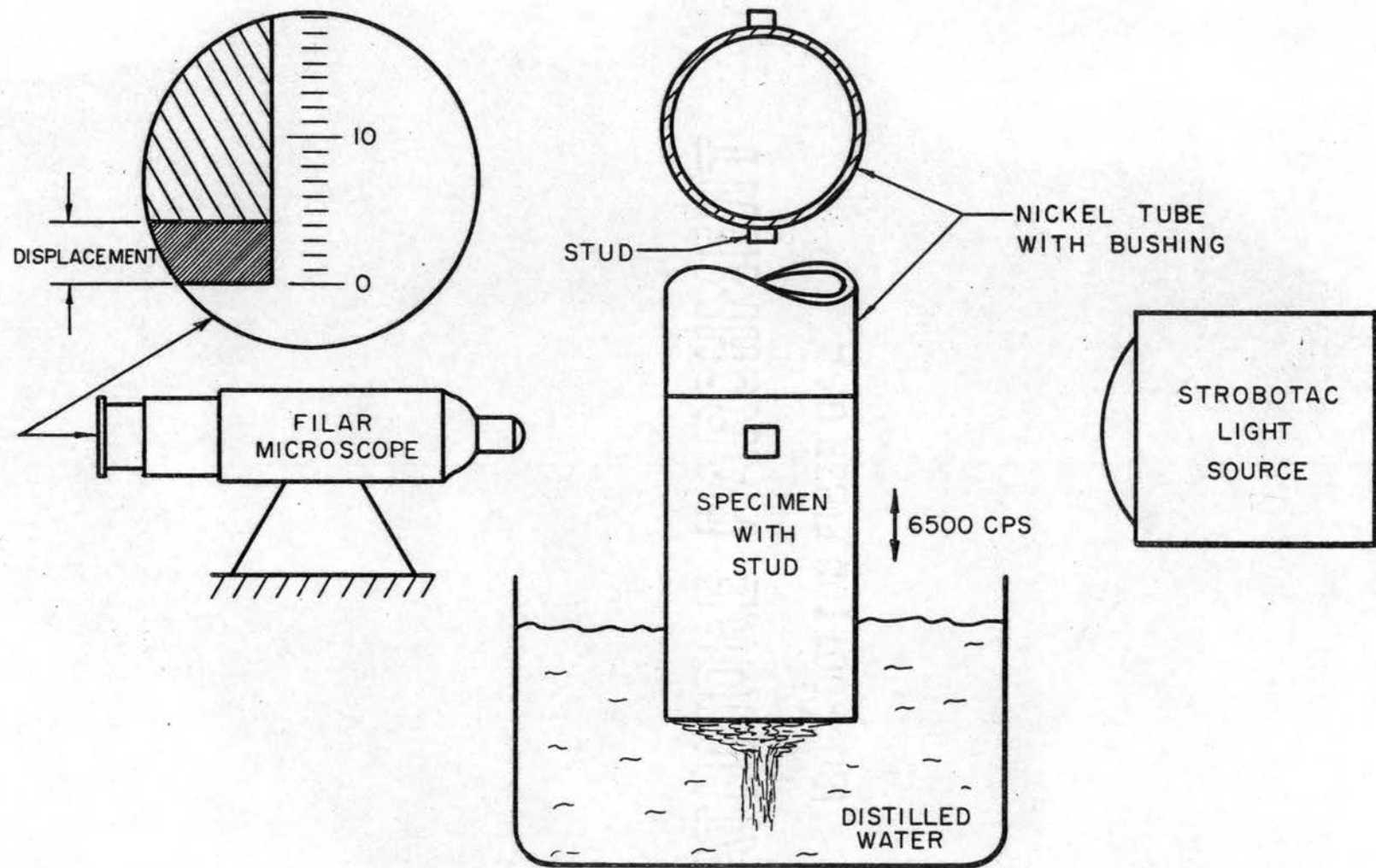


Figure 3-4. Schematic Representation of Calibration Equipment

top of the stud looking into the light source. By adjustment of the frequency of the light source near that of the frequency of the nickel tube, the distance between the extremities of the blurred area can be measured and is equal to the peak-to-peak displacement of the test specimen. It was necessary to calibrate each time a new nickel tube was used. The tests were conducted in filtered (0.45 micron millipore filter pads) distilled water using special sample containers (see Appendix A) which had been cleaned and filled in the Clean Room of the Mechanical Engineering Laboratory at Oklahoma State University. Each material was tested initially to determine the interval of time for each sample period. The amount of contaminant that could be evaluated easily and accurately was the basis upon which the time interval was specified. It was found that for 1100-H18 aluminum the sample period necessary for the determination of the particle size distribution was approximately one minute, while for 304 stainless steel the sample interval was five minutes in length. Intervals of 15 seconds duration were run in some instances to determine the incubation zone for specific materials. As can be seen, in some instances (see Figure 4-1) a weight loss was given by the gravimetric analysis of the fluid sample, while a microscopic observation of the pad revealed no material particles. This discrepancy can be attributed to the background contaminant (from the

fluid and air). Several tests were conducted to determine the accuracy of the method used to weigh the amount of material lost from the samples as a result of cavitation. The samples (which had been weighed before being cavitated) were cavitated in distilled water containers, and the weight of contaminant lost was determined by the weighing of particulate in the distilled water (see Appendix A). The samples were then removed from the machine and weighed. It was found that the weight measured by the weighing of the particulate in the distilled water was two per cent greater (maximum variation) than that of weighing the specimen before and after cavitation.

Analysis of Fluid Samples

All samples taken during the testing of each individual specimen were evaluated as to their weight loss during the test interval. This data was used to plot the cumulative weight loss versus time for each specimen. In addition, these samples were divided into one of the following groups for evaluation:

Group 1. Those samples in which the largest particle size generated was to be determined, and

Group 2. Those samples in which the particle size distribution was to be evaluated.

The samples placed in Group 2 were those taken during the

steady state region (rate of weight loss is constant) and were evaluated by the procedure given in Appendix A. The steady state region was chosen for the evaluation of the particle size distribution since this region has been found to be a point where the strain energy of materials correlates very well with rate of volume loss. The largest particle size generated during each sample period was determined by surveying a major portion of the filter pad area using a low power objective setting on the microscope. Materials such as 1100-H18 aluminum and copper generated very large particles and the larger sizes could be identified visually and then measured with the aid of a split-image eyepiece on the microscope for the determination of the largest particle size generated.

CHAPTER IV

EXPERIMENTAL RESULTS AND CONTAMINATION DATA CORRELATIONS

Introduction

The analysis of hydraulic systems during the last five to ten years with respect to contamination has been primarily concentrated on the cause and effect of the particulate distribution which is present or characteristic of the fluid system. Current test programs are being conducted to determine the existing distribution in a typical system and what distribution is harmful to this system. The analysis of a system's fluid is necessary for several reasons:

- (a) To determine if the system is operating in a contaminant distribution that is tolerable to all components,
- (b) To determine if the present filtration equipment will adequately handle the volume of generated contaminant, and
- (c) To determine, upon location of a contaminant generator, what type and size of filter is needed to protect those components

downstream which are not shielded by the system filters.

The determination of the largest particle size generated by some mechanism normally is of no significance to filter designers since the large sizes will be eliminated if a majority of the smaller particles are removed. However, the largest size generated is important when it comes to the placement of the filter in the system since the generating mechanism may produce particle sizes large enough to cause a decrease in performance or subsequent failure. For example, if there is a valve upstream of a cylinder which generates particles large enough to score the cylinder walls causing leakage, the filter will not solve the problem unless it is placed correctly even though the contaminant level is below that of its tolerable value.

Knowledge of the distribution $N(\mu)$ of the particles produced by the various mechanisms of contaminant generation assists the filtration designer to determine the filter characteristics (mesh area, pore size, number of layers, etc.) necessary to produce a specified distribution output (contaminant tolerance level).

Largest Particle Size Generated

The largest particle size generated for the various materials tested exhibited the same general characteristics

as the rate of weight loss curve of the specific materials (see Figures 4-1 through 4-6). In the incubation zone, the material surfaces for the softer specimens, such as 1100-H18 aluminum and copper, were deeply dented. However, the filtrate pads did not show any generated particles although the gravimetric weight indicated a slight weight loss. This weight can be attributed to the background contaminant present in the fluid which cannot be removed easily even by stringent clean room techniques. The length of the incubation periods for some materials was not determined since the initial sampling period extended into the second zone of cavitation damage rate (accumulation zone). However, as can be seen from Figures 4-1, 4-3, and 4-6, incubation periods of 0.5 to 15 minutes were determined during which particle generation was non-existent. During the second zone of cavitation, damage rate (the accumulation zone, which is characterized by an increase in the rate of weight loss), the largest particle size generated increased to a maximum value. The time necessary to reach this maximum particle size value is equivalent to the time the rate of weight loss curve approaches its maximum value. For all materials tested except 1100-H18 aluminum, the largest particle size generated remained constant (at the maximum value reached during the second zone of cavitation damage rate) during the remainder of the testing period. However, commercially

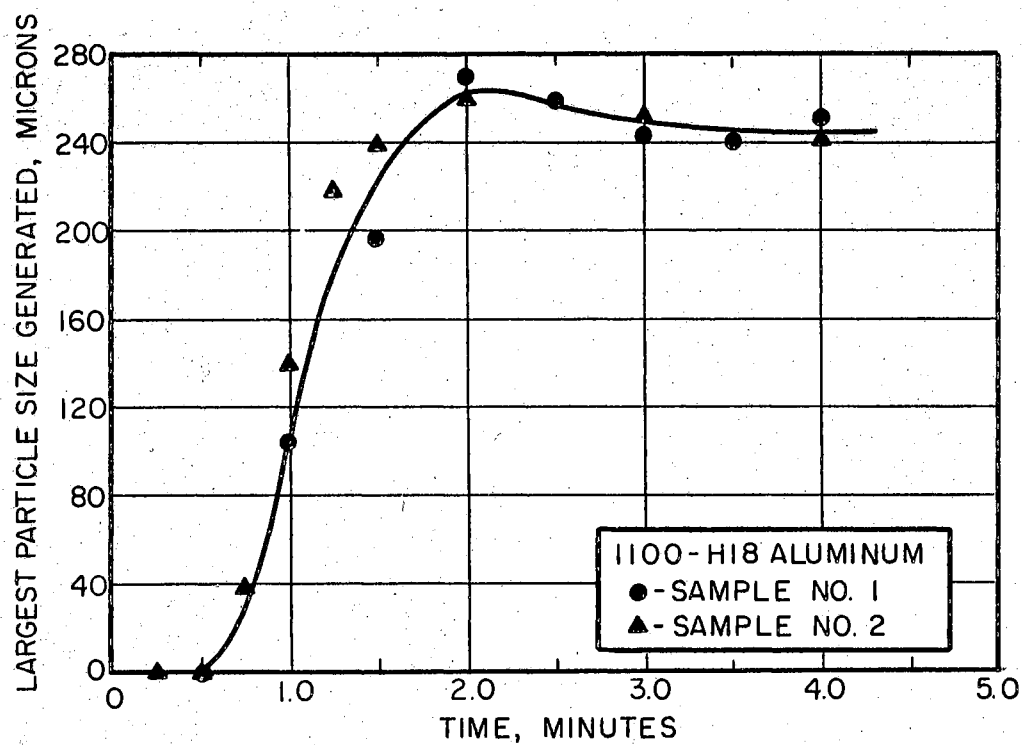
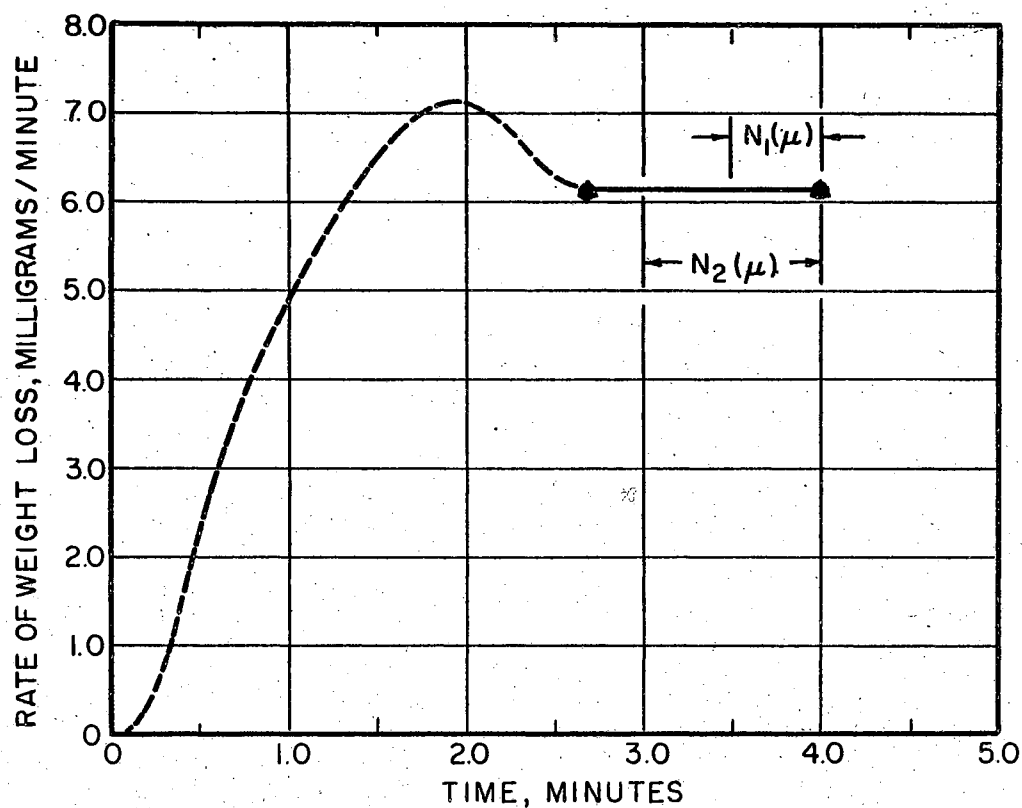


Figure 4-1. Rate of Weight Loss and Largest Particle Size Generated for 1100-H18 Aluminum

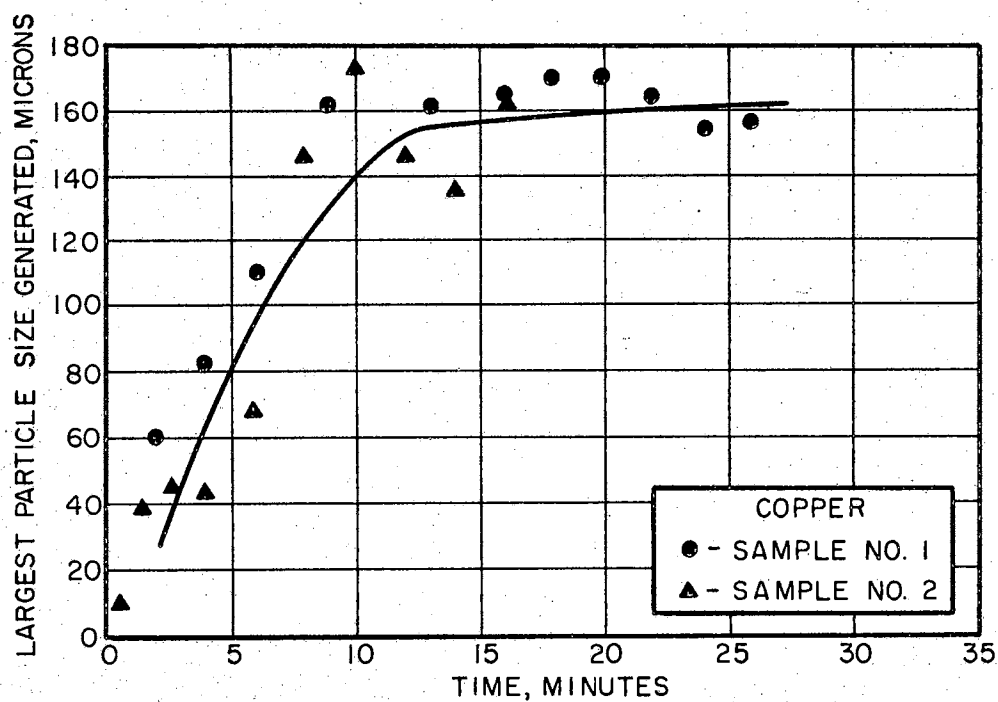
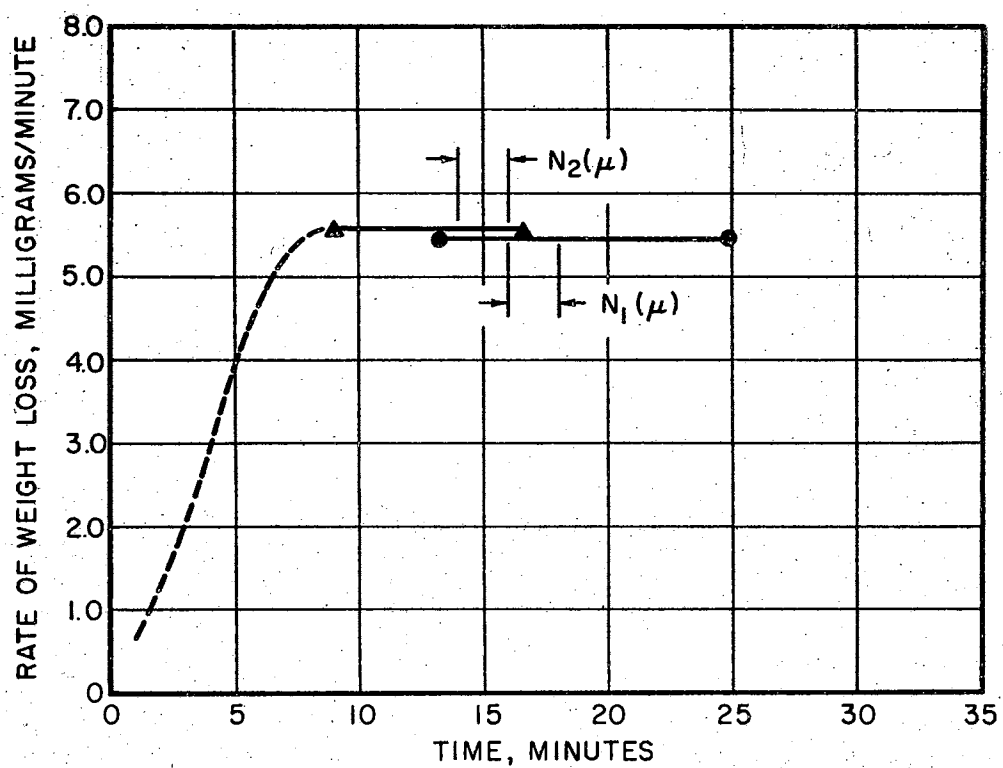


Figure 4-2. Rate of Weight Loss and Largest Particle Size Generated for Copper

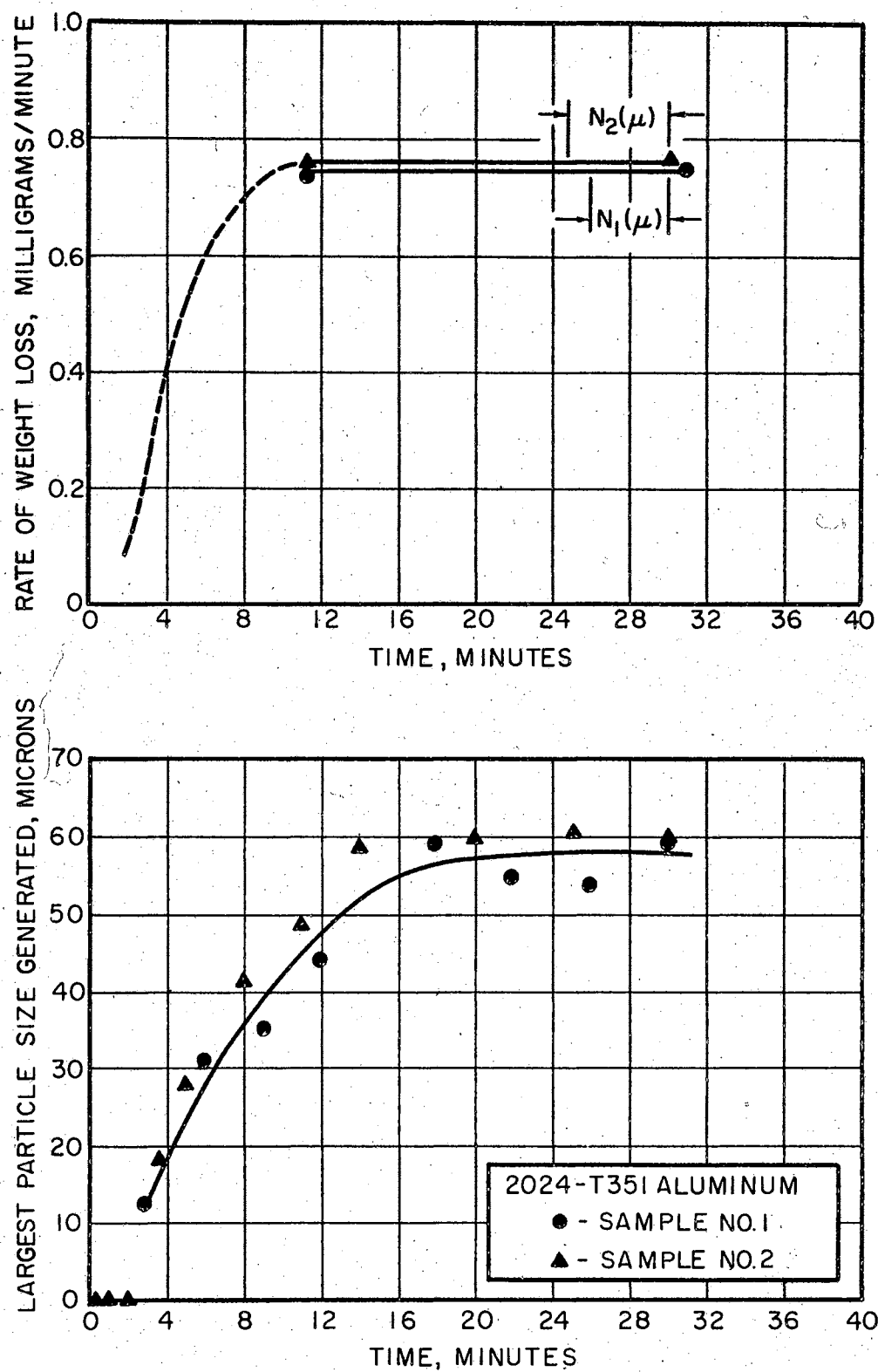


Figure 4-3. Rate of Weight Loss and Largest Particle Size Generated for 2024-T351 Aluminum

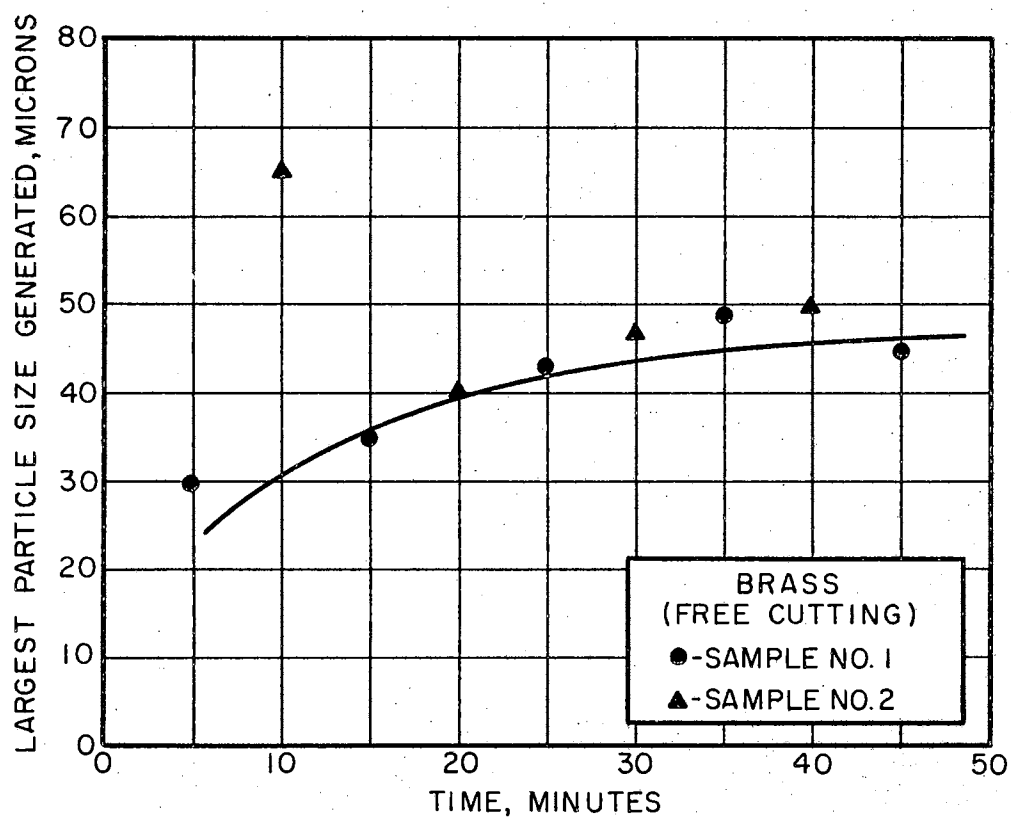
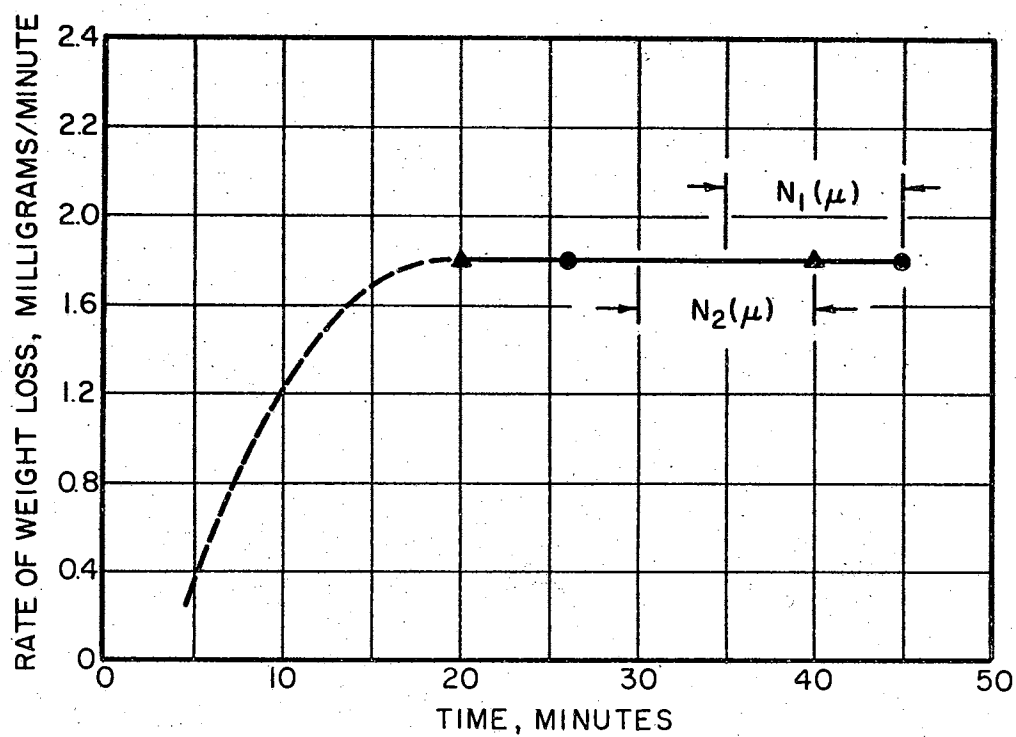


Figure 4-4. Rate of Weight Loss and Largest Particle Size Generated for Brass (Free Cutting)

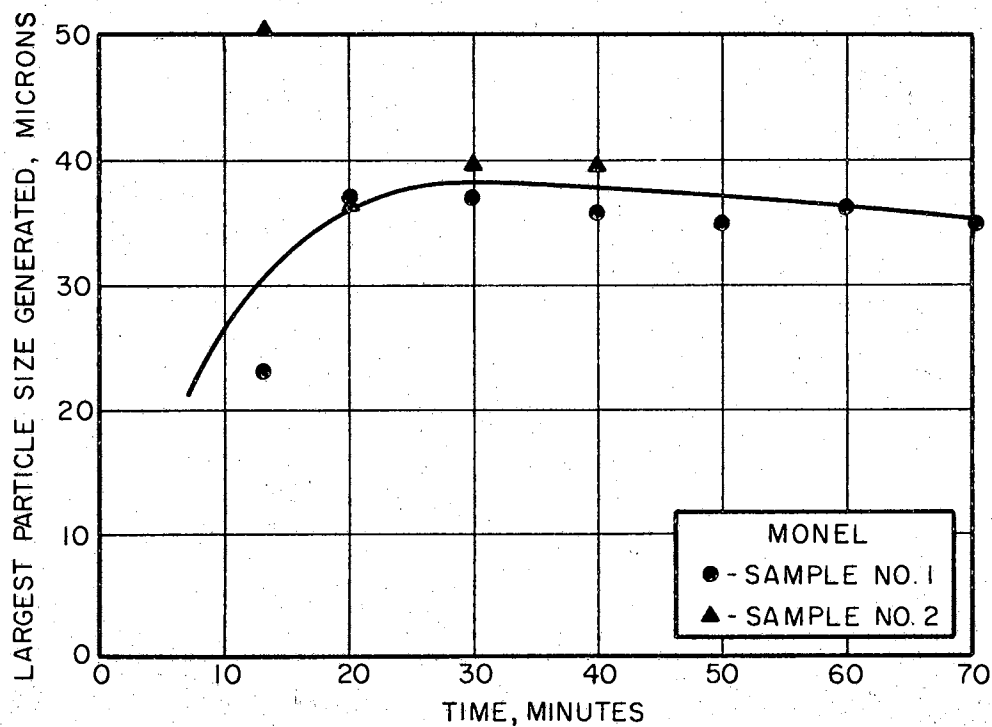
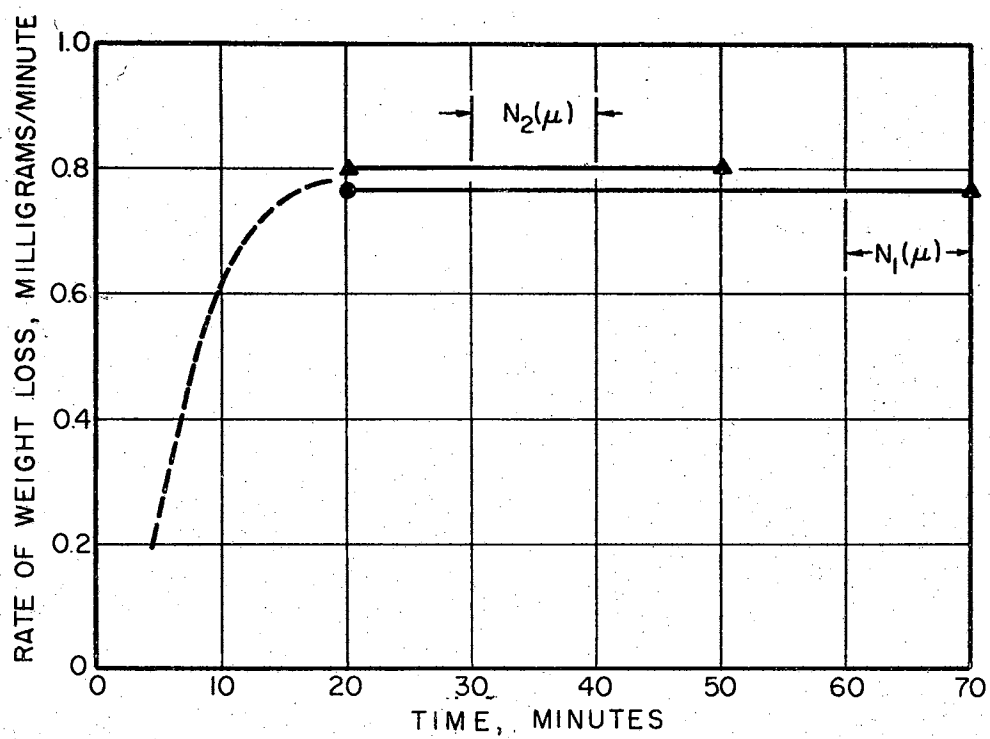


Figure 4-5. Rate of Weight Loss and Largest Particle Size Generated for Monel

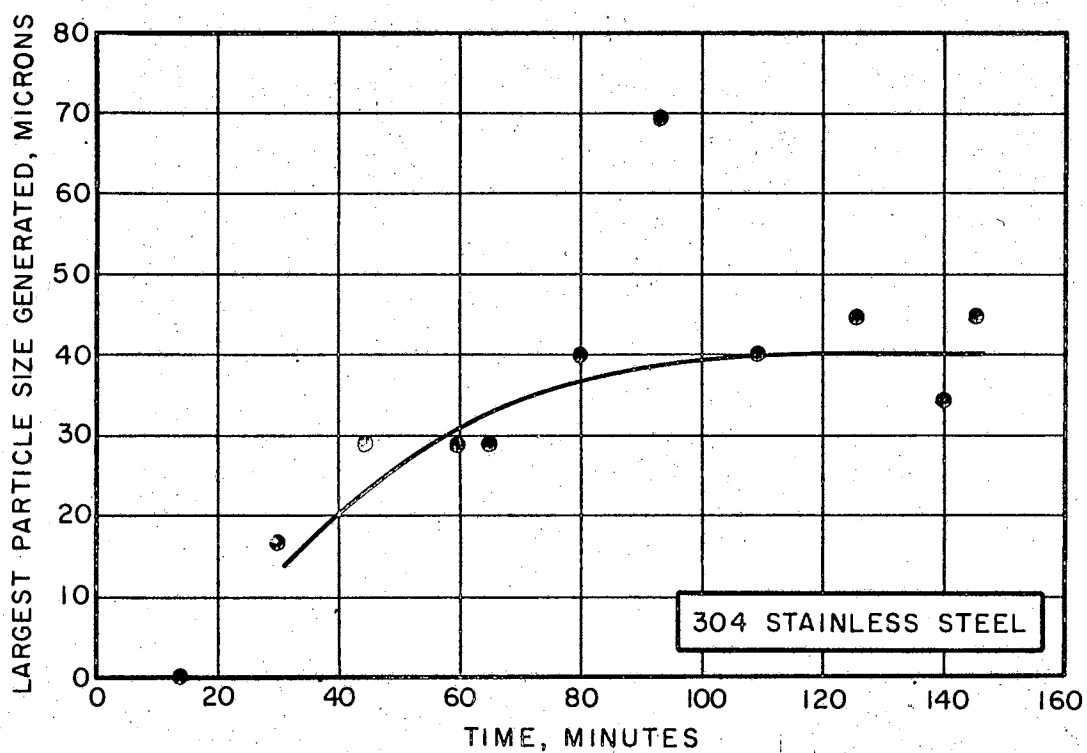
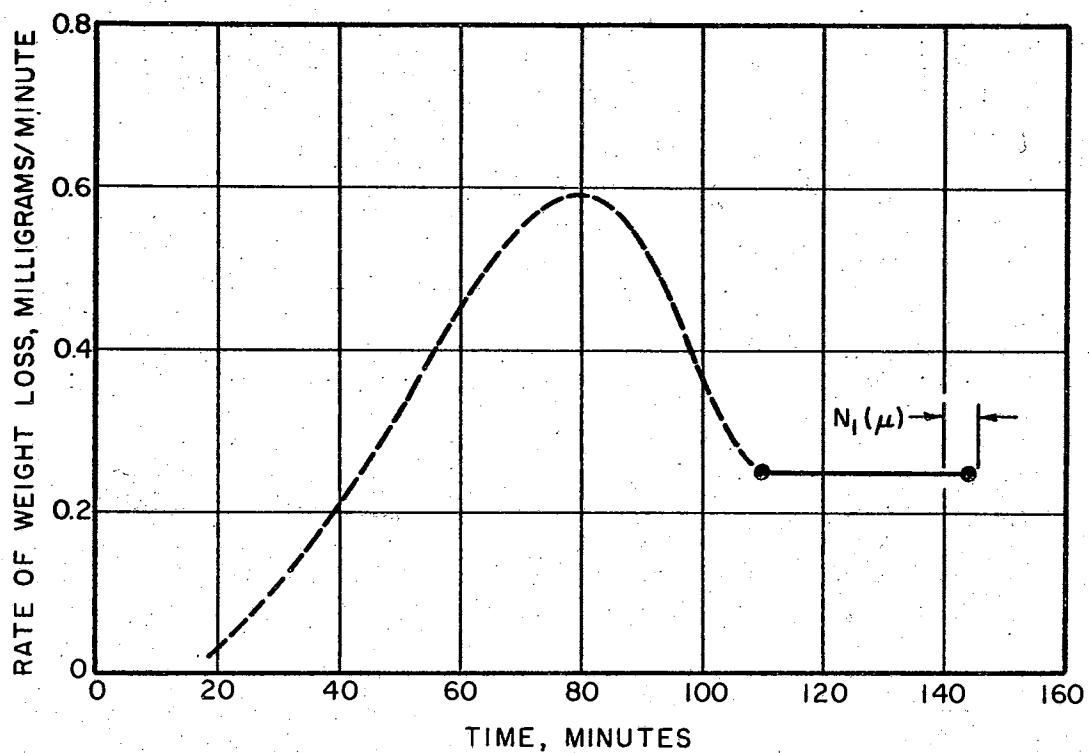


Figure 4-6. Rate of Weight Loss and Largest Particle Size Generated for 304 Stainless Steel

pure aluminum, 1100-H18, gave a slight reduction in the largest size generated during the third zone of cavitation damage rate. A particle size attenuation zone was not detected for the group of materials investigated in this study.

Figure 4-7 gives a plot of the largest particle size generated at steady state conditions versus the strain energy of the material. As can be seen from Figure 4-7, stainless steel with a strain energy of nearly twice that of monel generates particles of approximately equal magnitude as that of monel. From Figures B-5 and B-6 in Appendix B, it can be seen that the stainless steel sample loses only one-half the weight that the monel sample loses in equal 80 minute tests. Therefore, the strain energy of the material can be used to measure the volume of material lost but does not give a satisfactory measure of the magnitude of particle sizes generated for the group of materials tested. The concept of using strain energy as a measure of volume loss was conceived by Thiruvengadam (6).

A plot of the largest particle size generated at steady state conditions versus the Brinell hardness of the material is shown in Figure 4-8. This investigator determined from this plot that the diameter of the largest particle generated for ductile materials with Brinell hardness numbers between 30 and 250 can be estimated by the following empirical relationship:

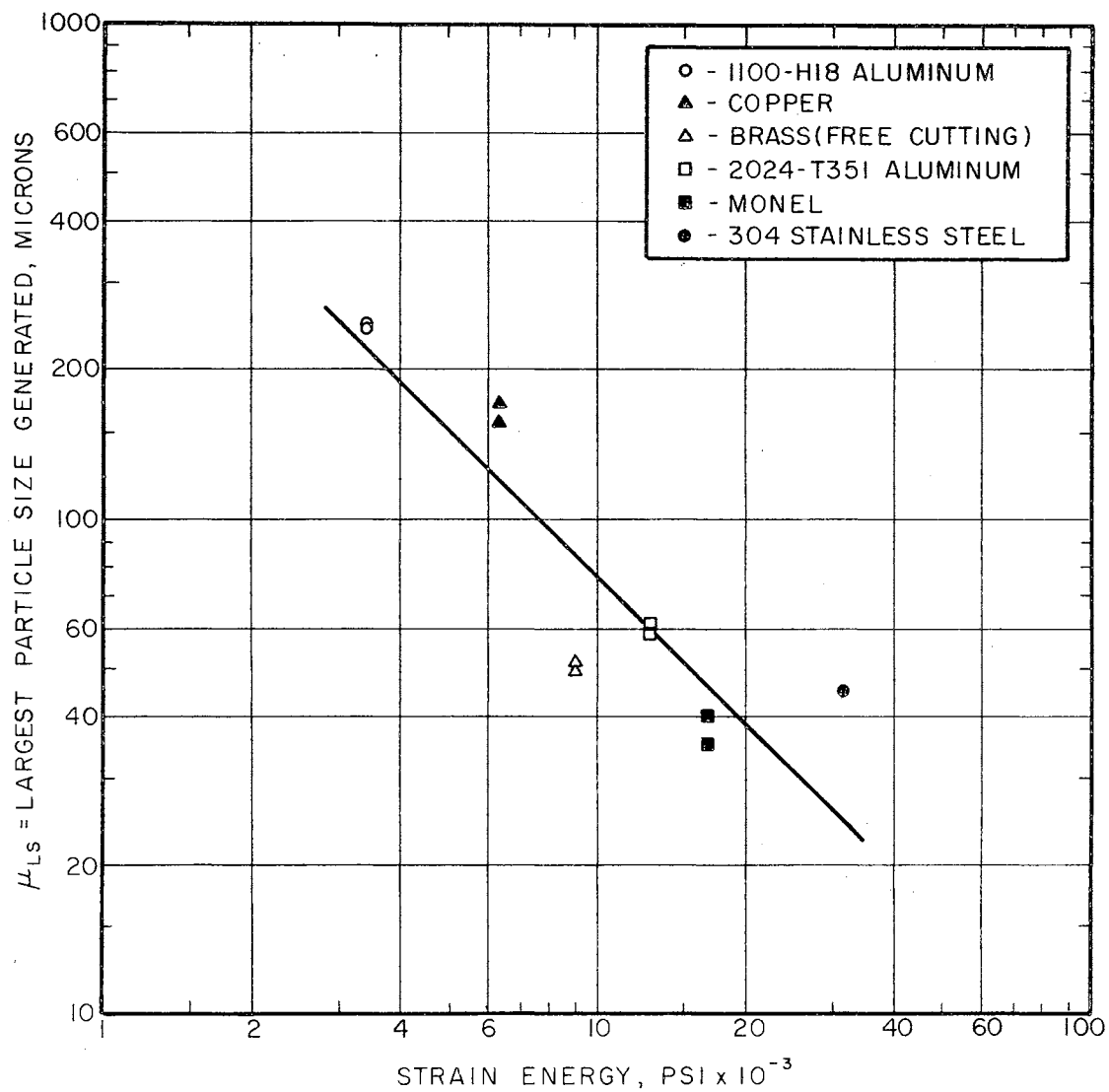


Figure 4-7. Correlation Between Largest Particle Size Generated and Strain Energy at Steady State Conditions

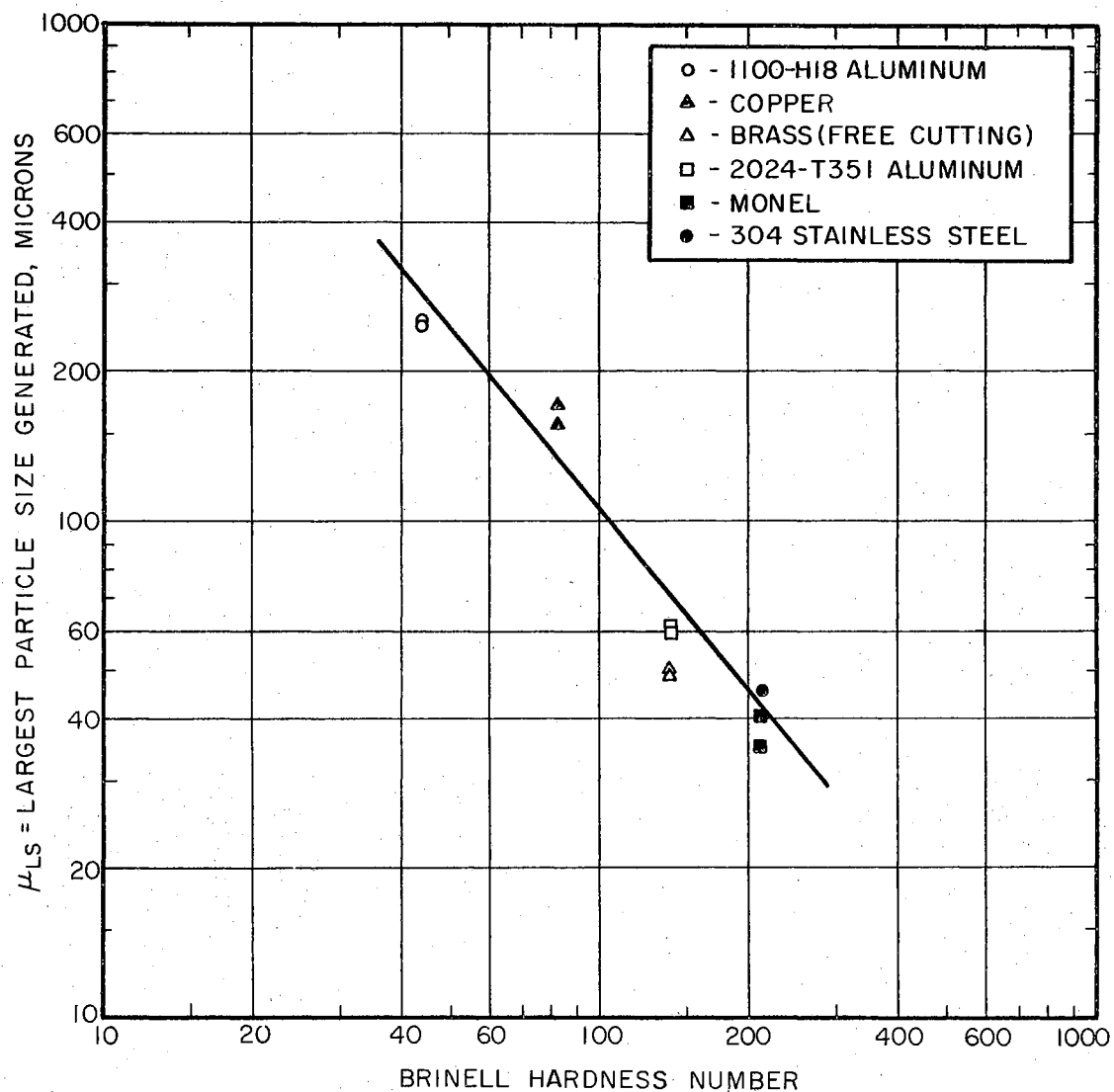


Figure 4-8. Correlation Between Largest Particle Size Generated and Brinell Hardness Number at Steady State Conditions

$$\mu_{LS} = 26,400/\text{BHN}^{1.195} \quad [4-1]$$

where

μ_{LS} = Diameter of the largest particle size
generated, microns

BHN = Brinell hardness number.

The hardness of a metal implies a resistance to permanent or plastic deformation (31) and is equal to the applied load divided by the surface area of the indentation or

$$\text{BHN} = \frac{P}{\left(\frac{\pi D}{2}\right) \left(D - \sqrt{D^2 - d^2}\right)} \quad [4-2]$$

where

P = Applied load, kg

D = Diameter of ball, MM

d = Diameter of impression, MM.

As the BHN increases, the area of indentation decreases, thereby decreasing the volume of plastic deformed material. From the collapse of bubbles near the material surface, a layer of plastic deformed material is produced due to the indentations. Subsequent blows chip off this extruded plastic deformed material in various irregular sizes and shapes. Plesset and Ellis (7) and Plesset and Devine (8) have shown by the use of X-ray and electrolytic polishing techniques the depth of plastic deformation ranging from 21 to 69 microns for a Brinell hardness range of approximately 60 to 175 for various materials. There

was no correlation between the depth of plastic deformation and BHN in the data reported by them (7, 8). The depth of plastic deformation was smaller than or equal to the largest size particle generated as given in Figure 4-7 for the corresponding BHN. From a microscopic examination shown in Figures C-1 through C-5 in Appendix C, it can be seen that the particles in general have a flat appearance or a measured diameter to an observed depth ratio greater than unity. This indicates that the particles are flat with the depth being equal to or less than the depth of plastic deformation and the diameter a function of the Brinell hardness. Figure 4-9 gives a plot of the rate of volume loss versus the strain energy of the materials tested and is equal to the ratio of the rate of weight loss at steady state conditions to the density of the material.

Particle Size Distributions

The steady state region of the rate of weight loss curve was chosen as the point where the particle size distribution $[N(\mu)]$ was determined for contaminant generated by cavitation. As was shown in Figures 4-1 through 4-6, this is the point at which the largest particle size generated remains at a constant maximum value. From a periodic examination of the test specimens, it was observed that the initiation of the steady state region was the

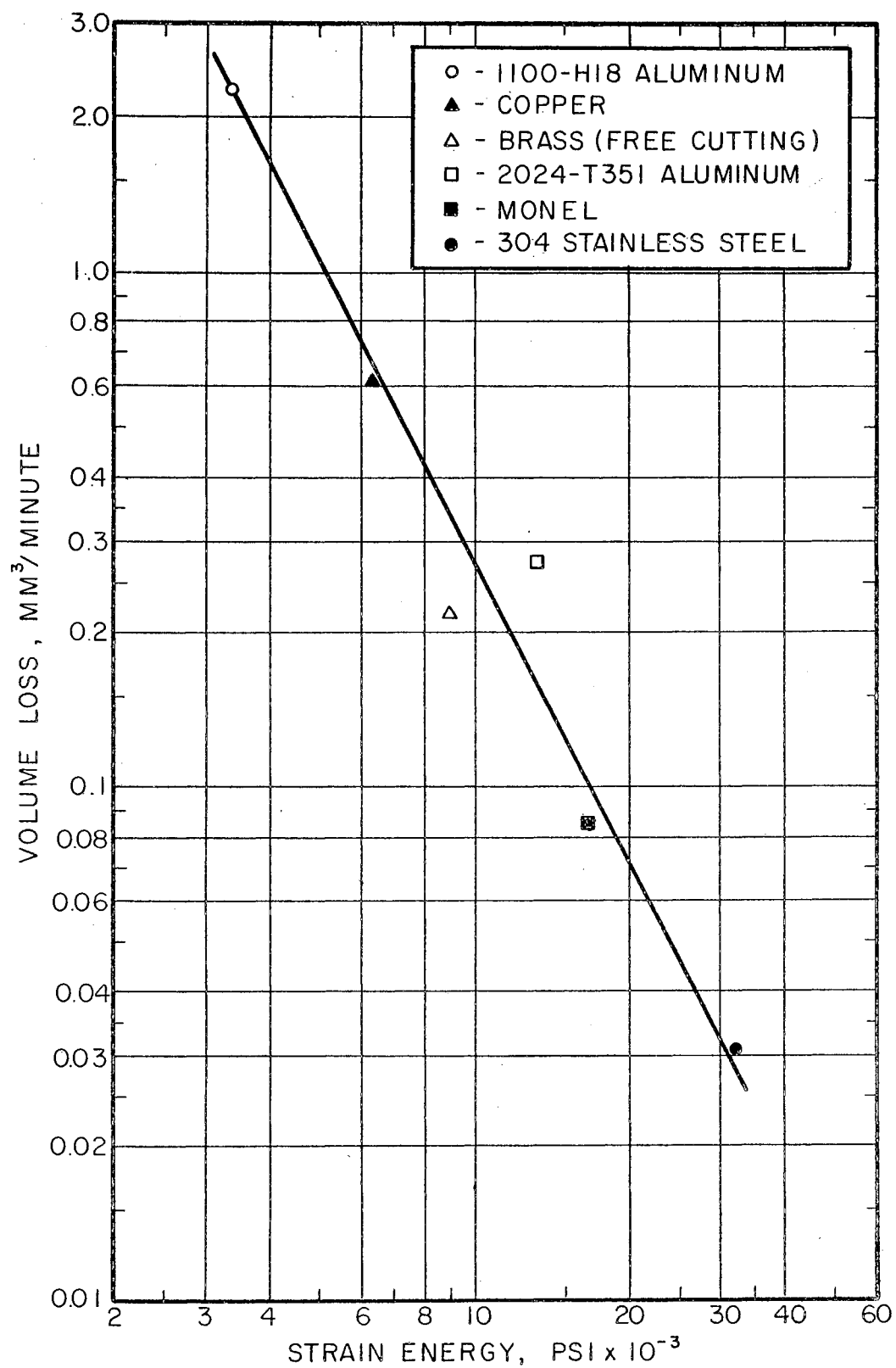


Figure 4-9. Correlation Between Volume Loss and Strain Energy at Steady State Conditions

point at which the damaged specimen surface changes from a uniformly damaged appearance to a surface exhibiting individual deep pits.

The particle size distribution curves shown in Figures 4-10 through 4-15 represent the number of particles generated per one-fifth square inch of exposure area of the material tested. These generation curves have the same form of empirical relationship as the generation characteristics of piston pumps that have been tested by the Fluid Power and Controls Laboratory at Oklahoma State University. Figure 4-16 represents the contaminant distribution generated by a piston pump and was obtained by taking the difference between the number of particles appearing at the case drain (generated distribution output) and the suction (distribution input).

The particle size distribution curves for contamination due to cavitation plot as straight lines on semi-log coordinates except for a small interval at the end of the distribution curve which represents the decay in the number of larger sized particles generated. This point of deviation of the distribution from a straight line will be defined as the particle cutoff size. The particle cutoff size versus the Brinell hardness number is given in Figure 4-17 and has a greater slope than the curve (given in Figure 4-8) of the largest particle size generated. The diameter of the particle cutoff size generated for ductile

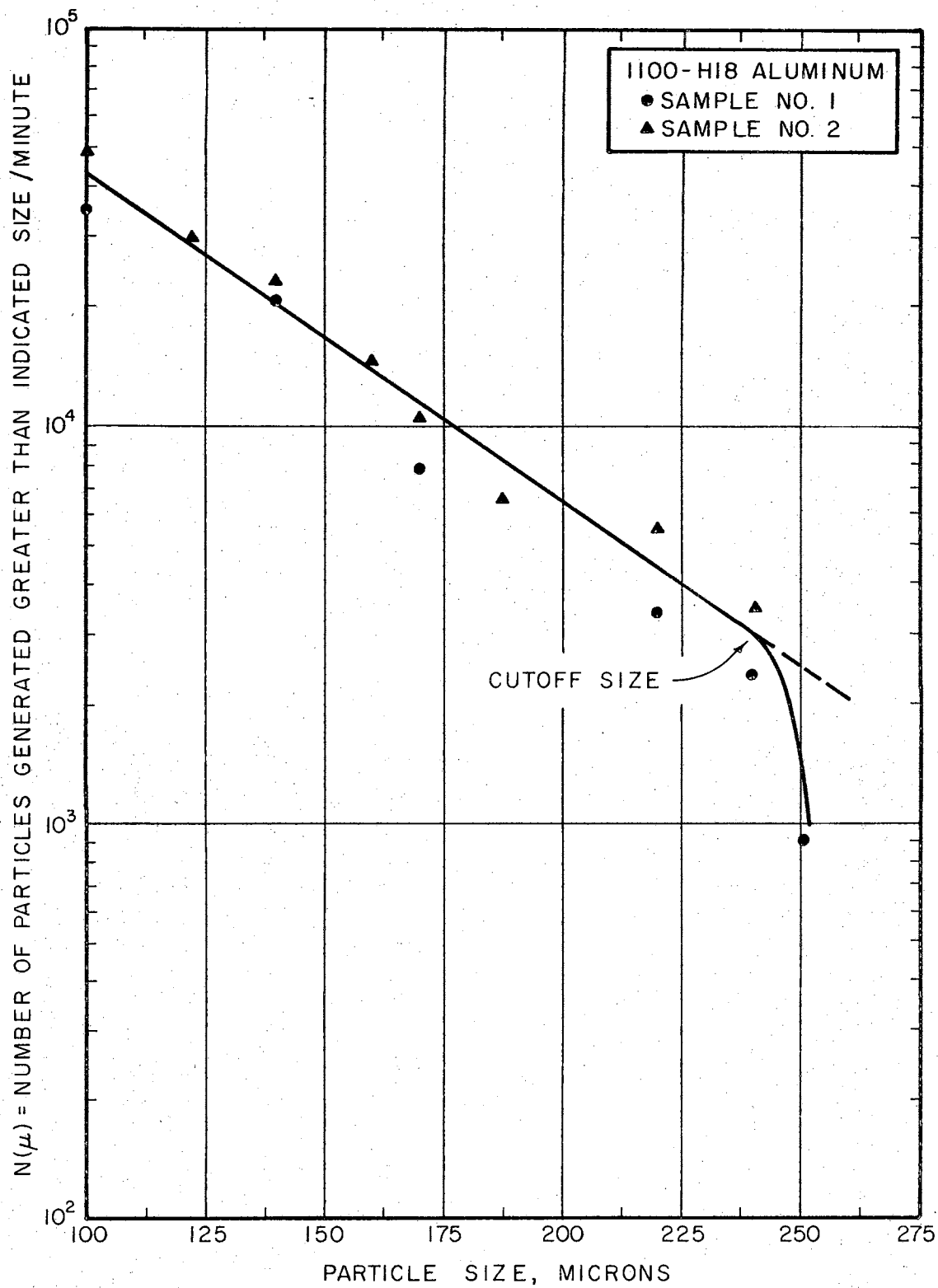


Figure 4-10. Cumulative Particle Size Distribution Curve for 1100-H18 Aluminum

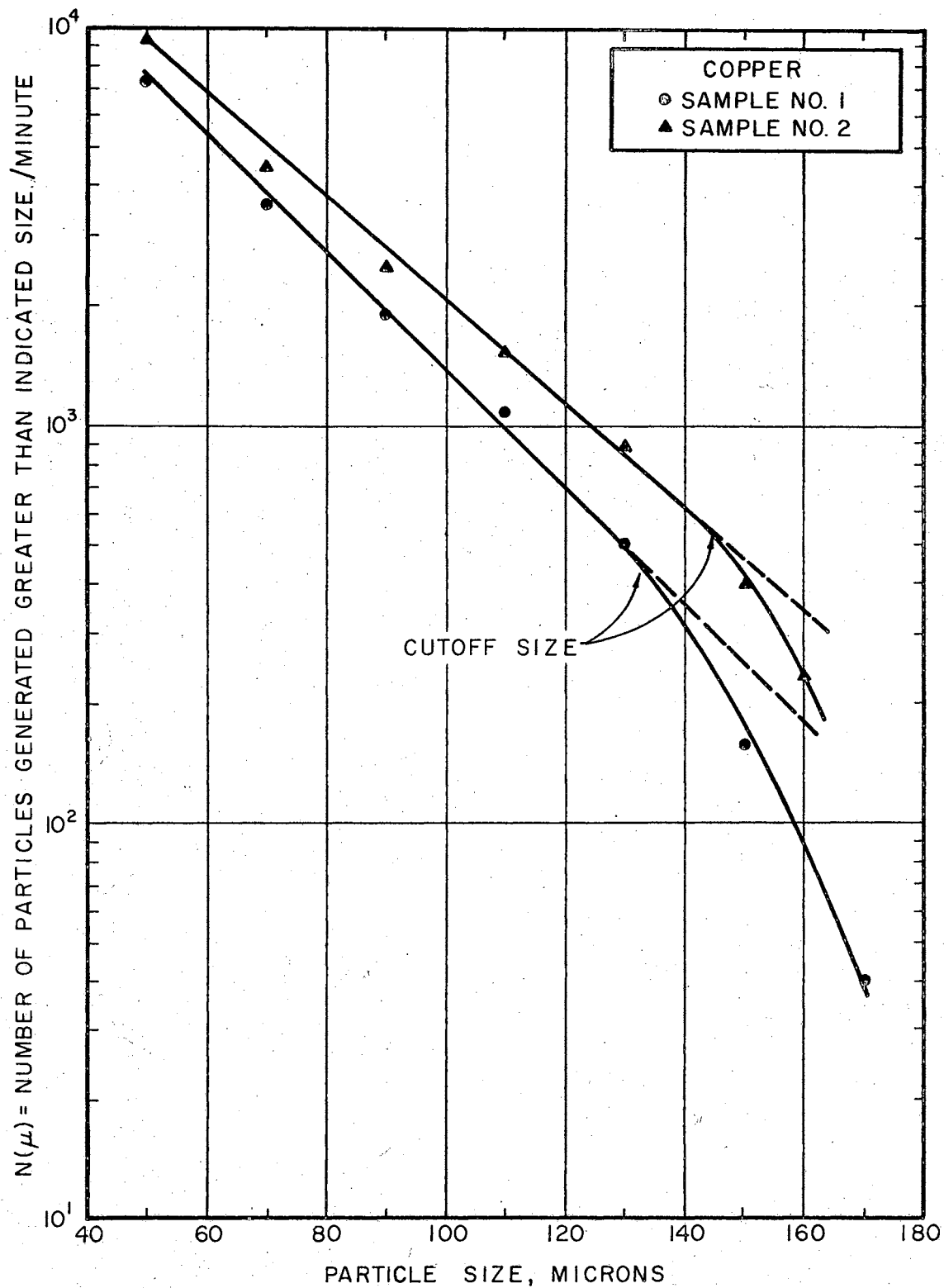


Figure 4-11. Cumulative Particle Size Distribution Curve for Copper

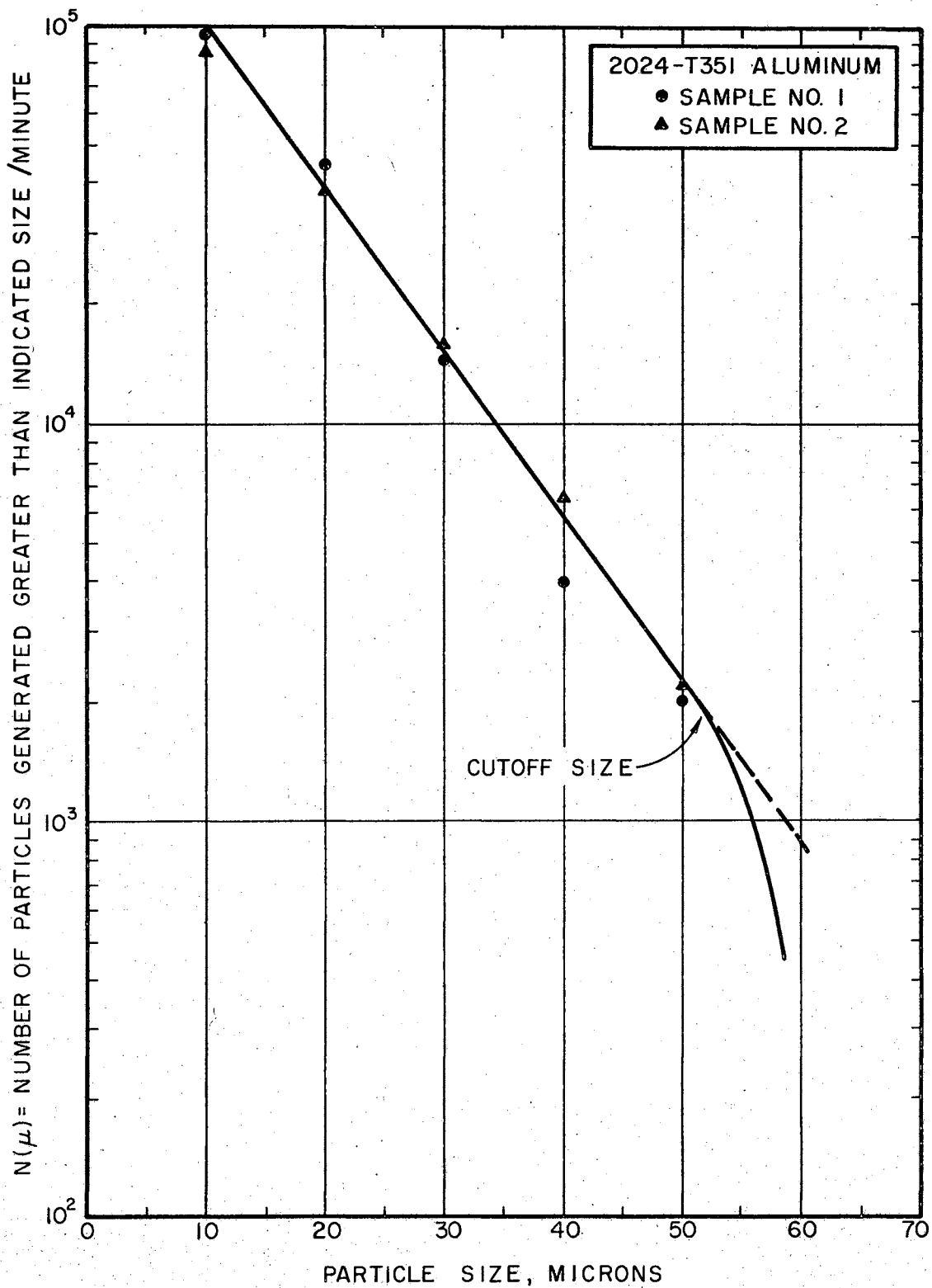


Figure 4-12. Cumulative Particle Size Distribution Curve for 2024-T351 Aluminum

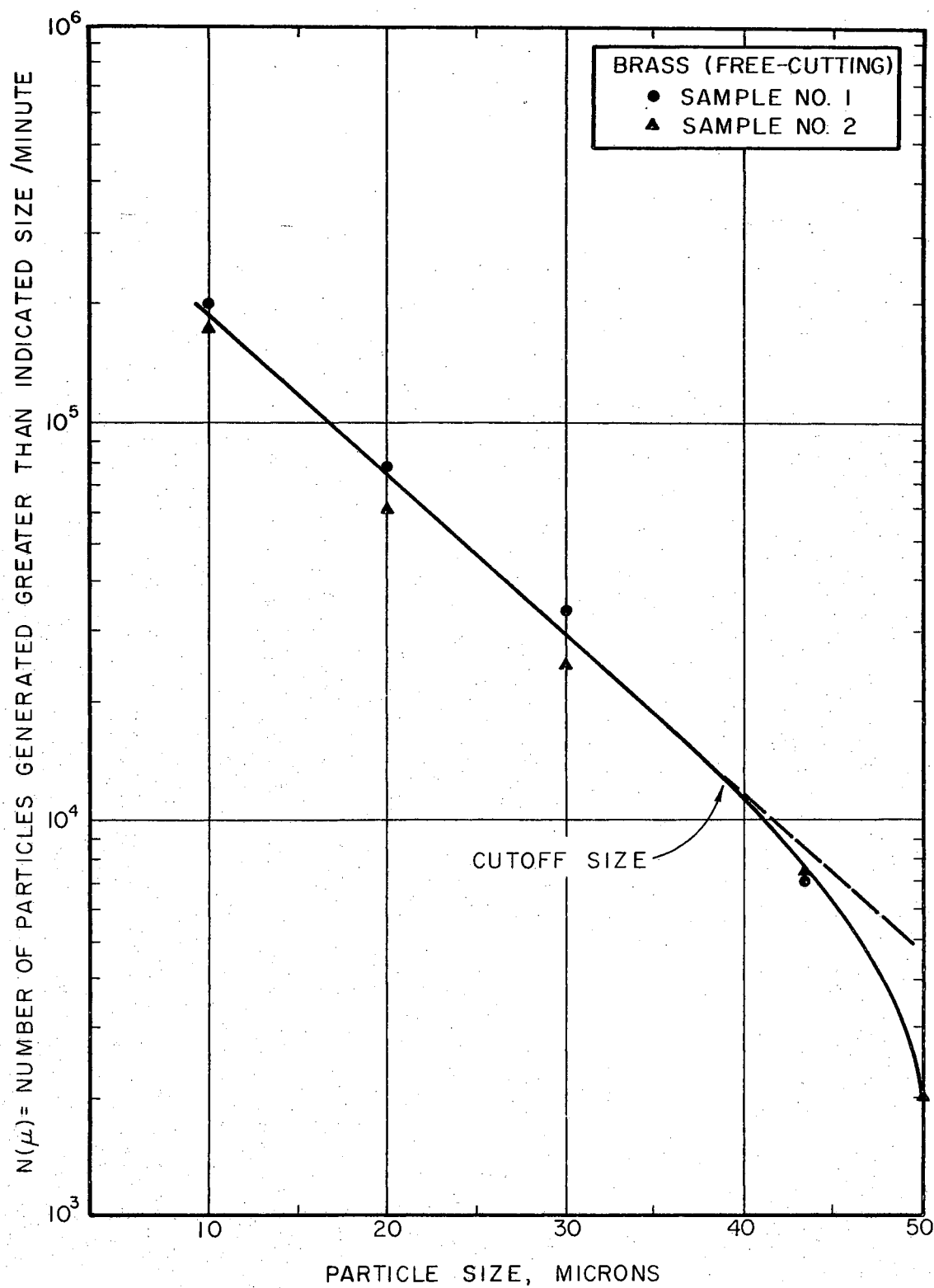


Figure 4-13. Cumulative Particle Size Distribution Curve for Brass (Free Cutting)

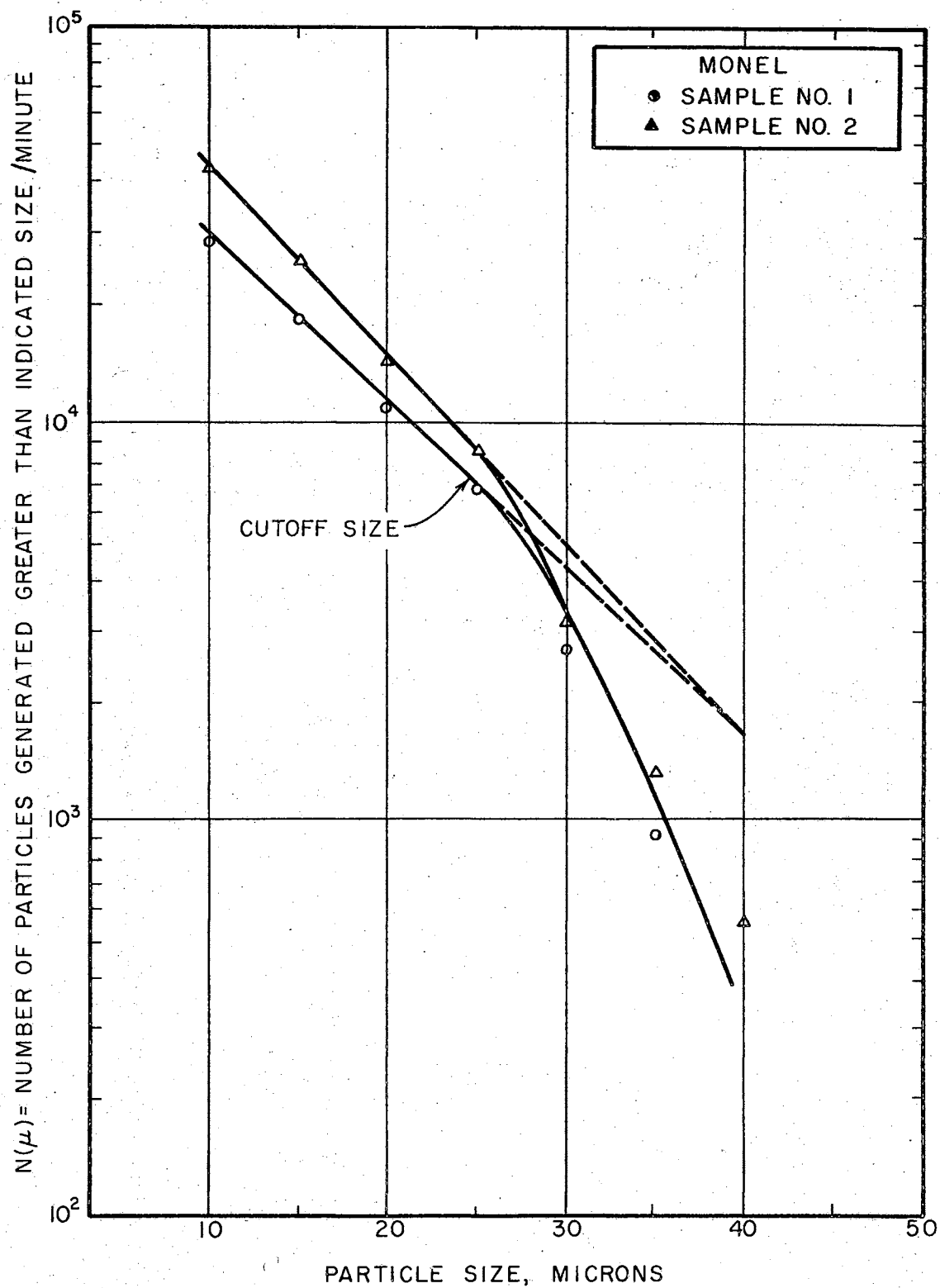


Figure 4-14. Cumulative Particle Size Distribution Curve for Monel

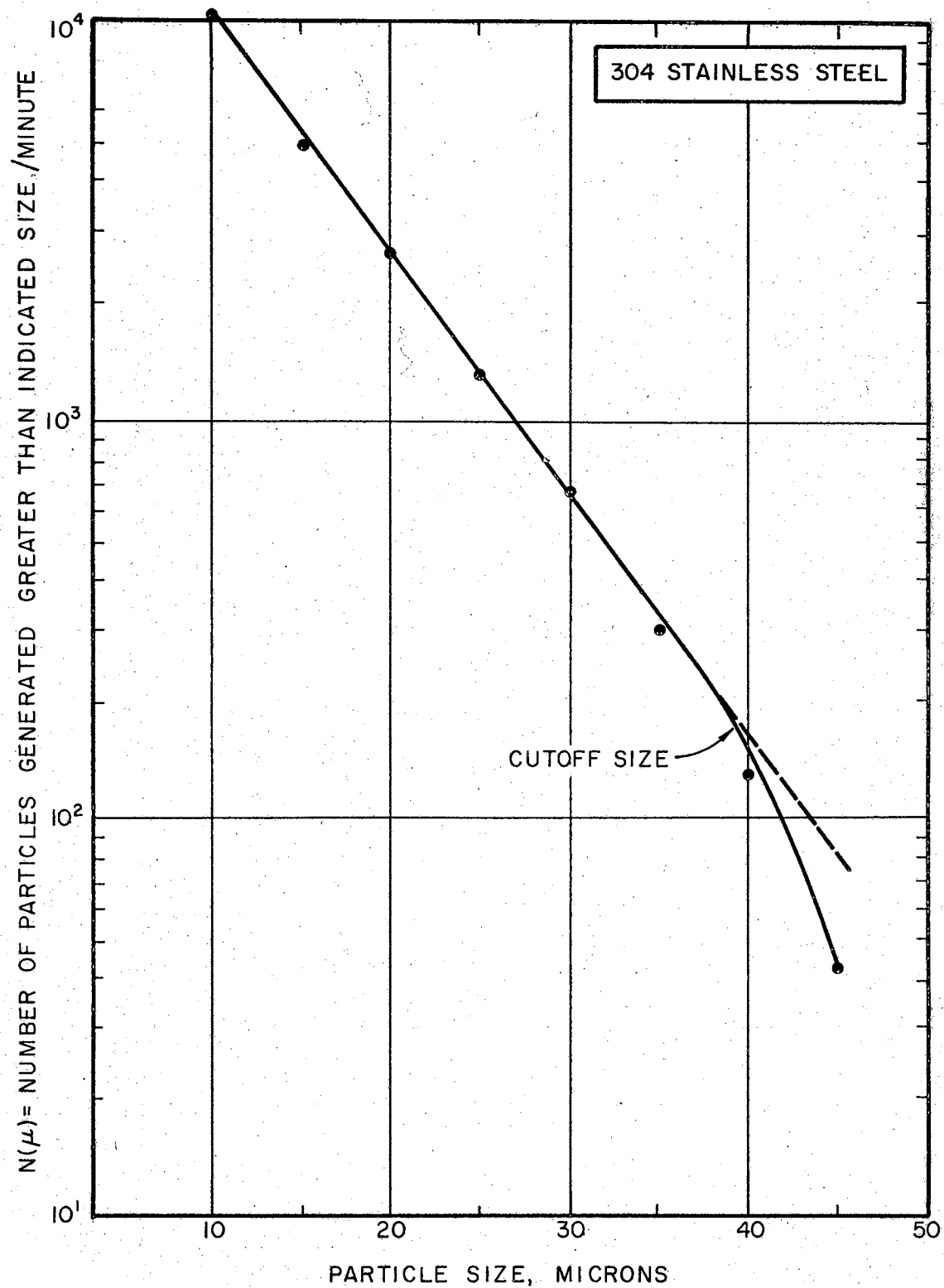


Figure 4-15. Cumulative Particle Size Distribution Curve for 304 Stainless Steel

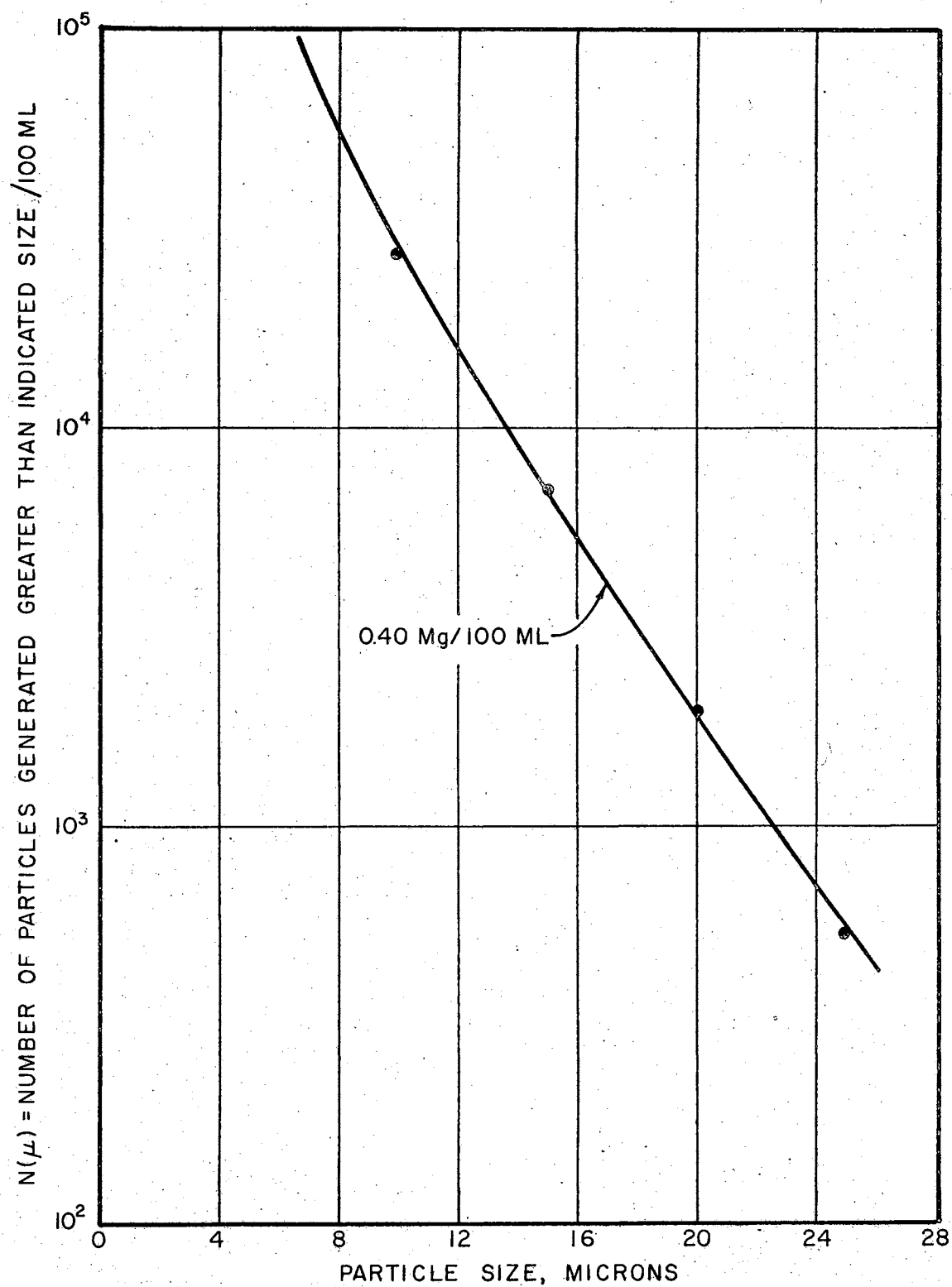


Figure 4-16. Cumulative Particle Size Distribution Curve of Aircraft Field Data

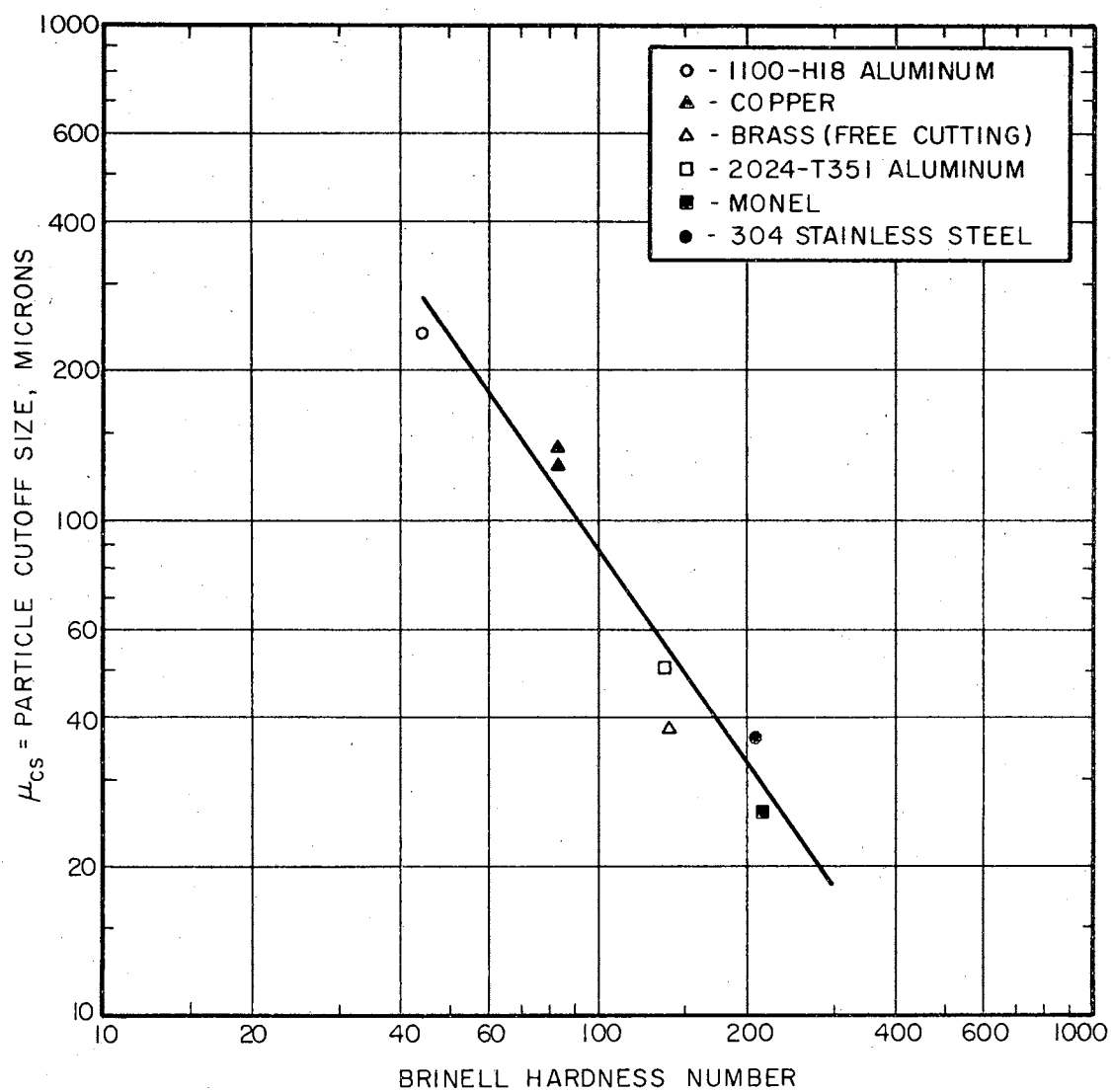


Figure 4-17. Correlation Between Particle Cutoff Size and Brinell Hardness Number

materials whose Brinell hardness ranges from 30 to 250 derived from Figure 4-17 is

$$\mu_{CS} = 58,600/BHN^{1.416} \quad [4-3]$$

where

μ_{CS} = Particle cutoff size, microns

BHN = Brinell hardness number.

Figure 4-18 is a plot of the distributions of all the material tested during the study. As can be seen from Figure 4-18, the slope of the distribution curves increases as the strain energy of the material increases. In Figure 4-19 is given a plot of the slope of these distributions versus the strain energy of the materials. The relationship for the slope of the distribution curves for particulate generated by cavitation for Figure 4-19 is:

$$M_d = 2.17 - 5.5 \log_{10} S_e \quad [4-4]$$

where

M_d = Slope of the distribution curve, $\times 10^2$

S_e = Strain energy, PSI $\times 10^{-3}$

and is valid for ductile materials whose strain energy is less than 35,000 PSI.

Assuming a constant bubble density, the number of bubbles collapsing will increase per unit volume of material loss for an increase in the strain energy of a material producing a greater overlapped damage. This results

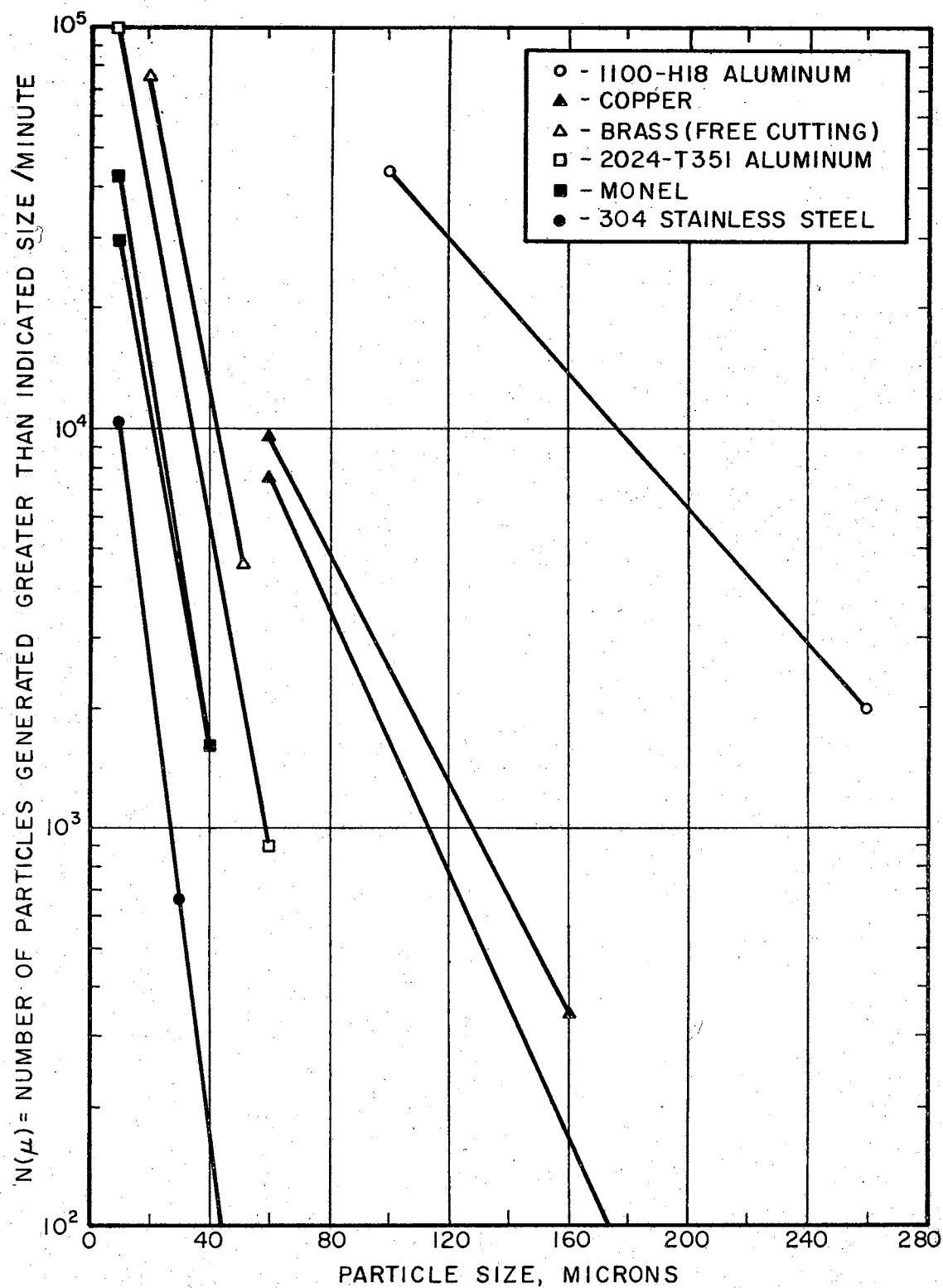


Figure 4-18. Cumulative Particle Size Distribution Curves for all Materials Tested

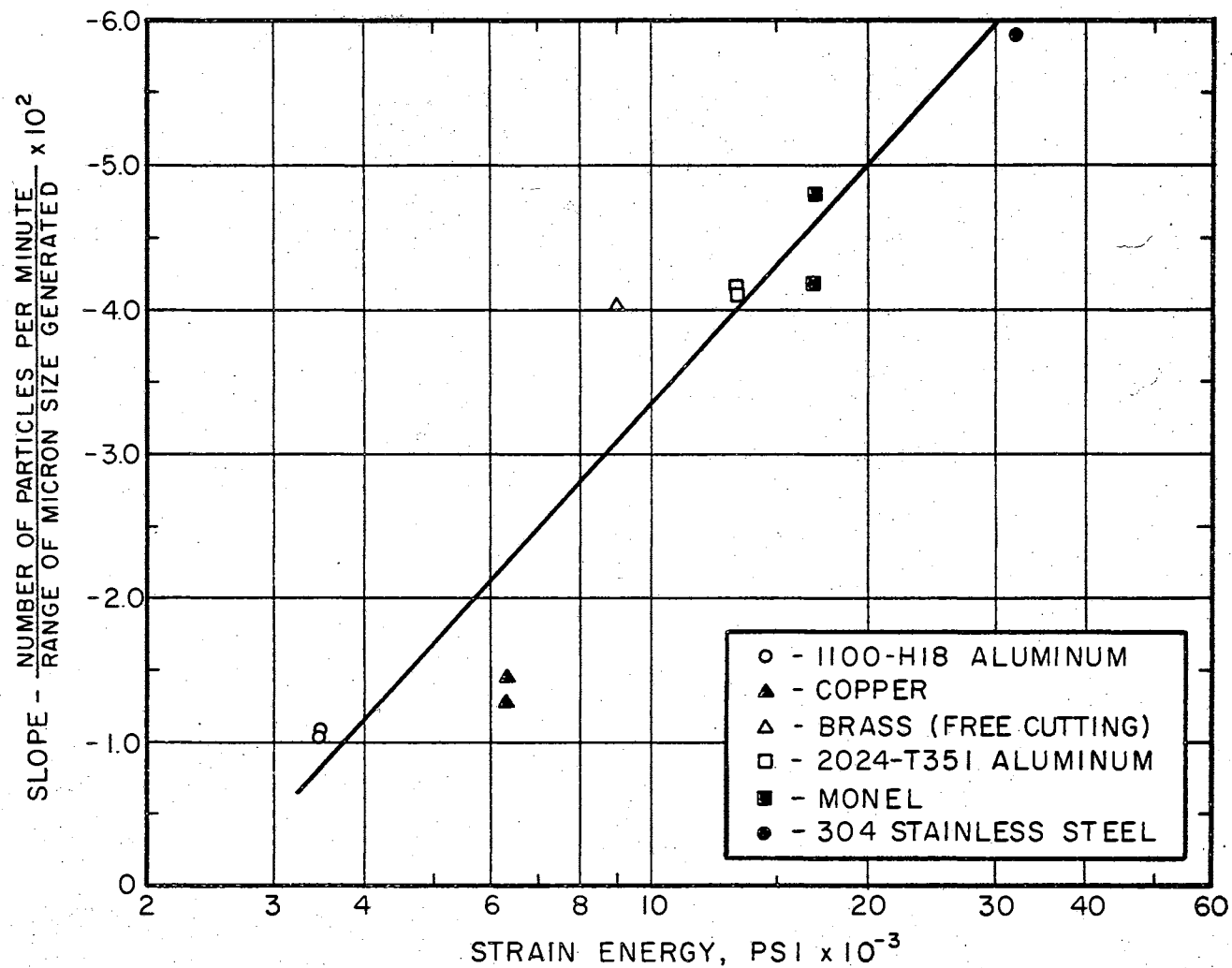


Figure 4-19. Correlation Between Slope of the Cumulative Particle Size Distribution Curves and Strain Energy

in a greater rate of generation for a particular size particle when the strain energy of the material increases. The effect of fatigue cracks, grain boundaries, inclusions, weak intercrystalline substances, etc., must not be ignored as additional reasons for the increase in the slope of the distribution curves. However, it is beyond the scope of this study to include the effects of such mechanisms.

The size can be determined at which a constant number of generated particles exists for each distribution. At $N(\mu) = 7,000$ particles (Figure 4-20), a horizontal line is drawn intersecting each distribution curve. From these points of intersection, lines are projected down to the abscissa of the curve which determines the values of the particle size at $N(\mu) = 7,000$. This size is designated as μ_s . The plot of strain energy for all materials tested versus the particle size μ_s at $N(\mu) = 7,000$ particles is given in Figure 4-21.

The empirical relationship for μ_s which represents the size at which a constant number of particles are generated for each distribution derived from Figure 4-21 is

$$\mu_s = 750/S_e^{1.185} \quad [4-5]$$

where

μ_s = Particle size at which 7,000 particles

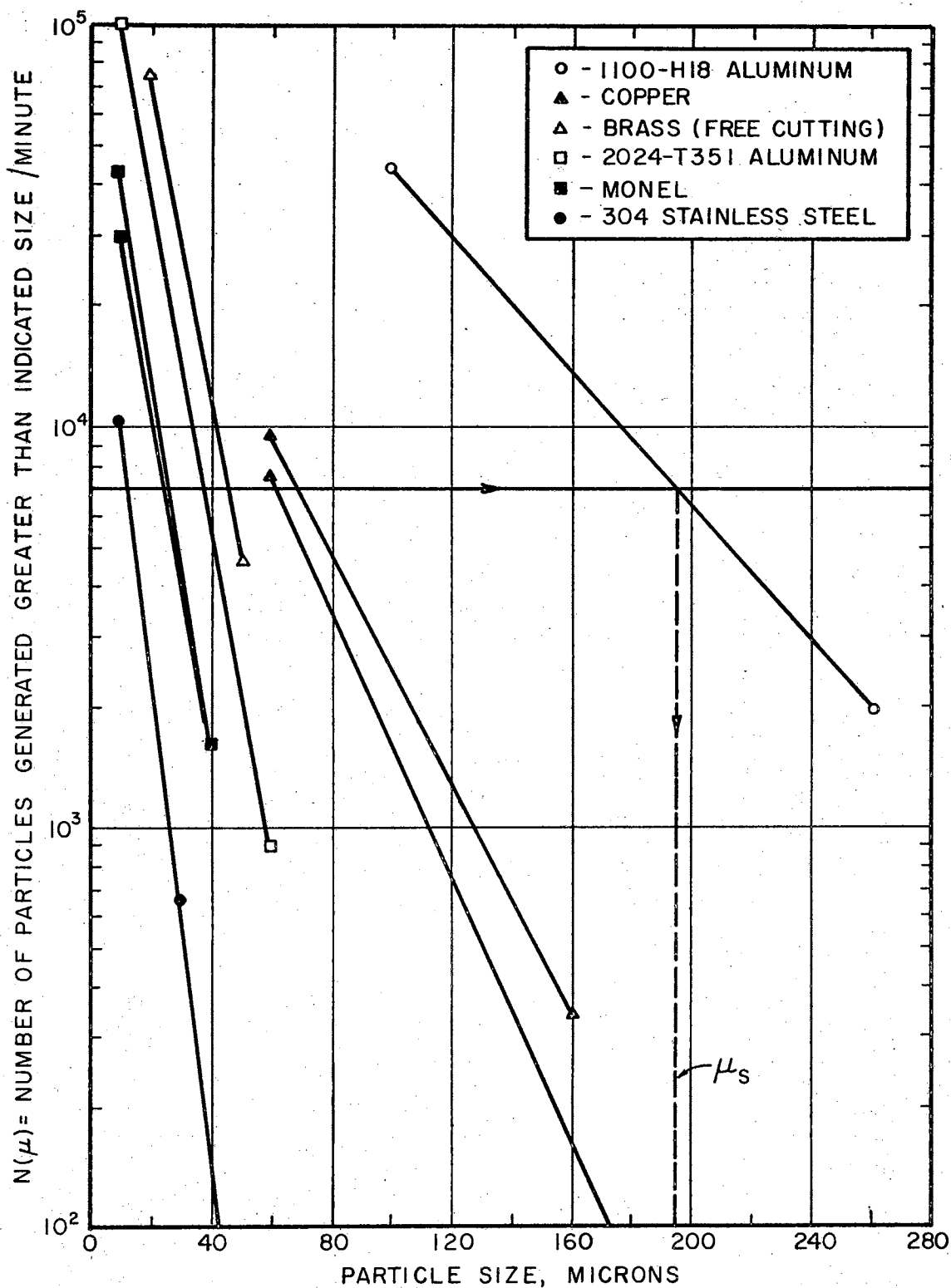


Figure 4-20. Sketch Showing the Determination of μ_s for $N(\mu)$ Equal to 7,000

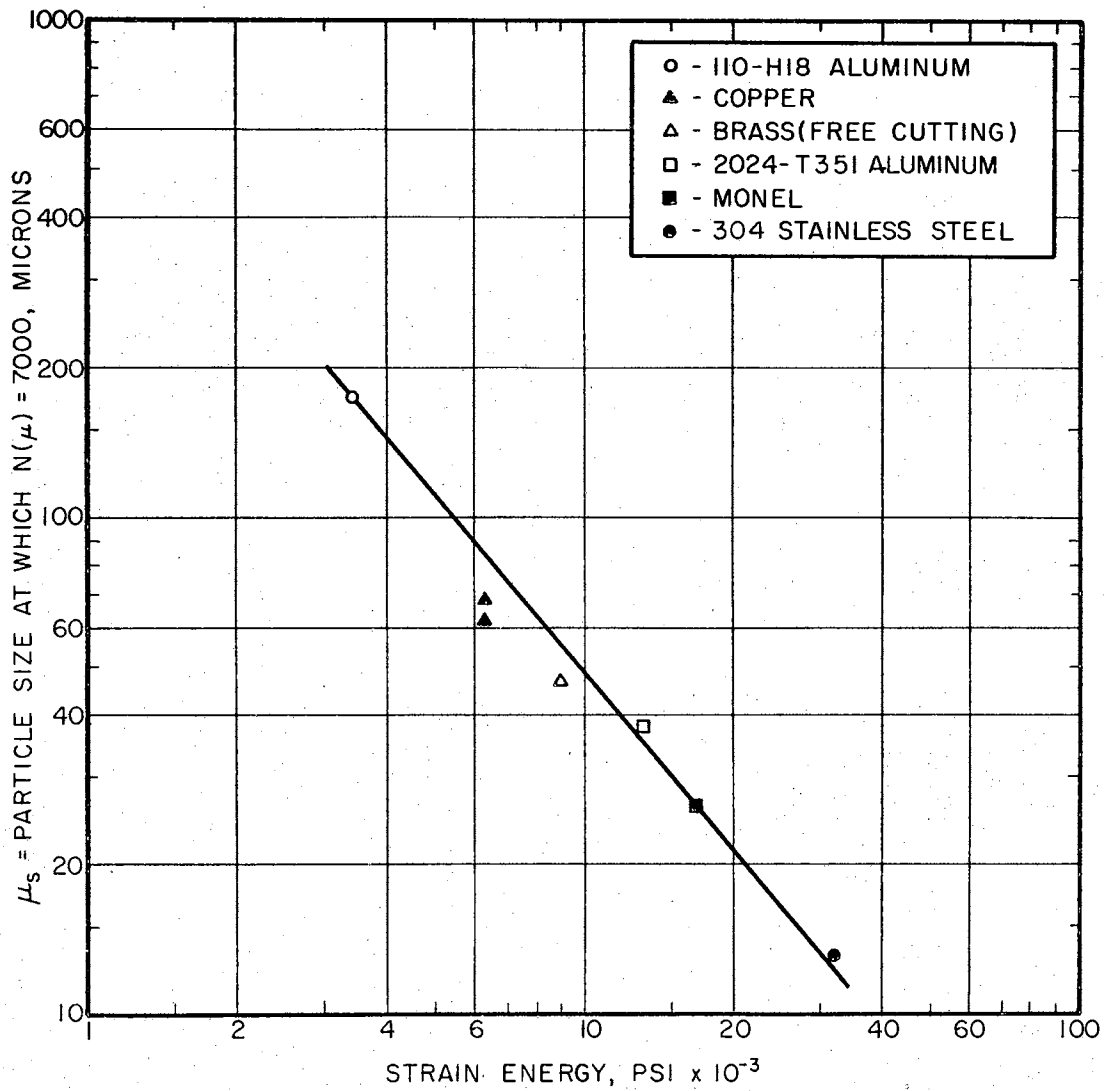


Figure 4-21. Correlation Between μ_s and Strain Energy for $N(\mu)$ Equal to 7,000

greater than μ_s are generated per minute,
microns

S_e = Strain energy, PSI $\times 10^{-3}$.

The relationship should be valid for ductile materials whose strain energy is less than 35,000 PSI. The tests were conducted in distilled water at 80 ± 5 degrees Fahrenheit at a calculated "Intensity" I of 2 watts per square meter.

A correlation, covering the entire range of materials tested, between μ_s and the strain energy for larger particle distribution values [$N(\mu) > 7,000$] does not exist since the copper sample distribution intersects the distributions of materials with a larger strain energy. However, for the materials normally used in component structures (exclusion of copper and 1100-H18 aluminum), the relationship between μ_s and the strain energy should be valid for a large range of $N(\mu)$ values (see Figure 4-20).

To determine the particle size distribution curve generated as a result of cavitation, the following items are necessary:

- (a) The largest particle size generated or the point at which the distribution terminates,
- (b) The slope of the distribution curve, and
- (c) The coordinates of a point on the curve.

The largest particle size generated or the point at

which the distribution terminates is needed to completely define the particle distribution curve since each material has a maximum size at which no larger particles are generated. The value of the largest particle size generated can be obtained from either Figure 4-8 or Equation [4-1]. The slope of the distribution curve can be obtained from either Figure 4-19 or Equation [4-4]. The coordinates of a point on the curve can be determined by either Figure 4-21 or Equation [4-5].

Effect of Fluid Viscosity on Particulate Contamination Generation

The effect of fluid viscosity on the size of particulate generated was investigated by conducting tests in:

- (a) distilled water
- (b) MIL-H-5606 hydraulic fluid
- (c) 20W Motor oil (non-detergent).

A brass sample was cavitated in the distilled water until the steady state region of weight loss had been reached. The same specimen was then cavitated in the other fluids. The largest particle size generated decreased with an increase of fluid viscosity. However, to theorize that the largest particle size decreases as a result of an increase in viscosity is questionable since:

- (a) The rate of weight loss was not determined for the tests and a decrease in intensity

may have resulted with the increase in viscosity, and

- (b) The depth of plastic deformation from the initial test (distilled water) may have influenced the results of the other tests.

Since the "Intensity of Cavitation Damage" is defined as the energy absorbed by the material per unit area, there was a possibility that a decrease in intensity occurred even though the frequency and amplitude remained constant during the tests.

To the author's knowledge, a relationship is not known between the depth of plastic deformation and cavitation "Intensity." In one instance (7), the depth of plastic deformation is reported, but the intensity, which was determined in another study (19) on the evaluation of testing devices, was at a constant level. It is the opinion of this author that an increase in the intensity level (pure mechanical action, with no erosion, etc.) will result in an increase of the slope of the distribution curve with a slight decrease in the maximum size generated. The effects of inclusions, grain boundaries and other mechanical or material properties may have a different influence on the generation characteristics at high cavitation intensities. The influence of a higher viscosity should have the same effect as a decrease in intensity.

Although distilled water with a low viscosity was used for the tests to determine the relationships derived from this study, the expressions should be valid for typical hydraulic systems. The relationships may possibly approach the maximum conditions encountered in a hydraulic system as a result of mechanical action. However, the validity of the expressions may be questionable in systems where the cavitation intensity is very low and corrosion may become a major factor in the removal of material.

CHAPTER V

APPLICATION OF EMPIRICAL RELATIONSHIPS

Although a system may incorporate a centralized filtration unit generally capable of producing a specific contaminant tolerance level in a portion of a system, contaminant generated downstream from a filter may produce non-tolerable levels at strategic points. After identifying the sources of the contamination, it is necessary to determine or establish the generating mechanism. Knowing the mechanism and the characteristics or parameters governing the process will permit the prediction of system reliability and performance.

The characteristics or parameters of contaminant generation caused by cavitation can be determined by the information derived from this study if the Brinell hardness and strain energy of the material are known. The determination of the Brinell hardness is a relatively simple standardized test. The strain energy of a material can be estimated by Equation [3-1] from the properties of the specific material which are normally given in metallurgical tables.

The empirical relationships derived from this study

cover the properties of those materials normally used in hydraulic component design and are valid for materials whose strain energy is between 3,000 and 35,000 PSI. They also encompass a Brinell hardness range of 30 to 250. Empirical relations to approximate the particle size distribution of cavitation generated contaminant up until this time have been non-existent. These relationships make it possible to determine the distribution generated as a result of cavitation in a hydraulic system. The ability to estimate the particulate contaminant generated by a specific mechanism represents a major accomplishment in the study of the cause and effect of fluid contamination.

The following example illustrates the use of the relationships derived from this study to approximate the particle size distribution $N(\mu)$ generated as a result of cavitation:

For a hypothetical material whose Brinell hardness is equal to 150 and has a strain energy of 15,000 PSI, the largest particle size generated can be estimated by the empirical relationship

$$\mu_{LS} = 26,400/\text{BHN}^{1.195} \quad [4-1]$$

and is equal to 66 microns. The slope of the cumulative distribution curve can be estimated

by the relationship

$$M_d = 2.17 - 5.5 \log_{10} S_e \quad [4-4]$$

and is equal to -4.3×10^{-2} or -0.043 particles generated per minute per micron.

The micron size μ_s at which there are 7,000 particles generated greater than μ_s is given by the relationship

$$\mu_s = 750/S_e^{1.185} \quad [4-5]$$

and is equal to 30.2 microns. Figure 5-1 is the distribution approximated by the relationships.

From particle size distribution information such as derived in the preceding example, it is possible to quantitatively specify the required performance characteristics of the system's filters.

If the contaminant tolerance level (which may be a specific size or concentration of a size) of unprotected downstream components is known, then the information can be used to determine if an additional filter is required to protect these components. The larger generated particle sizes can be estimated to determine if they are capable of plugging small orifices of control valves.

Another important application for the technology gained from this research is its use to identify certain

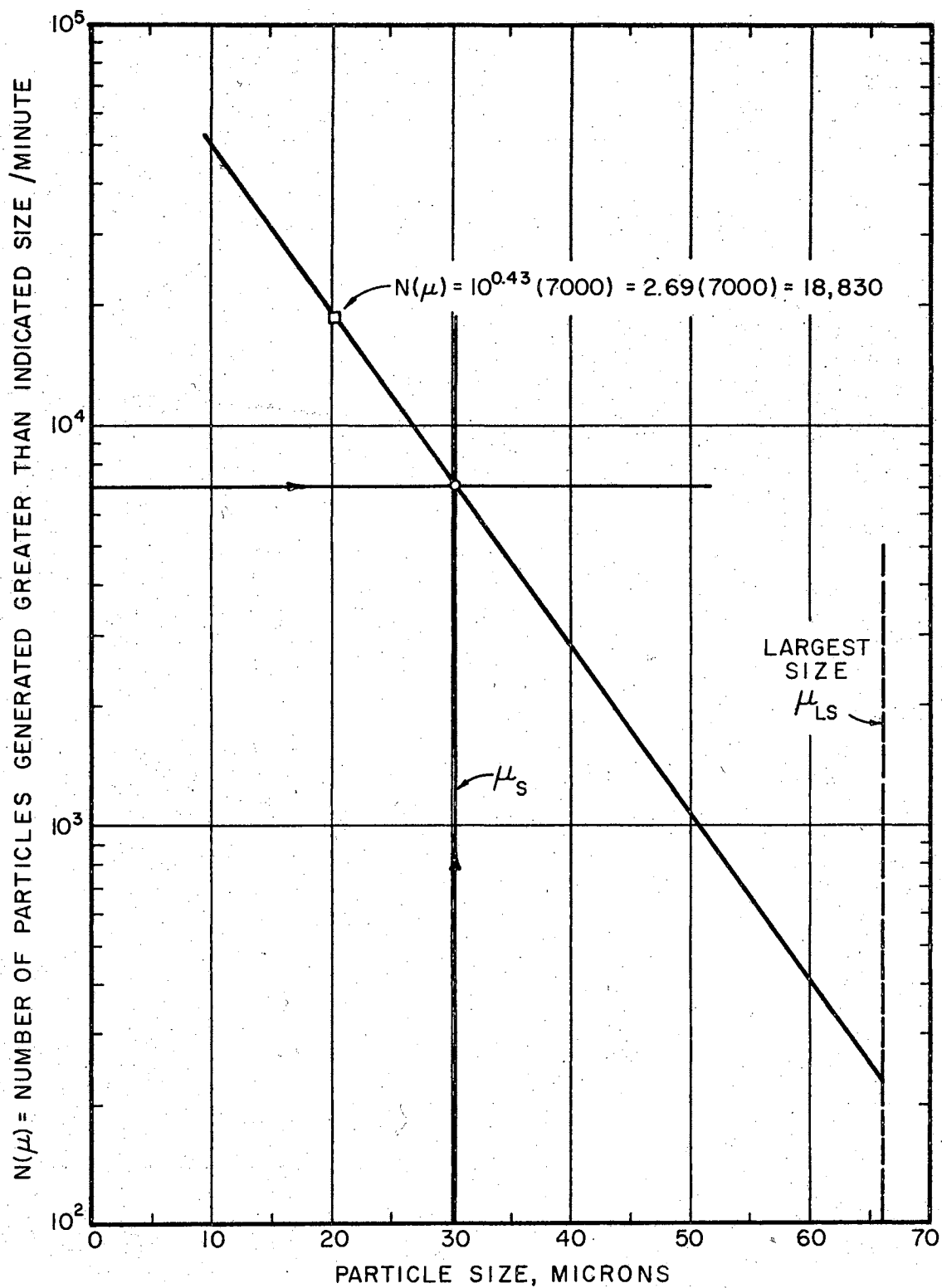


Figure 5-1. Estimation of $N(\mu)$ Using Empirical Relationships

specific types of contaminant generators. The relationships between the slope of the particle size distribution curves and the strain energy of materials for various mechanisms of contamination generation might be used as a "non-destructive" evaluation of the type of wear or the identification of the component producing abnormal quantities of contamination. The contaminant distribution (see Figure 4-16) generated by a particular piston pump has a slope more than twice that of the distribution generated by cavitation of 304 stainless steel. The large slope of this distribution curve is caused by the breaking down of the larger particles due to the sliding action between the moving members of the pump. The presence of cavitation in the pump might be detected if the slope of the distribution curve of the system's fluid would indicate a gradual decrease between sampling intervals.

CHAPTER VI

SUMMARY AND CONCLUSIONS

The parameters necessary to determine the particle size distribution curve are the slope of the distribution curve, the termination of the distribution size and a means of determining the volume of particles or an ordinate value on the distribution curve. The results of this study have provided the necessary information to determine the particle size distribution curve for specific materials. The conclusions drawn from this study are summarized as to (a) the largest particle size generated for the various materials, (b) the volume of material lost, and (c) the characteristics of the generated distribution curves.

Summary

Largest Particle Size Generated

The largest particle size generated for the group of materials tested gives the best correlation with the Brinell hardness number which is a measure of the material's resistance to indentation. As the BHN increases, the area of indentation decreases, thereby decreasing the

volume of plastic deformed material. From the collapse of bubbles near the material surface, shock waves or fluid jets impinge upon the surface producing indentations in the material and results in a volume of plastic deformed material. Subsequent blows to the material chip off this extruded plastic deformed material in various irregular sizes and shapes. The largest diameter of these particles can be predicted by the empirical relationship

$$\mu_{LS} = 26,400/BHN^{1.195} \quad [4-1]$$

where

μ_{LS} = Largest particle size generated, Microns

BHN = Brinell hardness number.

The strain energy of the materials was not a good correlation parameter for the determination of the terminal (largest size) particle size of the distribution. The time necessary for the largest particle size generated to reach its maximum value corresponds to the time at which the rate of weight loss of the specimen reaches its maximum value. The existence of a particle size attenuation zone for this particular group of materials was not detected except in the case of commercially pure aluminum (1100-H18). However, the soft aluminum had very deep pits which results in a less dense bubble cloud and a corresponding decrease in the damage rate (8).

A particle cutoff-size exists for the generated

particles due to cavitation and is defined as the micron size at which the particle size distribution $N(\mu)$ (plotted on semi-log coordinates) deviates from a straight line. The relationship for the particle cutoff-size is

$$\mu_{CS} = 58,600/BHN^{1.416} \quad [4-3]$$

where

μ_{CS} = Particle cutoff-size, Microns

BHN = Brinell hardness number.

Volume of Material Lost

While the strain energy is not the best judge of the particle size generated, it is a very strong function of the rate of volume of material loss for the group of materials tested. The concept of using the strain energy as a measure of volume loss is attributed to Thiruvengadam (6), and for the group of materials tested can be estimated by

$$V_L = 25.8/S_e^{1.985} \quad [6-1]$$

where

V_L = Rate of volume loss, MM^3 /minute

S_e = Strain energy, $PSI \times 10^{-3}$.

The rate of volume loss is the ratio of the rate of weight loss at steady state conditions to the density of the material.

Particle Size Distributions

The particle size distribution curves for contamination due to cavitation plot as straight lines on semi-log coordinates except for a small interval at the end of the distribution curve which represents the decay in the number of the terminal larger sized particles.

The slope of the distribution curves is a relatively strong function of the strain energy of the material and can be approximated by

$$M_d = 2.7 - 5.5 \log_{10} S_e \quad [4-4]$$

where

M_d = Slope of the particle size distribution
curve $\times 10^2$

S_e = Strain energy, PSI $\times 10^{-3}$.

The spacing interval of the distribution curves is a function of the strain energy of the materials. The value for the particle size, μ_S , at which each distribution of the materials tested has the same number of particles generated per minute can be estimated by the relationship

$$\mu_S = 750/S_e^{1.185} \quad [4-5]$$

where

μ_S = Particle size at which 7,000 particles
greater than μ_S are generated per
minute, Microns

S_e = Strain energy, PSI $\times 10^{-3}$.

A correlation, covering the entire range of materials tested, between μ_S and the strain energy for larger particle distribution values [$N(\mu) > 7,000$] does not exist since the curve of the copper sample distribution intersects the distributions of materials with a larger strain energy.

Attempts in the past have been made to correlate the cavitation resistance of a material (weight loss in a specific time interval) with the material's hardness. In general, the cavitation resistance of a material increases as the hardness increases. However, in most cases (18, 22) a strong correlation was evident between the hardness and weight or volume loss only when various hardnesses of the same material were tested. This loss of correlation outside the specific group may be explained by the fact that the hardness is a measure of the range of particle sizes generated while the strain energy of the material measures the rate of volume loss.

Conclusions

The conclusions are based on an "Intensity of Cavitation Damage" I of two watts per square meter as defined by Thiruvengadam (19) using Equation [2-1]. The mechanism of cavitation damage using the magnetostriction device is primarily a mechanical action. "Intensities" of 3,000

watts per square meter (29) in a flowing system are rather large and might suggest that erosion together with cavitation mechanical action may be the mechanism of material removal.

Although straight lines (determined by the method of least squares) were drawn through the observed data for the particular range of material properties of the specimens tested, an extension of the relationships to a much larger interval may result in a large error. The empirical relationships should be valid for ductile materials whose Brinell hardness ranges from 30 to 250 and strain energies from 3,000 to 35,000 PSI.

To the author's knowledge, this dissertation has given for the first time the relationships between cavitation generated particulate and properties of the material. The contributions to the field of filtration and to system contamination analysts as a result of this study are as follows:

1. If a component of a system is allowed to cavitate under certain conditions, then the relationships can be used to determine the sizes generated. If the sizes generated are harmful to components downstream, then additional filters must be placed in the system.
2. Filter design parameters can be determined

since it is possible to determine the generated particle size distributions using the derived relationships.

3. The occurrence of cavitation in a system can be detected by the distinct characteristic slope of the generated particle distribution which is associated with this mechanism of contaminant generation.
4. Materials can now be selected for hydraulic component design which will minimize the buildup of contamination caused by cavitation in a fluid system.

The information derived from the study was far greater than that anticipated initially. The possibility of identifying various mechanisms of contaminant generation for wear characteristics by an analysis of the system's fluid should stimulate further research into the area of contamination generation.

Recommendations for Future Study

As a result of this study, the following recommendations are made:

1. Tests should be conducted to determine the particle distribution characteristics and parameters of various intensity levels.
This information is needed since intensities

greater than that encountered in this study have been reported for various hydraulic components. This study would reveal if an increase in weight loss (which is characteristic of an increase in cavitation "Intensity") is caused by (a) the generation of larger particles, (b) an increase in the slope of the distribution generated, or (c) a simple parallel displacement of the distribution curve.

2. Studies should be conducted to determine the particulate generated as a result of other mechanisms of contaminant generation. The characteristics of these various generation mechanisms could be used as a non-destructive identification of abnormal wear or possible failure of a component.
3. The effect of fluid viscosity on the generation characteristics of various cavitation "Intensities" should be determined. This information can be used to determine the complete range in which the results derived from this study are applicable.

SELECTED BIBLIOGRAPHY

- (1) Parsons, Sir C. A., and S. S. Cook. "Investigations Into the Causes of Corrosion or Erosion of Propellers," Engineering, Vol. 107 (1919), 515-519.
- (2) Föettinger, H. "Uersuche über einige typische Kavitationerscheinungen." Hydromechanische Probleme des Schiffsantriebes, Hamburg, 1932; quoted in (6).
- (3) Boetcher, H. N. "Failure of Metals Due to Cavitation Under Experimental Conditions," trans. ASME. Vol. 58 (1936), 355-360.
- (4) Poulter, T. C. "The Mechanism of Cavitation Erosion," trans. ASME. Vol. 64 (1942), A-31--A-37.
- (5) Wheeler, W. H. "Indentation of Metals by Cavitation," trans. ASME. Vol. 82, Part D (1960), 184-194.
- (6) Thiruvengadam, A. "Prediction of Cavitation Damage" (unpub. Ph.D. thesis, Indian Institute of Science, Bangalore 12, 1961).
- (7) Plesset, M. S., and A. T. Ellis. "On the Mechanism of Cavitation Damage," trans. ASME. Vol. 79 (October, 1955), 1055-1064.
- (8) Plesset, M. S., and R. E. Devine. "Effect of Exposure Time on Cavitation Damage." ASME. Paper No. 65-WA/FE-23.
- (9) Kornfeld, M., and L. Suvorov. "On the Destructive Action of Cavitation," Journal of Applied Physics. Vol. 15, No. 6 (1944), 503-504.
- (10) Robinson, M. J. "On the Detailed Flow Structure and the Corresponding Damage to Test Specimens in a Cavitating Venturi" (unpub. Ph.D. thesis, University of Michigan, August, 1965).

- (11) Naude, C. F., and A. T. Ellis. "On the Mechanism of Cavitation Damage by Nonhemispherical Cavities Collapsing in Contact With a Solid Boundary" (paper presented at ASME-EIC Conference, Montreal, Canada, May 7-10, 1961).
- (12) Hammitt, F. G. "Observations on Cavitation Damage in a Flowing System," trans. ASME. Vol. 85 (September, 1963), 347-359.
- (13) Nowotny, H. "Werkslooffzerstörung durch Kavitation." V.D.I. Verlag Gimbh, Berlin, NW 7 (1942); English translation published by Edwards Brothers, Ann Arbor, Michigan.
- (14) Robinson, L. E., B. A. Holmes, and W. C. Leith. "Progress Report on Standardization of the Vibratory Cavitation Test," trans. ASME. Vol. 80 (1958), 103-107.
- (15) Kerr, S. L. "Determination of the Relative Resistance to Cavitation Erosion by the Vibratory Method," trans. ASME. Vol. 59 (1937), 373-397.
- (16) Leith, W. C., and A. L. Thompson. "Some Corrosion Effects in Accelerated Cavitation Damage," Journal of Basic Engineering, trans. ASME, Series D., Vol. 82 (December, 1960), 795-807.
- (17) Plesset, M. S. "The Pulsation Method for Generating Cavitation Damage," trans. ASME, Series D, Vol. 85 (September, 1963), 360-364.
- (18) Rheingans, W. J. "Accelerated Cavitation Research," trans. ASME. Vol. 73 (1950), 705-719.
- (19) Thiruvengadam, A. "A Comparative Evaluation of Cavitation Damage Test Devices." Tech. Rep. 233-2, Hydronautics, Inc. (November, 1963).
- (20) Thiruvengadam, A., and S. Waring. "Mechanical Properties of Metals and Their Cavitation Damage Resistance." Tech. Rep. 233-5, Hydronautics, Inc. (June, 1964).
- (21) Thiruvengadam, A., and H. S. Preiser. "On Testing Materials for Cavitation Damage Resistance." Tech. Rep. 233-3, Hydronautics, Inc. (December, 1963).
- (22) Mousson, T. M. "Pitting Resistance of Metals Under Cavitation Conditions," trans. ASME. Vol. 59 (1937), 399-408.

- (23) Stiles, G. F. "Cavitation in Control Valves," Instruments and Control Systems. Vol. 34, Part 2 (1961), 2091-2093.
- (24) Lichtman, J. Z., et al. "Cavitation Erosion of Structural Materials and Coatings." Corrosion-National Association of Corrosion Engineers. Vol. 17, Part 2 (October, 1961), 119-127.
- (25) Rao, N. S. G., and A. Thiruvengadam. "Prediction of Cavitation Damage," Proc. ASCE Jour. Hyd. Div., Vol. 87 (September, 1961), 37-62.
- (26) Thiruvengadam, A. "A Unified Theory of Cavitation Damage," trans. ASME. Vol. 85, Section 2, Part D (1963), 365-376.
- (27) Eisenberg, P. "Cavitation Damage." Tech. Rep. 233-1, Hydronautics, Inc. (December, 1963).
- (28) Knapp, R. T. "Recent Investigations of the Mechanics of Cavitation and Cavitation Damage," trans. ASME. Vol. 77 (1955), 1045-1054.
- (29) Thiruvengadam, A. "Intensity of Cavitation Damage Encountered in Field Installations." Tech. Rep. 233 Rep. 233-7, Hydronautics, Inc. (February, 1965).
- (30) Rasmussen, R. E. H. "Some Experiments on Cavitation Erosion in Water Mixed With Air." Proc. Symp. on Cavitation in Hydrodynamics, N.P.L. (Teddington), H.M.S.O. (1955), Paper No. 20; quoted in (19).
- (31) Deiter, George E., Jr. Mechanical Metallurgy. New York: McGraw-Hill Book Company, Inc., 1961.

Appendix A

Cleaning and Packaging of Sample Containers

Testing Procedure Using Packaged Sample Containers

Evaluation of Particle Size Distribution

The determination of the contaminant generating characteristics of cavitation required that stringent clean room techniques be followed during the preparation of the sample containers and the evaluation of the weight of material loss. Although strict rules were followed, the gravimetric weights obtained would indicate a weight loss even when no apparent generated particles appeared on the filter pad. However, this method of determining weight loss was considered quite satisfactory. The advantage of this method is that the specimen does not have to be removed for weighing at specific time intervals. However, the procedure requires a clean room for preparation of the sample containers and the generated weight analysis. Given below is the procedure used for the cleaning and packaging of the sample containers that were used to collect all material generated during the total testing of each individual material specimen.

Cleaning and Packaging of Sample Containers

1. The containers were washed in hot tap water and soap in an ultrasonic cleaner for 30 minutes.
2. The containers were rinsed twice in the ultrasonic cleaner changing the tap water before each rinsing operation.
3. The containers were then placed in an oven

at 180 degrees Fahrenheit for one hour for drying.

4. They were then taken into the clean room and rinsed twice with double filtered (0.45 micron pore size pad) distilled water.
5. They were then filled with 250 milliliters of double filtered distilled water.
6. Then, a layer of polyethylene film (rinsed with filtered distilled water) with a one-inch hole cut in the center of the film was placed over the mouth of the container and fastened with rubber bands. This hole in the polyethylene film allowed the nickel tube to extend into the test medium and also helped prohibit environmental contaminant from entering the containers during the test.
7. A second layer of polyethylene film was placed over the first layer to provide a protective cover for the containers during transportation and storage.

Testing Procedure Using Packaged Sample Containers

1. The nickel tube was washed down while vibrating with solvent to remove any

particles which may have been suspended on the tube.

2. The outer protective cover was not removed until after the machine was in operation (specimen vibrating in air).
3. The sample container was raised up by means of a screw jack until the specimen was immersed one-eighth of an inch into the test medium. The timer was also actuated at this time.
4. After a specified time interval (the time necessary to generate the amount of contaminant which could be counted easily and accurately), the timer was stopped and the sample container removed.
5. The outer protective cover was replaced immediately over the mouth of the container.
6. Steps 3, 4, and 5 were repeated until the weight loss had reached a steady state value. The time to reach the steady state value was determined from previous tests and the literature and could be identified by observing the test specimen surface during the test. The point at which the specimen surface changes from a uniformly damaged appearance to a surface with

randomly placed deep pits is normally the beginning of the steady state region.

Evaluation of Particle Size Distribution

1. A millipore pad (0.45 micron size pore diameter) was placed in a vacuum oven at 80 degrees Centigrade for 30 minutes and then placed into a desiccator allowing the pad to reach room temperature.
2. The pad is then weighed to the nearest one-hundredth of a milligram using a precision analytical balance.
3. The 250 milliliters of distilled water containing the generated contaminant is filtered through a 0.45 micron sized pore size pad rinsing down the walls and inside of the jar with double filtered distilled water to insure that all contaminant is placed on the pad.
4. Steps 1 and 2 are then repeated to give the weight of the generated contaminant and the pad.
5. The filter pad is then placed in a petri dish for counting to determine the particle size distribution.

A modified SAE Aeronautical Recommended Procedure

No. 598 for particle counting with a split image eyepiece and a calibrated scale was used to determine the particle size distribution of the generated contaminant. The calibrated scale was used as a reference line (or "gate") under which the particles were passed for counting. By passing the particles on the pad under the scale, their size is noted and those equal to or greater than the size set on the image splitter are tabulated. The total number of particles on the filter pad (0.47 MM diameter) in each size range can be determined by scaling the area of the filter actually counted to the total effective filter area and is given by

$$*T_p = 82.2 \frac{N_t}{N} M_o \quad [A-1]$$

where

T_p = Total number of particles of a given size range on the filter

N_t = Total number of particles counted in N unit areas

N = Number of unit areas, where a unit area is equal to the width of the calibrated scale times the distance between two grid lines

*The derivation of this equation is given in Progress Report No. 65-2, "Study of Filtration Mechanics and Sampling Techniques," Contract: NAS 8 11009, Prepared by School of Mechanical Engineering Fluid Power and Controls Laboratory, Oklahoma State University, Stillwater, Oklahoma.

on the millipore filter pad (47 MM diameter pad)

M_o = Objective power of the microscope.

A magnification of 520X was used to count particles whose size ranges were between 0 and 60 microns and was obtained by using the 40X objective on the microscope. Particle size ranges of copper and 1100 - H18 aluminum which were between 0 and 300 microns were counted using the 10X objective producing a magnification of 130X. Ten randomly selected unit areas were counted per pad to determine the particle size distribution for each specimen. After determining the particle size distribution, the entire pad was scanned using the 10X objective to determine the largest size particle. Generally, the largest size observed during the determination of the particle size distribution was comparable with the largest size found during the scanning of the entire pad at a lower objective power.

Appendix B

Cumulative Weight Loss Curves for Cavitated Specimens

Given are the cumulative weight loss curves for the materials tested for the determination of contaminant generation characteristics. As can be seen from Figures B-1 through B-6, all materials tested reached a steady state region (constant slope), and for the two specimens tested of each material the slopes were approximately equal at the steady state region. Only one specimen of 304 stainless steel was tested.

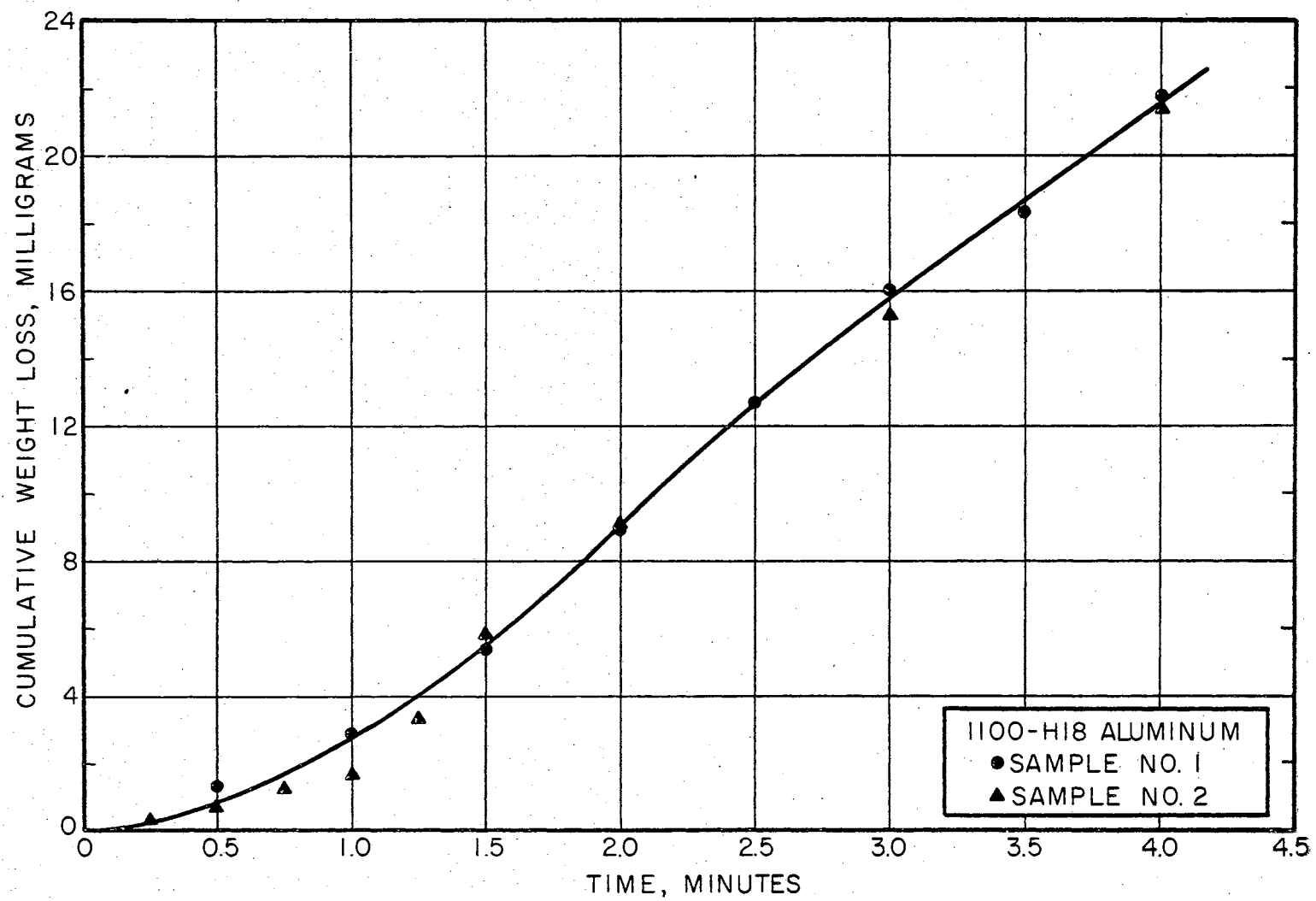


Figure B-1. Cumulative Weight Loss Curve for 1100-H18 Aluminum.

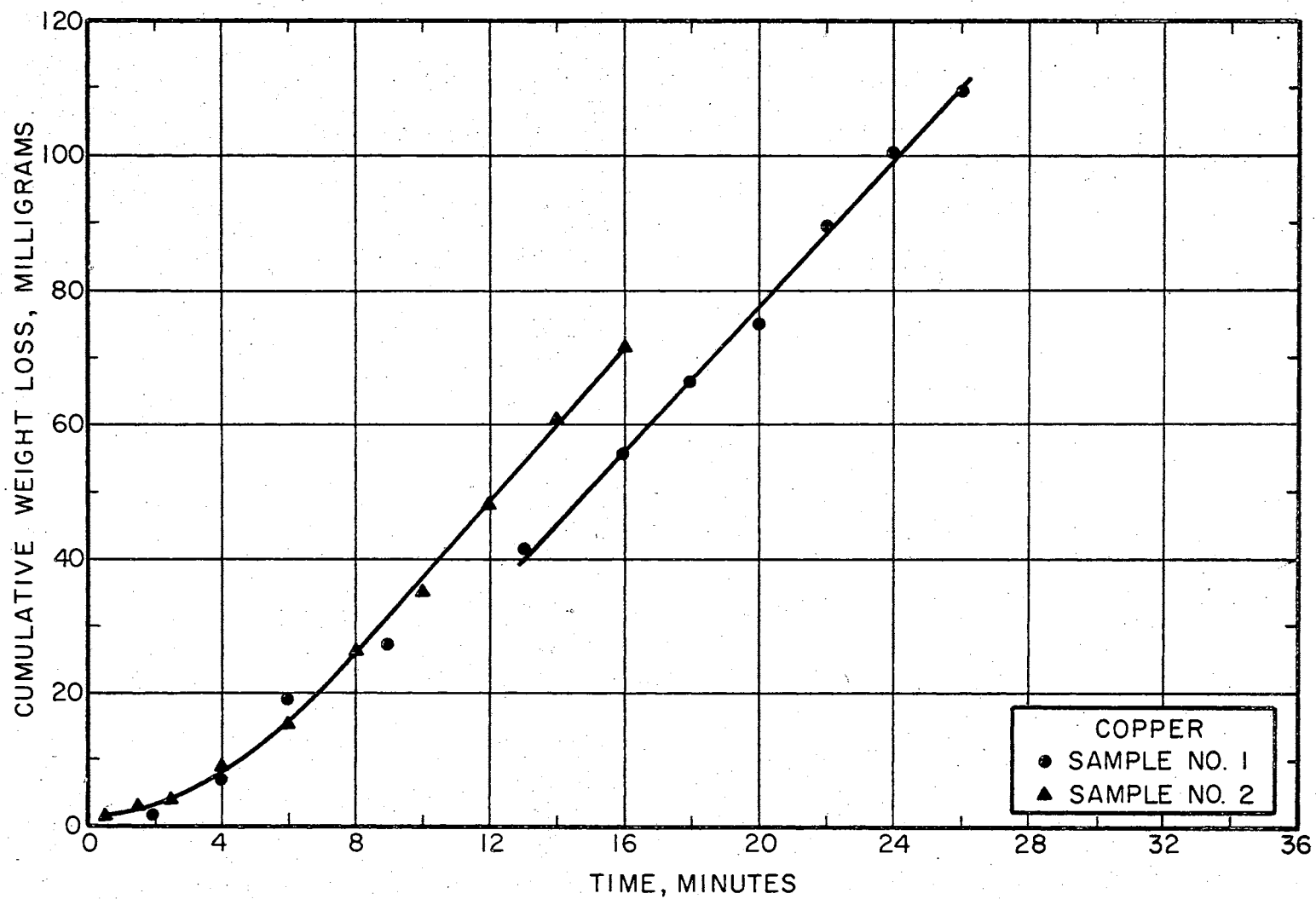


Figure B-2. Cumulative Weight Loss Curve for Copper

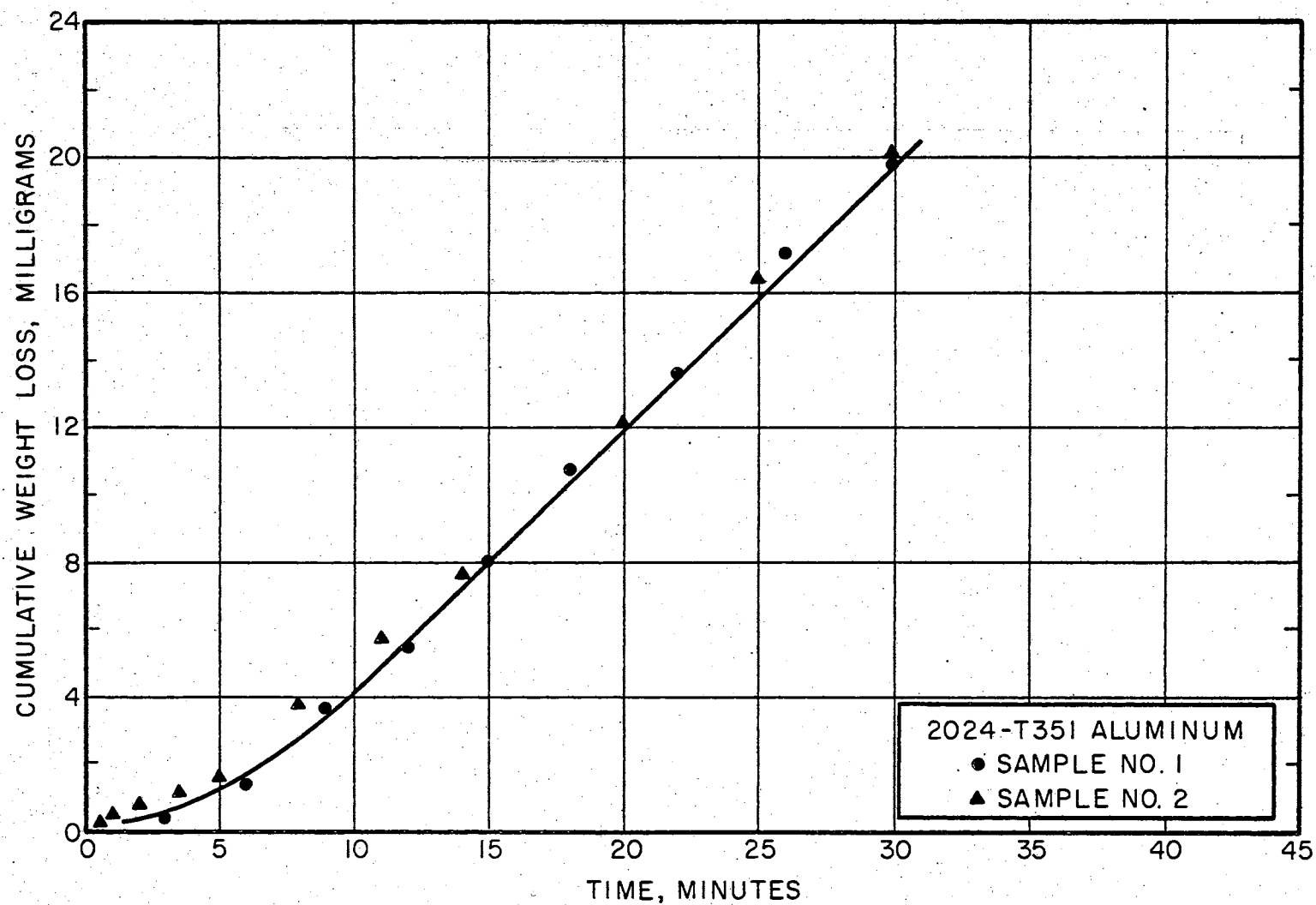


Figure B-3. Cumulative Weight Loss Curve for 2024-T351 Aluminum

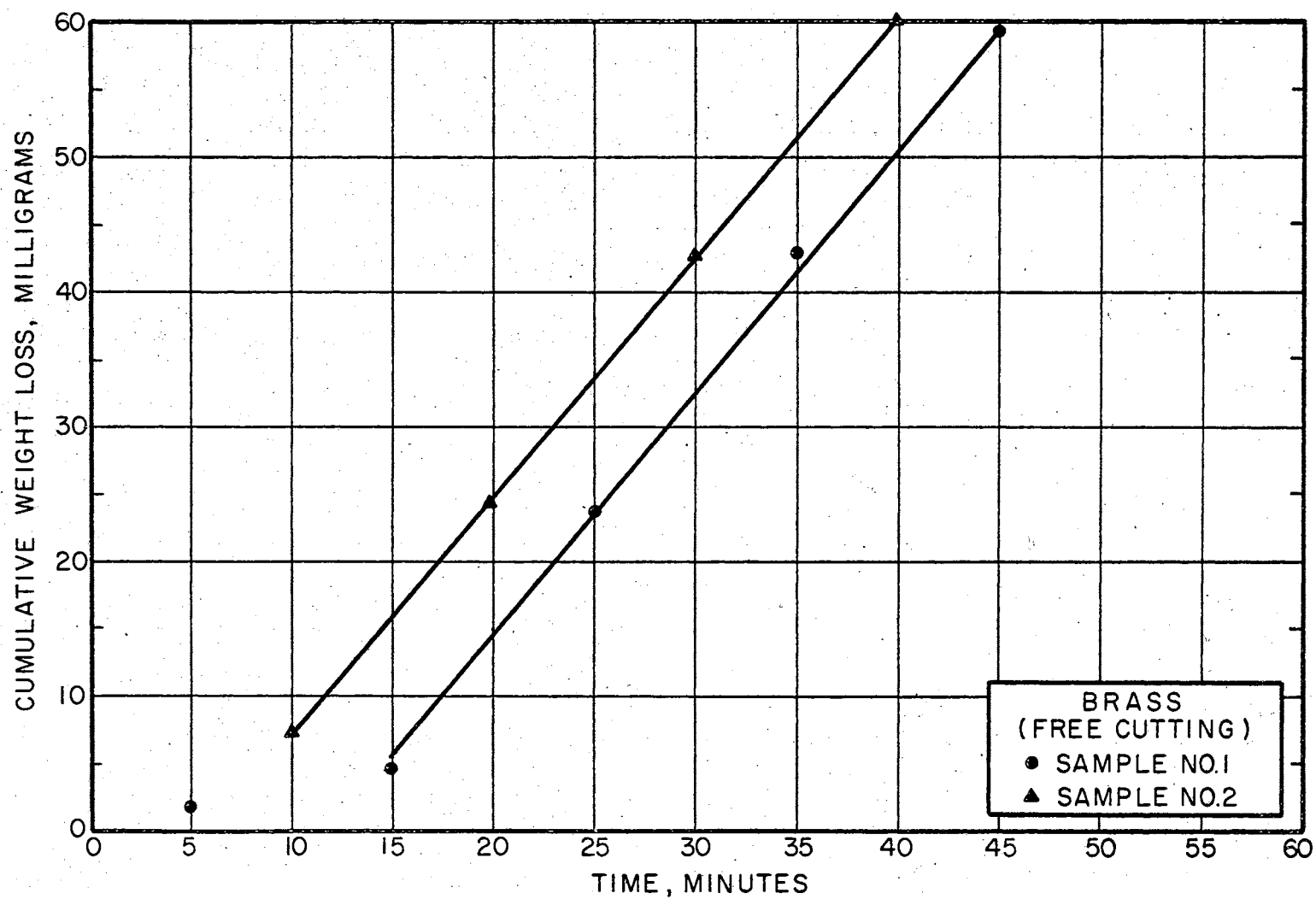


Figure B-4. Cumulative Weight Loss Curve for Brass (Free Cutting)

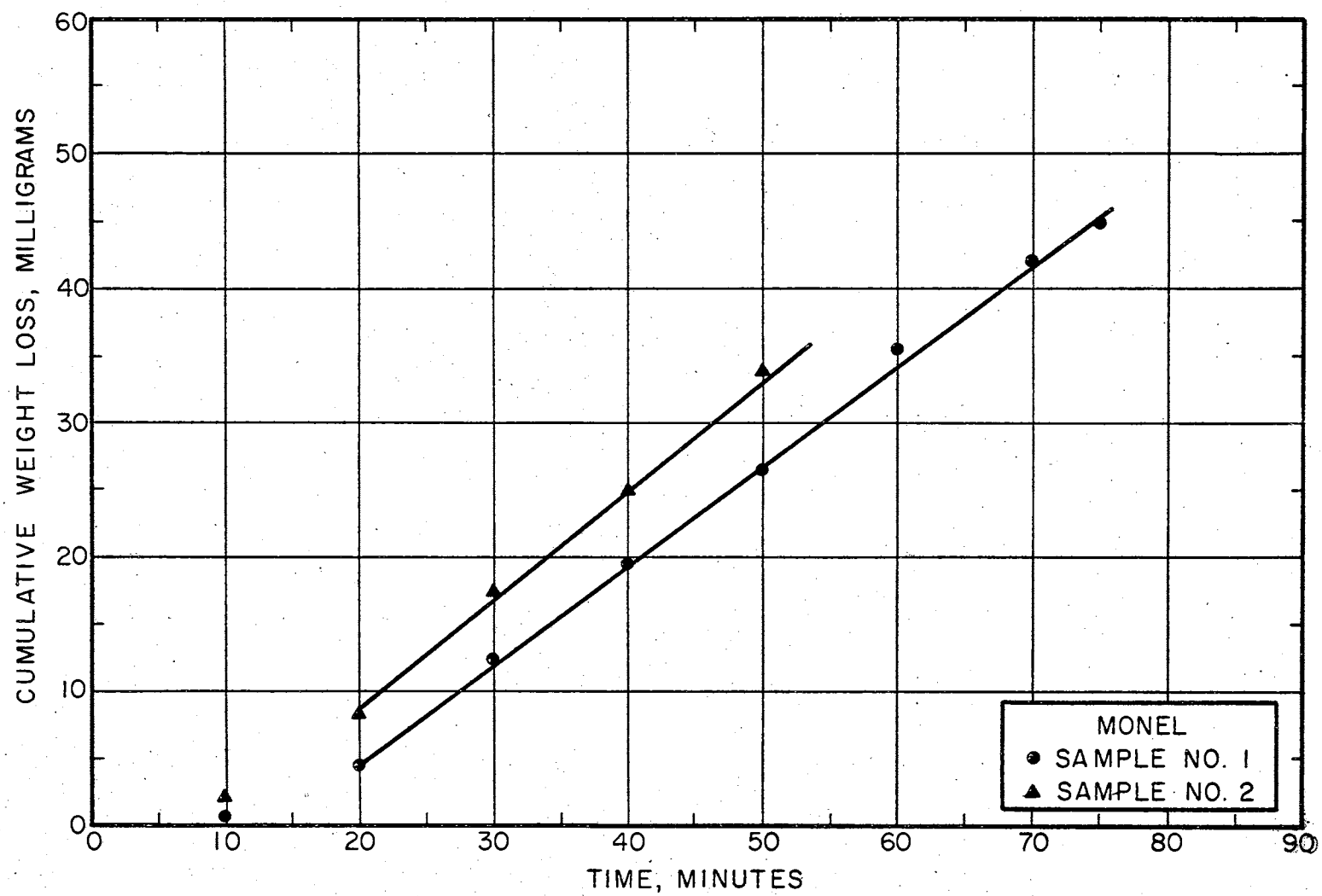


Figure B-5. Cumulative Weight Loss Curve for Monel

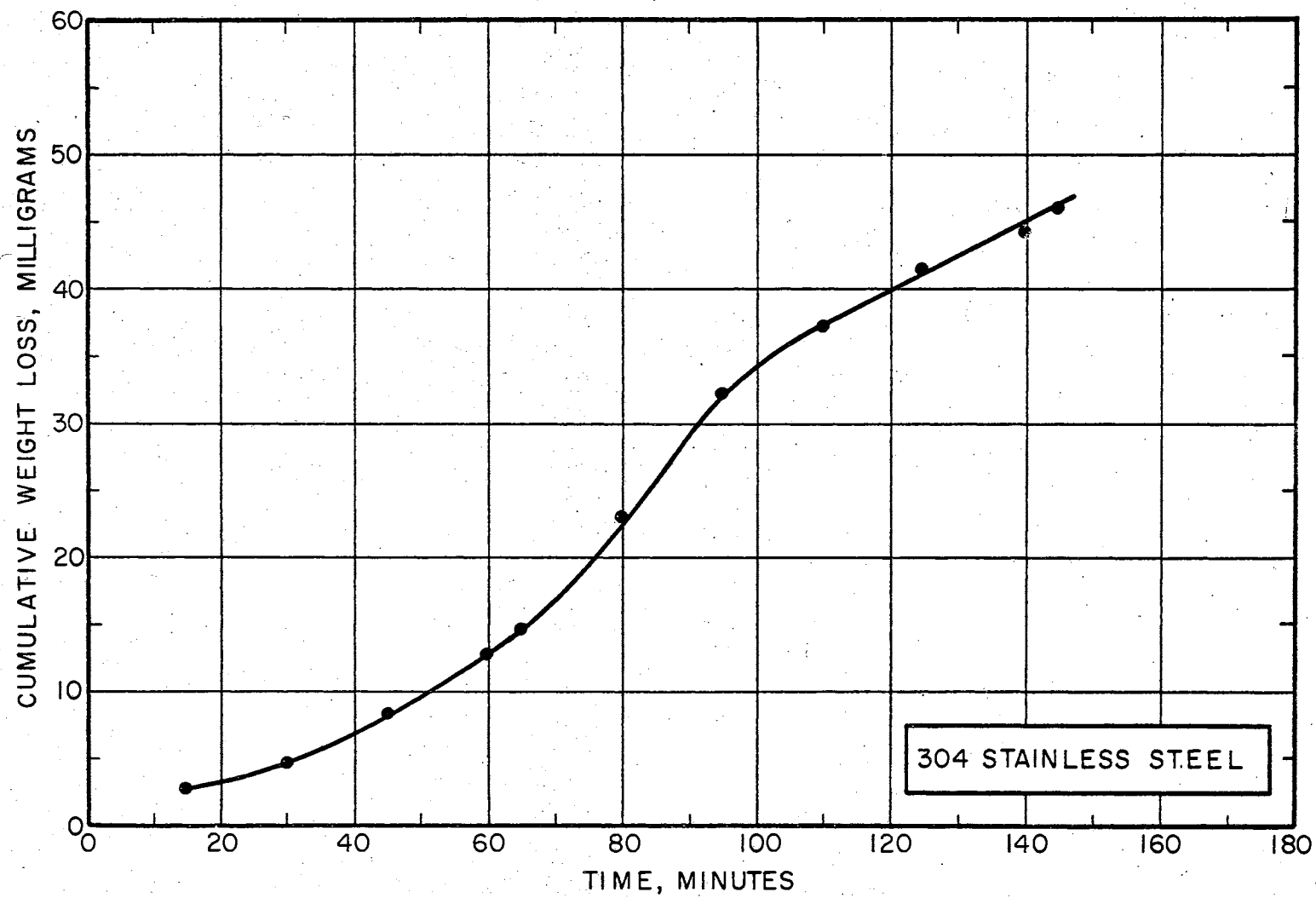


Figure B-6. Cumulative Weight Loss Curve for 304 Stainless Steel

Appendix C

Photographs of Generated Particulate

The photographs in Figures C-1 through C-5 show the particulate generated as a result of cavitation action on various materials. The width of the grid line in the photographs is approximately 100 microns. Photographs C-1 through C-4 were taken of particulate generated during the steady state region (rate of weight loss is constant). Figure C-5 is a photograph of 2024-T351 aluminum after an initial five minute cavitation exposure and is typical of the smaller sizes generated for the various materials during the accumulation zone (rate of weight loss increases with time).

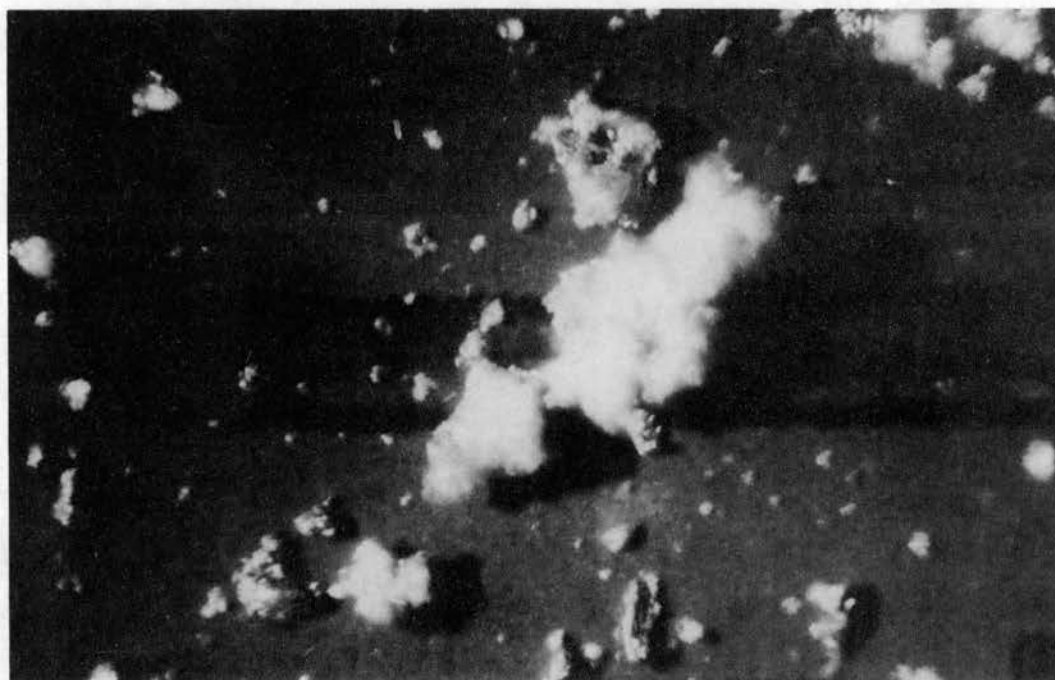
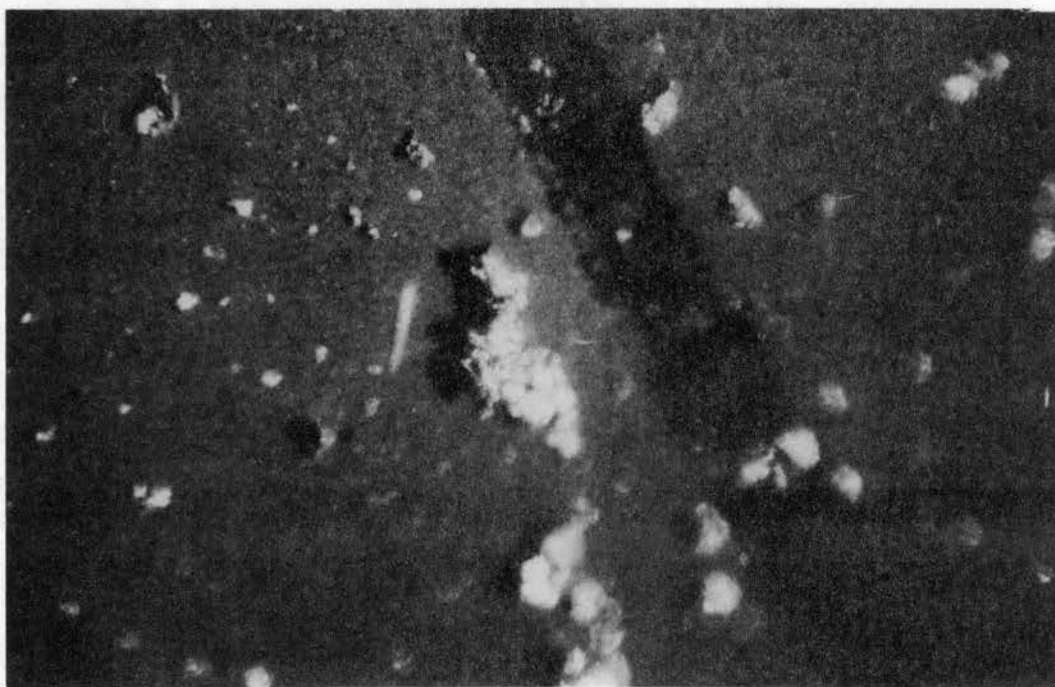


Figure C-1. Photographs of Generated 1100-H18
Aluminum Particulate at Steady ,
State Conditions

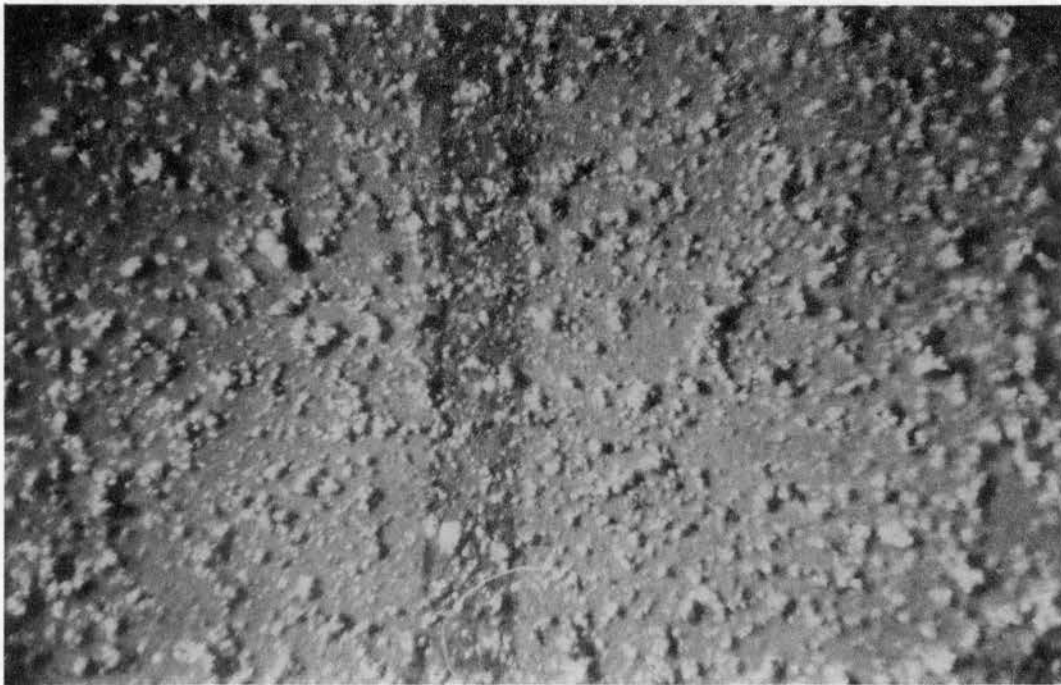


Figure C-2. Photograph of Generated Brass
Particulate at Steady State
Conditions

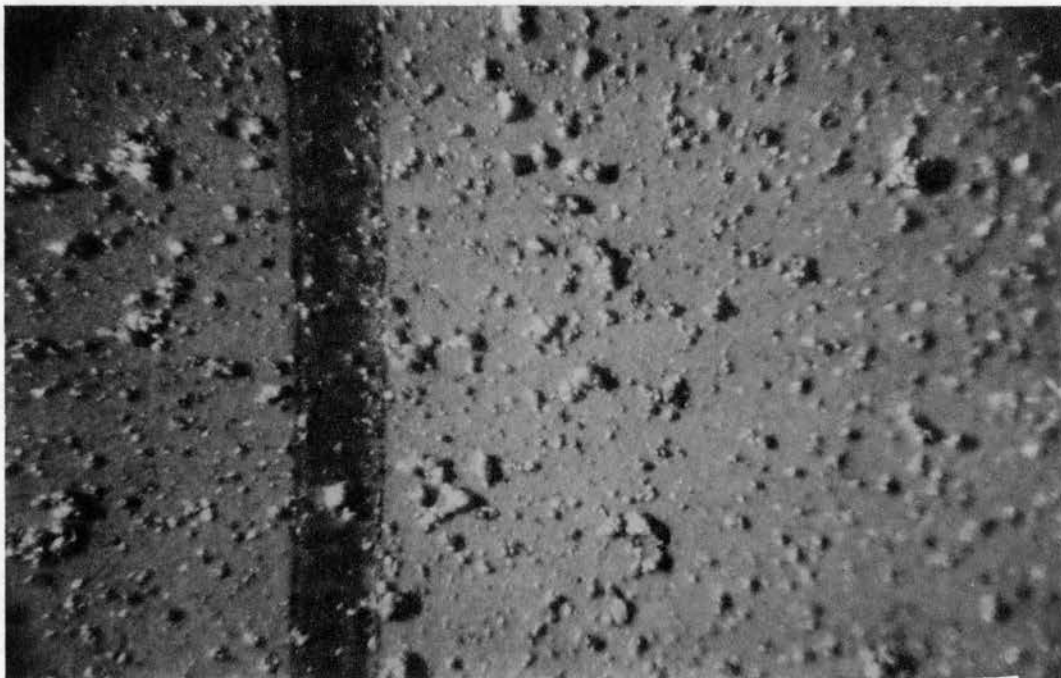


Figure C-3. Photograph of Generated Monel
Particulate at Steady State
Conditions

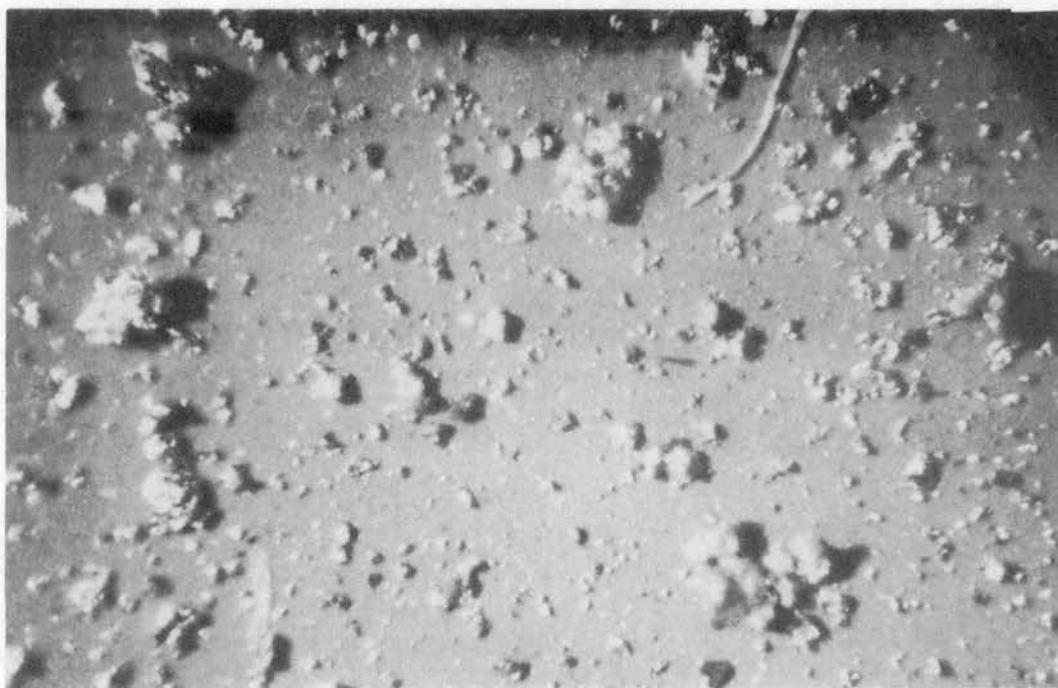


Figure C-4. Photograph of Generated Copper
Particulate at Steady State
Conditions

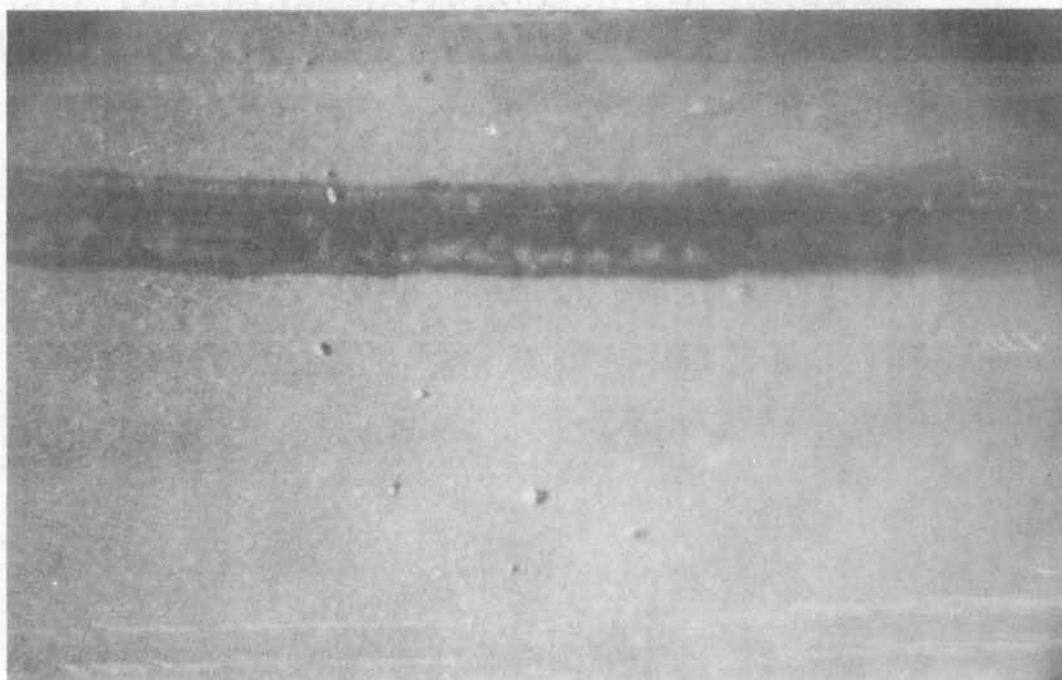


Figure C-5. Photograph of Generated 2024-T351
Aluminum Particulate After
Initial Five Minute Exposure to
Cavitation

VITA

Robert Elwin Bose

Candidate for the Degree of
Doctor of Philosophy

Thesis: THE EFFECT OF CAVITATION PARTICULATE
CONTAMINATION GENERATION

Major Field: Engineering

Biographical:

Personal Data: Born August 17, 1937, in Bessie,
Oklahoma, the son of Edward and Margaret Bose.

Education: Graduated from Clinton High School,
Clinton, Oklahoma, in May, 1955; received the
Degree of Bachelor of Science in Mechanical
Engineering from Oklahoma State University,
May, 1959; received the Degree of Master of
Science in Mechanical Engineering from Oklahoma
State University, May, 1962; completed the re-
quirements for the Degree of Doctor of Philo-
sophy in July, 1966.

Professional Experience: Employed by Oklahoma State
University from January, 1959 to September, 1961,
as a Graduate Assistant; from September, 1961 to
September, 1963, as a Graduate Research Assist-
ant; and from September, 1963 to August, 1966,
as an Instructor.

Professional Organizations: Member of the American
Society of Mechanical Engineers and Pi Tau Sigma.